Role of locomotor corollary discharges in sensory-motor integration in *Xenopus laevis* and *Ambystoma mexicanum*

Dissertation der Graduate School of Systemic Neurosciences der Ludwig-Maximilians-Universität München

Roberto Banchi

München, Juni 2015

Dissertation der Graduate School of Systemic Neurosciences, Ludwig Maximilians Universität München

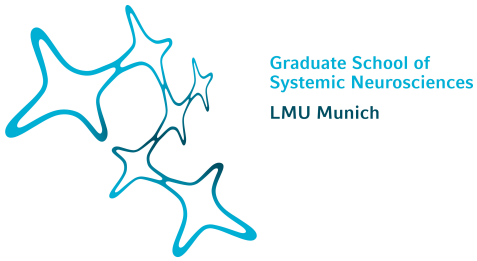

Role of locomotor corollary discharges in sensory-motor integration in *Xenopus laevis* and *Ambystoma mexicanum*

Submitted by

Roberto Banchi

Erstgutachter: Prof. Dr. Hans Straka

Zweitgutachter: Prof. Dr. Harald Luksch

Tag der mündlichen Prüfung: 29/10/2015

Affidavit/Eidesstattliche Versicherung

Hiermit versichere ich an Eides statt, dass ich die vorliegende Dissertation '**Role of locomotor corollary discharges in sensory-motor integration in *Xenopus laevis* and *Ambystoma mexicanum*'** selbstständig angefertigt habe, mich außer der angegebenen keiner
weiteren Hilfsmittel bedient und alle Erkenntnisse, die aus dem Schrifttum ganz oder annähernd übernommen sind, als solche kenntlich gemacht und nach ihrer Herkunft unter
Bezeichnung der Fundstelle einzeln nachgewiesen habe.

I hereby confirm that the dissertation '**Role of locomotor corollary discharges in sensory-motor integration in *Xenopus laevis* and *Ambystoma mexicanum*'** is the result of my own work and that I have only used sources or materials listed and specified in the dissertation.

München, den / Munich, date: 11.06.2015

Roberto Banchi

Acknowledgement

I would like to thank my TAC members for all the constructive discussions during the meetings. I am also very grateful to the GSN, which gave me the opportunity not only to acquire knowledge in the different fields of the neurosciences but also to personally develop by offering me a large variety of soft-skill courses.

Furthermore I want to thank the RTG[1373] and the IFB for the financial support during these years and also for the very interesting methods courses.

Many thanks also to all my co-workers/co-authors. We were and are all different in approaching problems and observing phenomena. I am grateful to all of you, who were not afraid of our 'biodiversity' and were open to understand, share and receive our individual talents. I truly believe that sharing with and receiving from others is the key crucial principle to achieve the absolute creative potential of a team, which is an emergent property of our combined individual unique talents.

Thanks to all of you,

Roberto

Table of Contents

1. Introduction

1.1 Corollary discharges (CDs): an overview

Sensory systems have evolved to provide animals with a reliable representation of the outside world allowing high fitness levels in exploration and navigation tasks.

An animal living completely stationary would only detect an input generated by the environment, an "exafference" stimulus (von Holst and Mittelstaedt, 1950). In contrast, an animal performing a motor behavior (e.g. locomotion, vocalization, breathing), would additionally experience an input that is a consequence of the motor activity, termed "reafference" (von Holst and Mittelstaedt, 1950). The concomitant detection of exafferent and reafferent stimuli can in principal produce ambiguity in assessing the cause of the sensation and result in an inefficient and disrupted perception of the outside world. Across the animal kingdom all species have evolved mechanisms to resolve ambiguity regarding the nature of the sensory inputs (Crapse and Sommer, 2008), in order to be able to perceive the world while moving. Interestingly, it seems that animals evolved a conceptually similar strategy for reducing the effect of reafferent stimulation. The intrinsic neuronal signal responsible for the motor behavior is also used to inform the sensory system about the impeding reafferent stimulation (efference copy signal, in von Holst and Mittelstaedt, 1950), reducing the ambiguity of perception and insuring a sensory-motor balance. The definition of "efference copy", initially given by von Holst and Mittelstaedt, is related to an actual copy of the motor signal (the efference), which produces muscle contraction. Sperry (Sperry, 1950) introduced the term "corollary discharge" (CD) to describe a motor-related signal that influences sensory processing, independently of the origin. The concept of CD will be preferentially used in this thesis since it also includes the definition of efference copy.

According to Crapse and Sommer (2008), CDs can be subdivided into higher and lower functional categories in relation to the complexity of the computational processes in which they are involved (e.g. learning or peripheral sensory gating). Lower-order CDs are responsible for reflex inhibition and filtering sensory signals. Reflex inhibition during swimming plays an important role in gating sensory inputs from skin receptors in *Xenopus* embryos (Sillar and Roberts, 1988) and in avoiding withdrawal responses in gastropods during feeding behavior which are otherwise present whenever the mechanoreceptors of the mouth are stimulated (Davis et al., 1973). In the latter example, CDs active during feeding decouple a motor response (withdrawal), which would be completely inefficient for the

feeding process. CDs have been shown to drive context dependent reflex control also in amniote vertebrates. For example, in monkeys the vestibulo-ocular reflex (VOR), responsible for gaze and posture stabilization during passive head motion, is suppressed during voluntary head movements (Roy and Cullen, 2004). In this case the CD contributes to the differential processing of passive and active head movements by the vestibular system.

Sensory filtering strategies have evolved simultaneously with the motor systems responsible for body motion in space or for acoustic communication (Crapse and Sommer, 2008). In case of acoustic communication, in insects (Poulet and Hedwig, 2006), fishes (Chagnaud and Bass, 2013) and mammals (Hage and Jürgens, 2006), CDs in the vocal motor centers suppress signal processing in auditory regions during self-vocalization, and thus maintain receptiveness for non-self-generated auditory stimuli.

Higher-order CDs are involved in more complex functions such as sensory analysis and stability, sensory-motor planning and learning, mostly present in amniote vertebrates (Crapse and Sommer, 2008). In monkeys CDs contribute to a stable perception of the visual world during saccadic eye movements (Schall, 2004) or to the planning of saccade sequences during visual exploration (Sommer and Wurtz, 2002). CDs of the vocal motor command play a crucial role in learning of songs in song birds (Brainard and Doupe, 2000; Margoliash, 2002). In a particular phase of vocal learning, the auditory signals of the actual emitted song, the memory trace obtained by listening to adult song birds (the tutors) and the vocal CD are reiteratively combined in order to refine the vocal motor command (Margoliash, 1997; Reiner et al., 2005). By taking into account the majority of studies related to CDs, it emerges that lower order CDs tend to inform sensory systems about the timing of the self-induced stimulation, whereas higher level CDs simultaneously encode multiple parameters (e.g. space and time).

1.2 Reafferent stimulation and CDs in mechanosensory systems

Amongst vertebrates, systems that are able to sense a physical displacement (mechanosensory systems) can be affected by reafferent stimulation during active movement in space of the body or of body parts. The mechanosensory hair cell systems like the vestibular and the lateral line system (in fishes and amphibians), are extremely sensitive to body motion or water waves, and are therefore affected by reafferent stimulation during locomotion. Other mechanosensory systems present on the body surface (e.g. touch receptors) are also potentially affected by self-induced stimulation and might necessitate mechanisms to resolve ambiguity regarding the nature of the sensory inputs.

1.2.1 Vestibular system

The vestibular system is responsible for detecting linear and angular body/head acceleration and for driving the appropriate counteracting motor commands to maintain stable posture and gaze during body movements (Angelaki and Cullen, 2008; Carriot et al., 2014). The vestibular nerve (VIII) of all vertebrates (reviewed in Straka and Dieringer, 2004) is composed of sensory afferent fibers with their somata in the ganglion of Scarpa in the peripheral nervous system (PNS). These fibers mediate motion information to the central nervous system (CNS), by making synaptic contacts with the different end-organ hair cells (Straka and Dieringer, 2004). The VIIIth nerve also comprises efferent fibers originating from a brainstem efferent nucleus. These fibers make peripheral synaptic contacts with hair cells and afferent fibers (Fritzsch, 1996). Due to this connection, the efferent neurons are potentially involved in regulating the peripheral sensory processing within the vestibular system and might be responsible for the suppression of self-induced stimulation. The activation of this nucleus might produce a wider dynamic range for the afferent signals encoding head/body motion (Highstein and Baker, 1985; Boyle et al., 1991). Electrical stimulation of the efferent nucleus in toadfish, in anesthetized monkeys and in chinchilla produced an increase in resting afferent discharge rate (Goldberg and Fernández, 1980; Highstein and Baker, 1985; Plotnik et al., 2002). In contrast, similar experiments in frogs and turtles revealed a combination of excitatory and inhibitory effects (Bernard et al., 1985; Rossi and Martini, 1991; Brichta and Goldberg, 2000). In toadfish the sensitivity of afferent fibers to passive head rotation was diminished during electrical stimulation of the efferent system.

Some evidence of behavioral activation of efferent fibers come from studies in toadfish and frogs (Russell, 1971; Roberts and Russell, 1972; Highstein and Baker, 1985; Boyle et al., 1991). In these animals putative efferent neurons were found to produce a burst of activity before the initiation of escape responses or during locomotor episodes. More recent studies however have shown that in awake monkeys, vestibular afferent fibers show the same sensitivities during passive and voluntary head motion (Cullen and Minor, 2002), indicating that the efferent nucleus is not active during this motor behavior or not able to produce an effect on peripheral sensory processing. Despite the potential mechanism of peripheral adaptation via efferent neurons, the sensory filtering during motor behaviors could also take place in the CNS, at the different levels of the sensory-motor processing. Vestibular neurons in monkeys receive direct projections from afferent fibers encoding passive and voluntary head motions (Cullen and Minor, 2002), compatible with the absence of a peripheral sensory gating. A subpopulation of these neurons, called vestibular only (VO) neurons, carry information about motion only during passive and not during voluntary head rotation (Boyle et al., 1996; McCrea et al., 1999; Roy and Cullen, 2001). These cancellation signals at the level of VO neurons were found only when the head of the monkey was left free to perform actual rotational movements. In a head-restrained condition, simple 'trying to attain' head rotations (measured by the presence of large saccadic eye movements) did not cause any change in the resting firing rate of the VO neurons (Roy and Cullen, 2004). It was concluded that an integration between efference copies of the signals going to the neck muscles and proprioceptive inputs coming from these muscles only during actual head rotation has to take place in order to generate the inhibition. Other evidence of CDs influencing the vestibular sensory processing come from studies in larval and adult amphibians. During undulatory axial-based swimming (larval stages) and limb-based swimming (adult stages), compensatory eye movements are produced via CD signals originating in spinal locomotor regions and are not related to vestibular inputs (Lambert et al., 2012; von Uckermann et al., 2013).

1.2.2 Lateral line system

The lateral line system is located along the head and trunk/tail regions of aquatic anamniotes (fishes and amphibians), serves to sense water waves and can be used for pray/predator recognition/localization and in navigational tasks (for a review see Bleckmann, 2008). The sensory processing of water waves produced by the external environment can thus be affected

by concomitant self-generated turbulences during locomotor activity (Montgomery et al., 2009). The anterior and posterior lateral line nerves (ALLN and PLLN) innervating the hair cell neuromasts on the head and trunk/tail regions are also composed of afferent and efferent fibers (Russell, 1968), as described for the vestibular nerve. The majority of efferent neurons are shared between the lateral line and vestibular system (Hellmann and Fritzsch, 1996). Similarly to the vestibular system, sensory processing of external lateral line stimuli (water waves produced in the environment) can be affected by concomitant self-generated stimuli (water turbulences created during locomotor activity). Also in this system, efferent projections to hair cells represent a possible candidate to suppress reafferent stimulation already at the level of the sensory periphery. Even though, an increase in activity of putative efferents during swimming in dogfish was reported in a previous study (Roberts and Russell, 1972), up to date, the physical origin of the neuronal inputs responsible for locomotion related activation of lateral line and vestibular efferents is unknown and the nature of this activation (sensory feed-back/feed-forward mechanisms) remains ambiguous. The possible relationship between the firing profile of efferent neurons and locomotion-related features (i.e. duration, amplitude and frequency) and the resulting effect on the sensory processing also remain unclear.

1.2.3 Somatosensory processing (touch)

The processing of touch sensation as described for other sensory modalities also occurs during active movements of the body (locomotion) and of the body´s appendages endowed with touch receptors (e.g. fingers, whiskers, tentacles). In 1962, Gibson already hypothesized that the difference between 'touching and being touched' could not only be given by the perception of movement (kinesthesis). He proposed that touch sensation has to be processed within two different channels, one 'extero-specific' and one 'proprio-specific'(Gibson, 1962). Studies in primate somatosensory cortex have confirmed this hypothesis showing that CDs are responsible for attenuated responses to self-produced versus externally produced tactile stimulation (Chapman, 1994). Intrinsic motor signals are also involved in suppressing self-induced tickling sensations/responses in humans (Blakemore et al., 1998). Rats use tactile information from their whiskers (vibrissae), which are actively moved to explore the environment (Kleinfeld et al., 2006). In the trigeminal nucleus, which supplies a part of the innervation for the whisker system, cells were found that specifically encode for only the

active deflection or for the pure touch of the whiskers (Szwed et al., 2003). Other studies in the barrel cortex of these animals showed that, neurons continued to encode amplitudes of active whisking also after the removal of proprioceptive inputs, indicating the presence of CD signals (e.g. Fee et al., 1997).

Mobile, elongated appendages, which emerge from the head or brachial regions are also present across fishes, amphibians and reptiles containing a large variety of different sensors (reviewed in Fox, 1999). Depending on the type of receptors present on the surface of these structures, they can be used for touch perception, electroreception, water motion detection and gustation. The tentacles of *Xenopus laevis* larvae, present between developmental stages 47 and 61 (Nieuwkoop and Faber, 1956), are an example for facial structures endowed with Merkel cell touch receptors (Ovalle, 1979; Ovalle et al., 1998). The presence of mechanoreceptors suggests a role in touch perception and recognition of surfaces (Maricich et al., 2009). At larval stages these animals are very active and live prevalently in a murky aquatic environment (Nieuwkoop and Faber, 1956), probably in the absence of adequate visual cues for orientation and navigation. Thus, tentacles might represent an evolutionary adaptation for this particular ecological niche. Interestingly these appendages are gradually lost before metamorphosis and are absent in adults. This loss might be related to the change in lifestyle of post-metamorphic frogs, which live at the clearer water surface and are mostly stationary.

Xenopus tadpole tentacles and rodent whiskers might have the same functional role in touch perception. As already emphasized, rats use whisker movements to explore the environment while walking along surfaces. *Xenopus* tadpoles swim slowly with their tentacles touching the wall or floor of the tank where they are kept. This behavior potentially serves to collect surface information via tentacle tactile stimuli. While, rodents control their whisker movements actively by differential activation of multiple muscles (Berg and Kleinfeld, 2003), tentacle motion in *Xenopus* larvae is controlled by a single muscle (producing retraction to a lateral position) and a spring-like antagonist (responsible for the passive return to the extended position). The motor (tentacle retraction) and sensory (touch sensation) innervation of the tentacles have been shown to originate from the mandibular and ophthalmic branches of the trigeminal nerve (Ovalle, 1979) .

During undulatory swimming of *Xenopus* tadpoles, the large oscillations produced by the tail cause a concomitant motion of the head (Lambert et al., 2012). The concurrent strong passive displacement of the extended, relatively long (up to 1/3 of the animal´s length) tentacles during swimming might impair their tactile function by damaging and/or over- stimulating

these sensory appendages. A potential protection of the sensors and an increase in hydrodynamic efficiency could be achieved by a retraction of the tentacles, especially during strong locomotor activity.

Starting from the anatomical knowledge that the tentacles of these animals are sensory and motor innervated by a subdivision of the trigeminal nerve (Ovalle, 1979), the goal was to reveal if this particular nerve subdivision receives locomotor-related CDs. Furthermore, this also included a study to investigate which kind of information about locomotion is transmitted to the trigeminal nucleus and its effect on tentacle motility.

1.3 Technical requirements for experimental approaches

In-vitro preparations of *Xenopus laevis* have been already used in a variety of studies on developmental aspects of the vestibulo-ocolomotor system (Lambert et al., 2008, 2013; Branoner and Straka, 2014) or on the role of swimming related spinal CD for eye movements (Combes et al., 2008; Lambert et al., 2012). All these studies were conducted by means of electrophysiological recordings of motor nerves and spinal cord ventral roots. In the framework of my thesis, I modified this semi intact *in-vitro* preparation and developed an electrophysiological technique (described below) for stable recordings of intact vestibular/lateral line afferent/efferent fibers as well as the activity of identified central vestibular/lateral line neurons by means of calcium imaging and electrophysiological techniques (see below). These recordings are possible in the presence and absence of locomotor activity. I also established axolotl (*Ambystoma mexicanum*) larval/juvenile (Fig.1 A, C) semi intact *in-vitro* preparations, which both are particularly suitable for imaging techniques.

In these *Xenopus* and axolotl preparations all the sensory-motor systems or a subset of them can be kept functional (Fig. 1 A, C). After disconnection of the forebrain, the head and the associated neuronal structures can be completely fixed. The entire or parts of the midbrain, hindbrain and spinal cord with the associated nerves can be exposed (Fig. 1 B, C) with the possibility to keep the sensory periphery intact and functional (note the accessibility of the VIIIth and of the other cranial nerves in Fig. 1 A together with the intact otic capsule). For both species parts or the entire osteomuscular elements of the trunk and tail can be maintained functional and free to perform spontaneous or induced (mechanically, electrically, pharmacologically) swimming/walking movements, as it is exemplified for the *Xenopus* preparation in Fig. 1 B. These reduced preparations, kept in Ringer solution (see Materials and Methods in the enclosed manuscripts), maintain their functionality for an average period of 2 days (*Xenopus)* and 7 days (axolotl). This long survival time, together with the accessibility and visibility of all nerves and brain regions makes it possible to conduct anatomical and physiological studies of identified neuronal subpopulations. In Fig. 2 some examples of retrogradely labeled projections and neuronal types in the hindbrain of axolotl (Fig. 2 A, D) and *Xenopus* (Fig. 2 B, C) are shown. The site of application and combinations of different color fluorescent tracers for both species are depicted in the inset in Fig. 2 B.

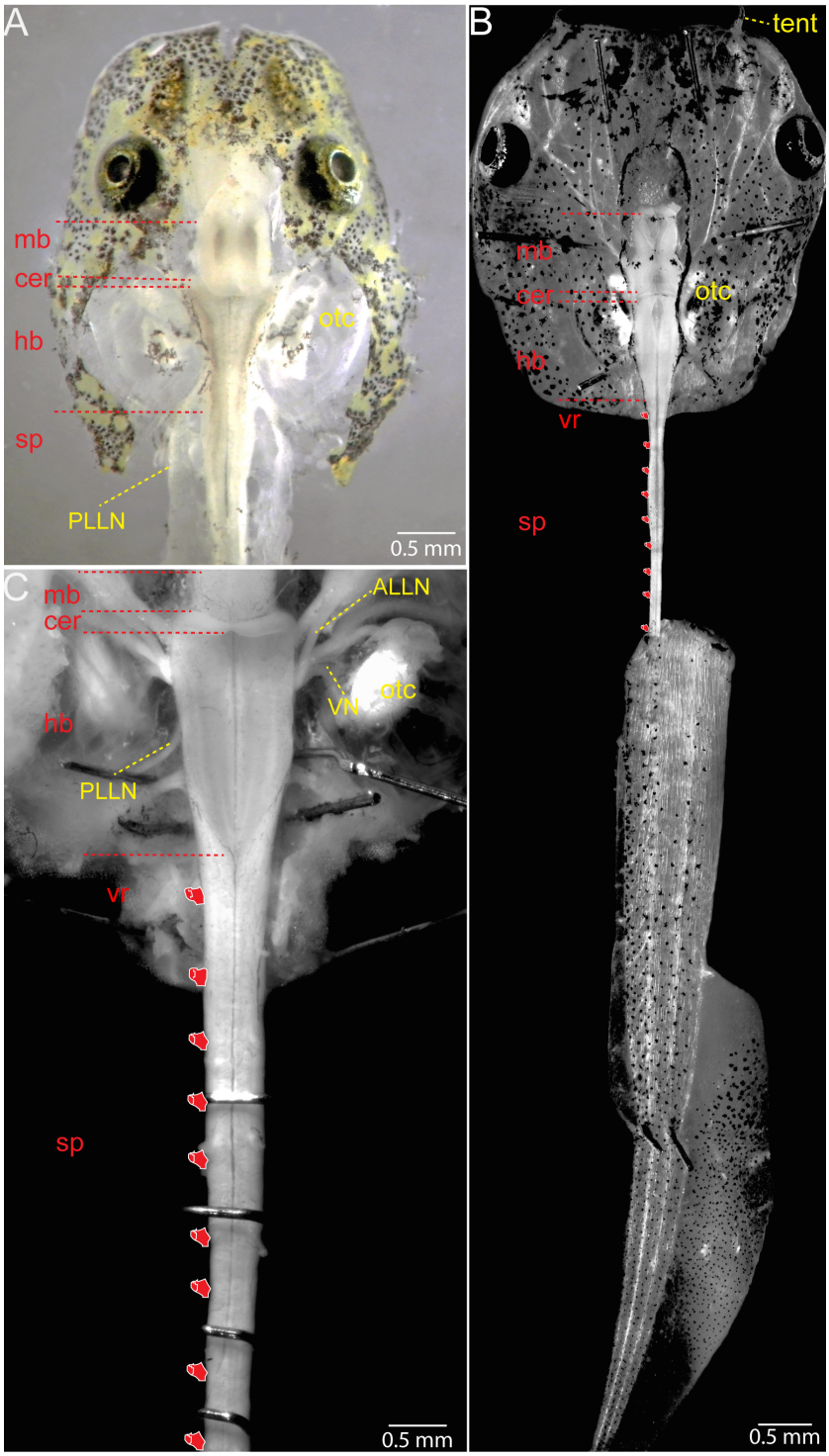

Figure 1

Semi-intact *in-vitro* preparations. Whole-head-spinal cord preparations of larval axolotl (A) and *Xenopus* (B) and of a juvenile axolotl (C) used for anatomical, behavioral and physiological studies. The intact head sensory structures and the exposed brainstem-spinal cord regions are shown together with the accessible cranial nerves and spinal ventral roots (A, B, C). In C, the caudal part of the tail was left intact to perform swimming movements. Abbreviations: mb, midbrain; cer, cerebellum; hb, hindbrain; vr, ventral roots; sp, spinal cord; tent, tentacle; otc, otic capsule; ALLN, anterior lateral line nerve; VN, vestibular nerve; PLLN, posterior lateral line nerve.

1.3.1 Anatomical localization of hindbrain neurons

The embryonic hindbrain of all vertebrates develops as a series of functionally and genetically distinct segments, called rhombomeres (r, Fig. 2 B) (for a review see Gilland and Baker, 2005). This evolutionary retained segmental organization allows the comparison of clusters or of individual neurons located in specific rhombomeric domains across species. Interestingly, this embryonic rostro-caudal bauplan can still be found during larval stages of some aquatic vertebrates (Straka et al., 2001; Gilland and Baker, 2005) and appears to be true also for larval *Xenopus* (Fig. 2 B). Due to the absence of a direct visualization of the segmental pattern in the axolotl hindbrain, the embryonic rhombomeric scaffolds at younger and at older larval stages were inferred by the sequential arrangement of reticulo-spinal neurons along the rostro-caudal axis of the hindbrain (red neurons circumscribed by dashed-withe-lines in Fig. 2 A). In many vertebrate species, these clusters of reticular neurons were shown to have a specific morphology, axonal projection pattern and rhombomeric origin during embryogenesis and retain their localization throughout development (Metcalfe et al., 1986; Hanneman et al., 1988; Lee and Eaton, 1991; Lee et al., 1993; Straka et al., 2001, 2006; Gilland and Baker, 2005; Gilland et al., 2014). Due to the well known properties of these neurons, the inferred rhombomeric scaffold was used to compare the segmental localization of subpopulations of vestibular neurons in axolotl and *Xenopus*. In Fig. 2 A, B (green cells circumscribed by dashed-blue-lines) vestibular neurons projecting to the same midbrain regions (see figure legend for details) were found to be located in the same homologous segments in axolotl (Fig. 2 A) and *Xenopus* (Fig. 2 B).

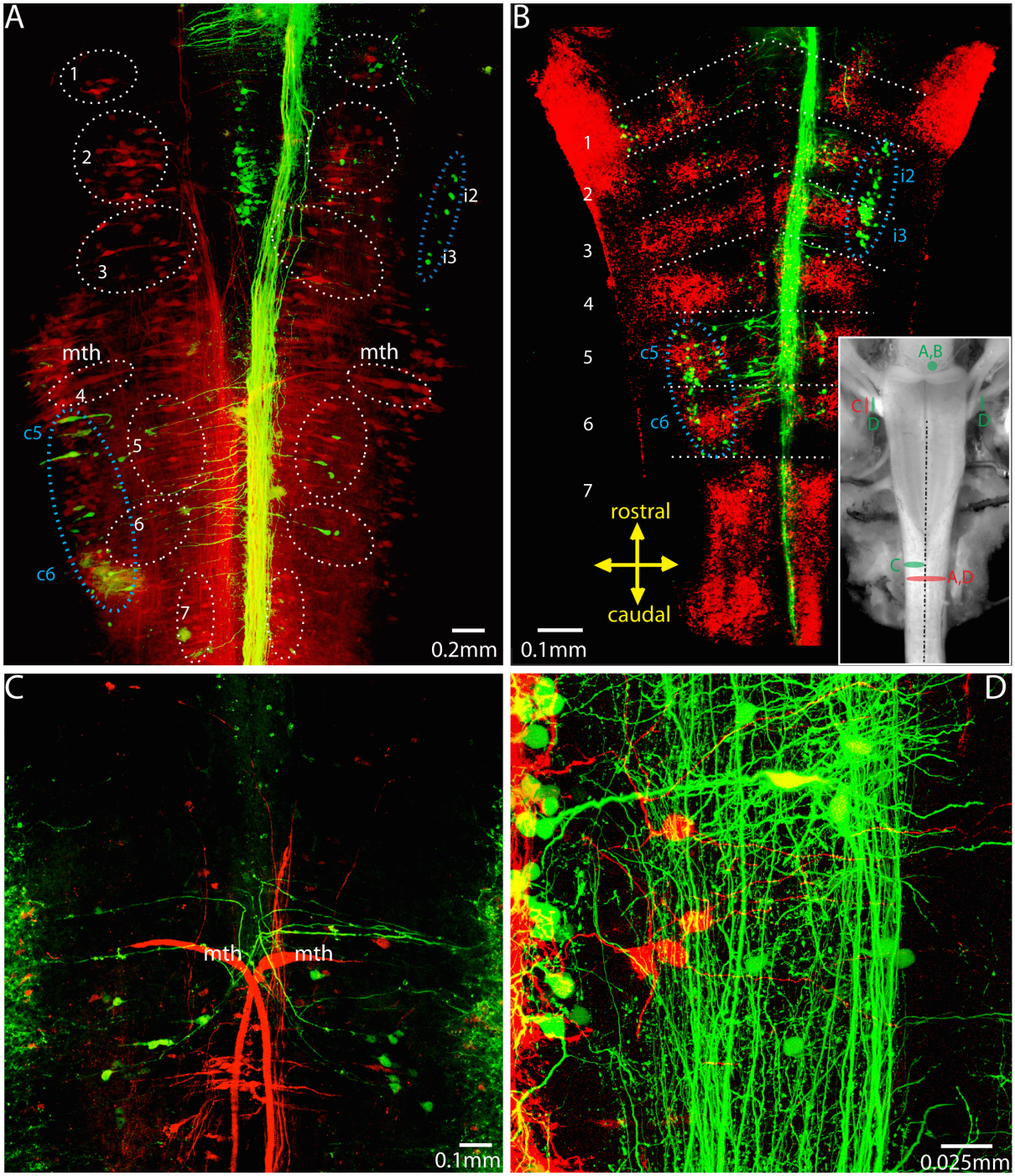

Figure 2

Rhombomeric arrangement of hindbrain motor nuclei. Confocal microscope reconstructions of hindbrain neuronal subpopulations in axolotl (A, C) and in *Xenopus* (B, D) after application of two different fluorescent tracers (green and red). The different combinations and sites of tracer application for both species and all preparations are depicted in the inset in B. A and B show homologous segmental allocation of ipsilateral and contralateral vestibulo-ocolomotor neurons (i2-3, c5-6; green cells circumscribed by the blue dashed lines) visualized by unilateral green tracer application to the oculomotor nucleus (see letters and colors in the insert in B). The rhombomeric domains were directly visible in *Xenopus* (1-7 and sequential dashed white lines in B) and inferred in axolotl from the rostro-caudally arranged clusters of reticulo-spinal neurons (1-7 and red cells circumscribed by the dashed lines in A). C, D. Labeling of efferent neurons/afferent vestibular projections (green in C, red in D)

and of reticulo- and vestibulo-spinal projections (red in C, green in D). Mth, Mauthner neurons in A and Mauthner neuron axons in C. The yellow arrows in B show the orientation of the hindbrain and apply to all the images.

1.3.2 Recording of nerve activity

Different electrophysiological techniques have been used across vertebrates to record the discharge of the entire nerve, of nerve portions or of single axons. The activity of the majority of the axons (units) composing a nerve or of isolated dissected nerve bundles can be acquired by placing the nerve tissue over electrodes and by electrically isolating this area with fatty compounds like mineral oils or Vaseline (Russell and Roberts, 1972; Combes et al., 2004). With this technique, the peripheral parts of the nerve can be both kept attached as well as transected before the innervation to the target structures (e.g. muscle, sensory organs, glands). After the transection two parts of the nerve are theoretically available for the recordings; one cut end is still attached to the periphery, whereas the other end (the central stump) is connected to the CNS. In case of a motor nerve, the activity recorded from the central stump corresponds to the discharge of the motor neurons located in the CNS (see Fig. 3), which would lead to a muscle contraction. The discharge acquired from the other side of the cut nerve, the part attached to the muscle, would be related to some still functional sensory fibers (e.g. proprioceptive from the periphery). If one considers a sensory nerve containing only afferent fibers, the only possible recorded activity would be the one coming from the peripheral stump. On the other hand, in mixed sensory/motor nerves containing efferent and afferent fibers, as described for the vestibular and lateral line system, the activity of the efferent fibers could be recorded from the central stump. The recording methods described above can be used in relatively large animals or at older developmental stages, where the nerves have acquired a sufficient size. Recordings from smaller nerve stumps (50-100 μm) have been made with glass suction electrodes (Combes et al., 2008; Lambert et al., 2008; Branoner and Straka, 2014) where the cut nerve end is sucked into a glass pipette with an adequate diameter to ensure a tight seal (see Fig. 3 B). This technique can be applied only to nerves that have been isolated from the peripheral targets (e.g. muscles). Alternatively, intracellular (Rossi et al., 1980) and extracellular electrodes (Cullen and Minor, 2002; Sadeghi et al., 2009) have been used for recordings of single or multiple afferent discharges in nerves with intact or disrupted peripheral and central projections. Even tough these approaches have been used for vestibular afferent recordings during rotations of the head or of an isolated otic capsule (Rossi et al., 1980; Cullen and Minor, 2002), they are only suitable

for larger axons and for nerves that remain relatively immobile with respect to surrounding structures and tissues. Some other disadvantages of the common extracellular recording techniques are that in most of the cases the signal is composed of the activity of many units, the signal to noise ratio is relatively poor and in some cases only the average of sequentially recorded traces can be analyzed.

The necessity to investigate the effect of vestibulo/lateral line locomotor related efferent activation on the discharge of afferent fibers of larval amphibians during natural stimulation (head movement, hydrodynamic stimulation) required a specific technique, which had to include all of the following aspects: 1) Efferent and afferent fibers and their connections to hair cells have to be intact; central or peripheral cut end recordings would not have revealed afferent adaptation given by efferent activity. 2) The recording method has to be suitable for relatively small and fragile nerves/afferent fibers present at larval stages (approximate diameter 1 μm); the axonal diameter would have been too small for intracellular recordings. 3) The recorded signal should include, with a high signal to noise ratio, the activity of one or a few afferent fibers. 4) The recordings have to remain stable during the natural stimulation of both sensory systems: lateral line nerves during hydrodynamic stimulation and of the vestibular nerve branches during head rotation.

To achieve this, the tips of sharp glass pipettes, normally used for intracellular recordings, were broken at a diameter of approximate 2 μm. The broken tips were observed under a microscope and only pipettes with sharp transversal apical apertures were used. Alternatively, patch-pipettes, around the same diameter, with a polished tip, were used (preferentially for lateral line nerve recordings). Prior to the experiments, the surface of the different nerve branches, close to their brain entrances, were completely cleaned from the surrounding tissue. After reaching the surface of the nerve with a preferential perpendicular approach, negative pressure was applied to and maintained in the glass electrode. This procedure resulted in a very tight connection between the electrode and the nerve patch. The activity of single or very few afferent fibers (due to the small tip size of the pipette) could be recorded with a high signal to noise ratio (due to the tight connection between the polished tip of the pipette and the completely clean nerve); the connection and the recording revealed to be remarkably stable also during rotational stimuli (rotation of the preparation on a turn table) or during movement of the liquid surrounding the nerve (hydrodynamic stimulation of the lateral line system). In some rare cases, the activity of an afferent fiber (red arrow in Fig. 3) could be

recorded *en passant* together with locomotor related activity of a closely located efferent fiber (blue arrows in Fig. 3). The newly established method is thus perfectly suitable for stable single/multiple discharge recordings of relatively small axons.

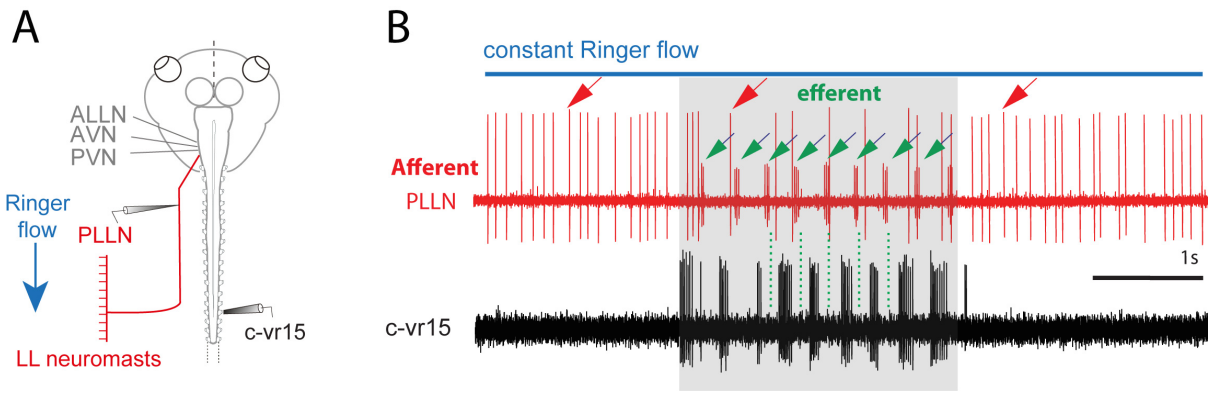

Figure 3
Peripheral sensory processing during locomotor activity. A, in this *Xenopus* preparation the posterior lateral line nerve (PLLN) is kept attached to the sensory periphery (LL neuromasts), which is stimulated via constant ringer flow. B, the red trace shows a single afferent unit (red arrows) of the PLLN active before, during (gray box) and after a fictive swimming episode. B, the smaller efferent unit (green arrows) is only active during fictive swimming, showing rhythmicity out of phase (dashed green lines) with the contralateral ventral root discharge (c-vr). The afferent encoding of water motion (Ringer flow) is reduced during the entire fictive swimming episode. ALLN, anterior lateral line nerve; AVN, anterior vestibular nerve; PVN, posterior vestibular nerve.

1.3.3 Fictive locomotion

After dissection of the trunk/limb muscles and isolation of the respective nerves, the neuronal correlate of swimming/walking can be recorded as left-right alternating bursts in the isolated spinal ventral roots (Fig. 4 A-C); this neuronal activity has been identified with the term ‘fictive locomotion‘ (e.g. Combes et al., 2004). This firing pattern is driven by a network of spinal premotor neurons (spinal central pattern generator, sCPG) and is responsible for rhythmic locomotion in animals (Combes et al., 2004; von Uckermann et al., 2013). As shown in Fig. 4 C, the motor activity was recorded from the cut ends of ventral roots by means of suction electrodes perfectly matched to the diameter of the roots. In these preparations locomotor activity can occur spontaneously or can be mechanically, electrically and pharmacologically induced.

The absence of motion-related sensory feedback during fictive locomotion (vestibular, lateral line, proprioceptive and visual inputs) due to the immobile experimental conditions or due to

the selective ablation of the sensory periphery makes it possible to unequivocally identify locomotor related CDs.

It is also possible to passively (externally) stimulate the different sensory systems in the presence and absence of fictive locomotion in order to study the effect of CDs on the different sensory processing relay stations. The immobility of the preparation during fictive locomotion represents also a big advantage for physiological techniques that require stability of the neuronal tissue and for imaging of body parts: Ca^{2+} imaging, photo-activation, electrophysiological recordings, electrical stimulation, video recordings of eye and appendage movements (e.g., *Xenopus* tentacle motion relative to the body).

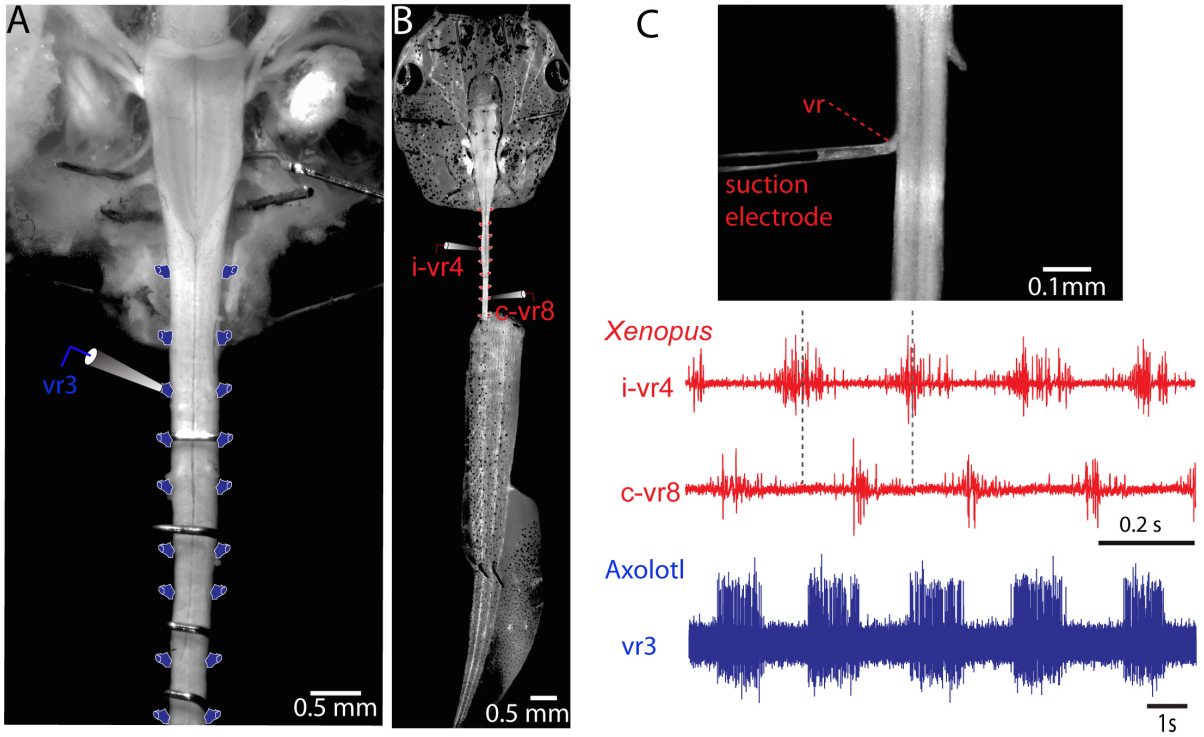

Figure 4

Fictive locomotion. Neuronal activity responsible for locomotor behaviors can be recorded in axolotl (A) and *Xenopus* (B) *in-vitro* preparations at different rostro-caudal levels of the spinal cord. C, suction electrodes adjusted to the size of the specific ventral root (vr, upper pannel). Red traces show the rhythmically alternating bilateral activity recorded from ipsi- and contralateral ventral roots (see B) during an episode of fictive swimming in *Xenopus* larvae. Blue trace, rhythmic motor activity recorded from a forelimb ventral root, (vr3 in A) during an episode of fictive walking in axolotl.

1.3.4 Recordings of peripheral and central activity

Figure 5 A-D shows examples of the advantages of the developed *in-vitro* preparations. Galvanic vestibular stimulation (GVS) can be applied selectively to the different vestibular end organs due to their clear visibility and accessibility (Fig. 5 A). This selective activation can be used to mimic angular and linear acceleration that would result from actual head motion in the different planes. The responses to GVS can be recorded as afferent fiber activity in the different branches of the intact vestibular nerve (anterior and posterior vestibular nerve, AVN and PVN in Fig. 4 B) by means of stable *en passant* electrodes (technique described in the previous paragraph). The simulation of head motion achieved with this technique represents a big advantage also for recordings of central neuronal activity. As described above, in these preparations, neuronal subgroups can be selectively back-filled and identified by tracer application to their peripheral/central projections (Fig. 2). Furthermore, these neurons can be allocated along the segments of the rhombomeric scaffold (Fig. 5 C). For physiological tract-tracing studies Ca^{2+}-sensitive dyes can be used, and the responses to GVS of certain end organs at different current frequencies and amplitudes can be inferred from imaging calcium transients (color coded traces in Fig. 5 D) at the level of the single neuron. The calcium traces in Fig. 5 D are the responses of a single central vestibular neuron in r2-3 (circumscribed by the blue-dashed line in Fig. 5 C), backfilled from its projection to the oculomotor nucleus.

The combination of all these applied and developed experimental approaches allows to compare the central and peripheral connectivity (site of tracer application, responses to activation of a specific end organ) and the characterized physiological responses (frequencies and amplitudes of GVS) with the genetic identity of single neurons (according to the specific rhombomeric localization).

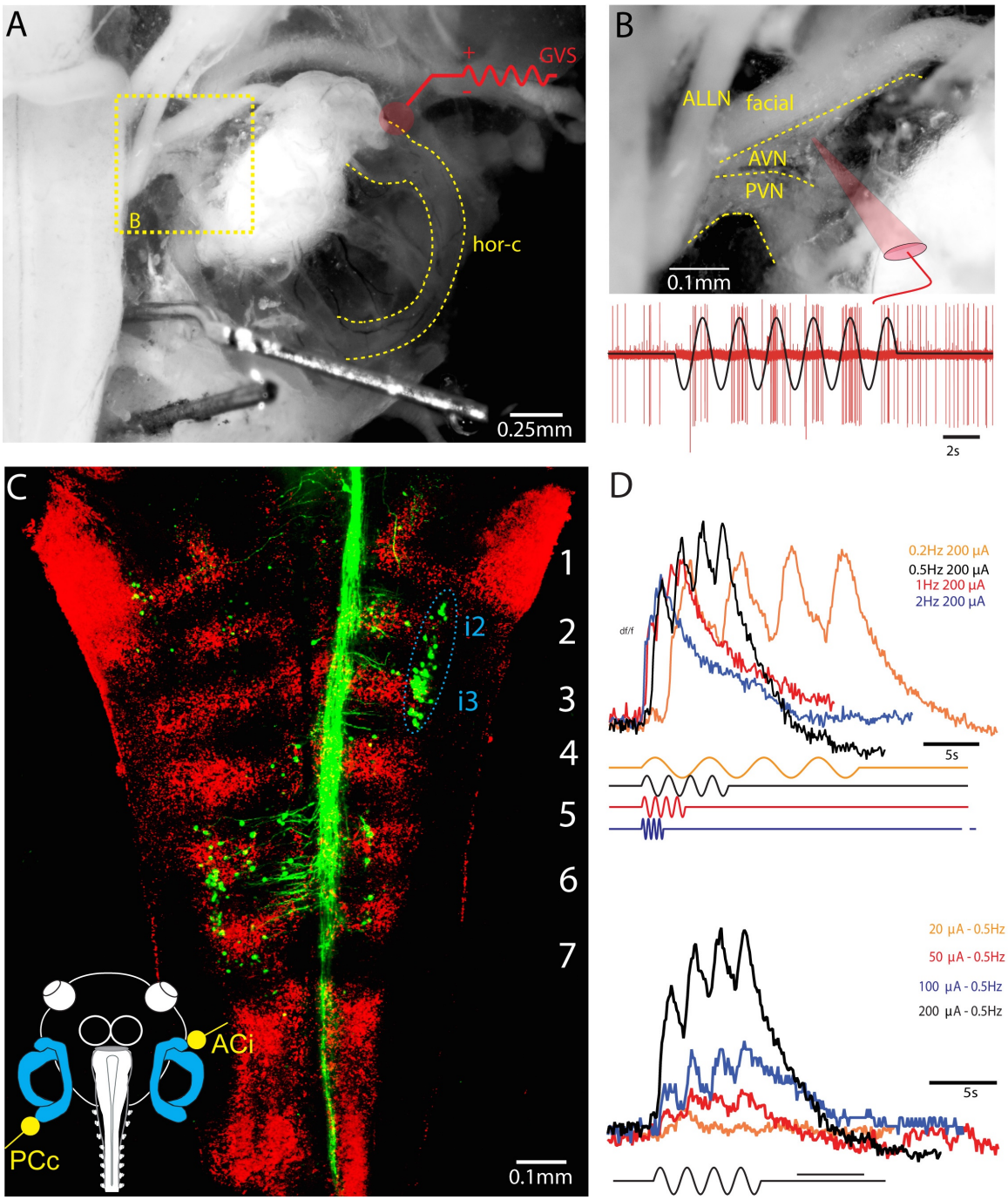

Figure 5

Physiological, anatomical and genetic characterization of vestibular circuitries. A, an example of axolotl preparation in which galvanic vestibular stimulation (GVS) can be used to exclusively activate clearly visible vestibular end organs (e.g. see the horizontal canal highlighted by the dashed yellow line; hor-c). B, the selective responses to GVS (black trace) of a single (multiple) afferent fiber(s) (red trace), with intact peripheral and central projections, can be recorded via suction electrodes (*en passant* recordings), from different vestibular nerve branches (AVN, anterior vestibular nerve; PVN, posterior vestibular nerve). C, D, calcium imaging of single central vestibular neurons within a specific rhombomeric domain (i2-3 circumscribed by the blue dashed line in C). These neurons reveal differential responses during increasing frequency (color coded traces in upper panel in D) or current amplitude (lower panel in D) of sinusoidal GVS applied to the ipsi-lateral anterior canal and to the contra-lateral posterior canal (ACi and PCc, schematic in C).

Electrophysiological recordings of identified central neurons were also achieved in these preparations. Fig. 6 shows an example of extracellular recordings from efferent neurons during locomotor activity in an axolotl preparation. The efferent nucleus (cells circumscribed by the green dashed line in Fig. 6 B) was visualized after fluorescent tracer application to the vestibular nerve. This allowed accurate positioning of the tip of the recording electrode (filled with a fluorescent dye) to the vicinity of the cell cluster. The recorded activity of the backfilled neurons can be seen in Fig. 6 C, D during episodes of fictive locomotion monitored via the ventral roots recordings.

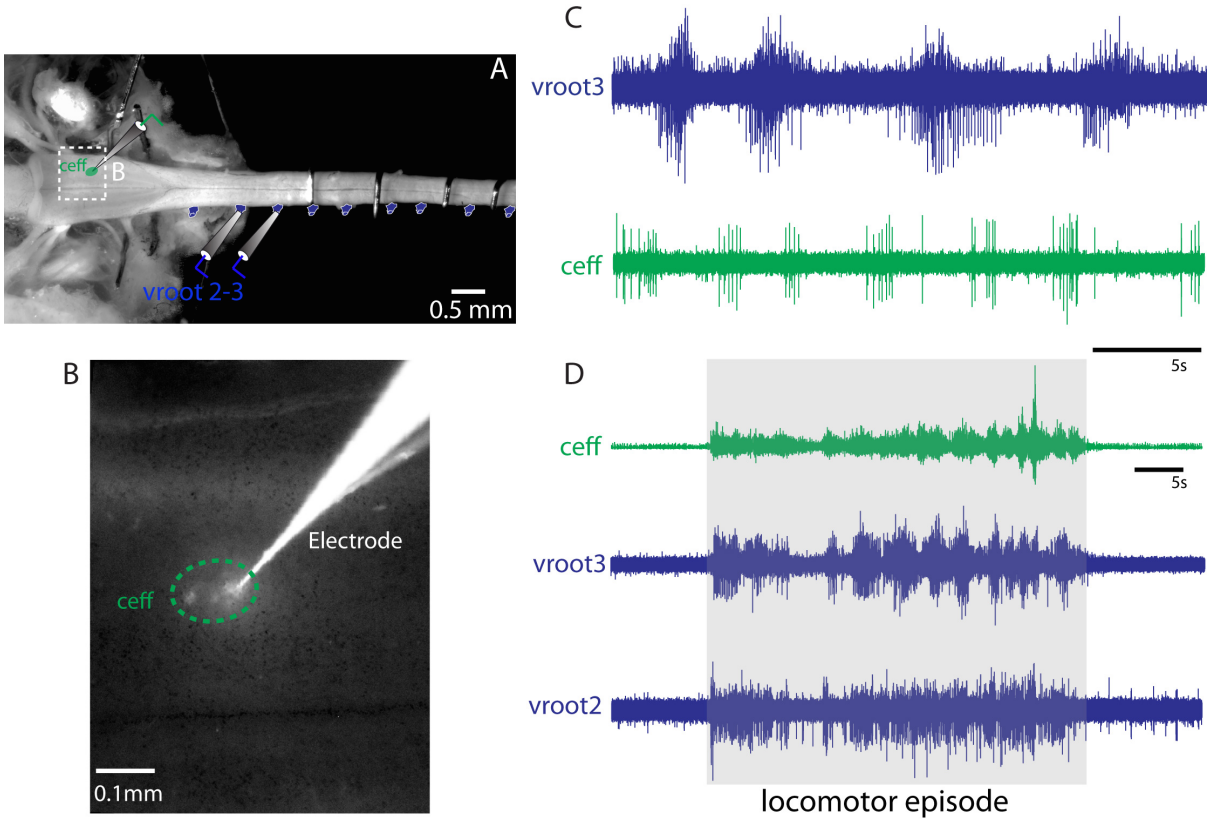

Figure 6

Electrophysiological recordings of identified central neurons during fictive locomotion in axolotl. Overview (A) and a higher magnification (B) illustrating the whole-head spinal cord *in-vitro* preparation, after tracer application to the vestibular nerve. The visibility of the back-filled contralateral vestibular efferent nucleus (green dashed line area, ceff, in B) was used to place the extracellular recording electrode in the close vicinity of the nucleus. C, D, green traces show the efferent discharges during locomotor episodes (blue traces, hind limb ventral root recordings). The gray box in D highlights the matching duration of locomotor and efferent neuronal activity.

1.3.5 Imaging techniques and advantages of the *in-vitro* preparations

Brain functions can be considered as emerging properties arising from the combined computational properties of single neurons and neuronal networks. The traditional electrophysiological approaches allow the study of either the combined simultaneous activity of many indistinguishable neuronal elements (extracellular, multi-units recordings) or the activity of few single neurons at a time. At the same time, the use of electrical currents to activate/inhibit brain regions is only suitable on a relative large spatial scale, not adequate to activate and thus understand the functional role of single neuronal components/networks. On the other hand, the more recently developed imaging techniques (Ca^{2+}, voltage imaging) potentially allow to acquire the simultaneous individual activity of many neurons over large brain areas. These innovative techniques makes it also possible to selectively activate/inhibit single neurons/networks, by means of optical uncaging of caged neurotransmitters (e.g. glutamate, GABA) or by light-induced opening of genetically encoded ion channels, (for a review see Häusser, 2014).

As already emphasized, in order to understand complex brain functions, which emerge from extended neuronal network dynamics, it is necessary to acquire temporally accurate activation profiles of many neurons at the same time. Thus, the ideal imaging setup would include the possibility to maintain high acquisition rates over large fields of view (FOVs), in order to acquire maximum information from spatially extended neuronal components. At the same time it would be very useful to independently control multiple FOVs to simultaneously activate/inhibit and record from spatially segregated or overlapping neuronal regions. In order to accomplish adjustable FOVs with spectrally and physically independent excitation pathways it would be necessary to quickly switch between imaging channels with different excitation wavelengths. Furthermore, a broad spectrum of different excitation wavelengths would allow to use the variety of existing Ca^{2+}/voltage sensors and caged compounds. All imaging systems currently available lack the combination of these prerequisites. Epifluorescence imaging setups, equipped with fluorescence lamps necessitate multiple mechanical filters, which have to be exchanged to obtain different excitation wavelengths resulting in a slow multi-color acquisition. Multi-photon imaging systems, due to the scanning processes, lack acquisition speed at large FOV (Grewe et al., 2010). Furthermore the installation of several laser lines for multi-channel scanning is still very expensive (Piston, 1999). In all the available microscopes, independently adjustable and spatially separated FOVs are also not present.

Based on the described requirements and on the framework of the already existing two-photon Intravital^{2P} microscope (TILL Photonics, FEI, Munich, Germany), a novel epifluorescence microscope equipped with 8 high-power light emitting diodes (LEDs) with seven different excitation wavelengths and two independently adjustable FOVs was developed. This setup provides the possibility to perform optical activation and imaging of neuronal activity via the two spatially independent FOVs with a wide range in size, from 800 x 680 µm to 40 x 40 µm. The presence of two multi-LED combiners also makes it possible to independently control the illumination timing and wavelength of the LED emitted on the two FOVs. Imaging setups that use illumination sources like fluorescent lamps have a broad spectrum of excitation wavelengths but necessitate time-consuming processes for switching filters for multi-color acquisition. The implementation of different wavelength LEDs, which can be controlled with high temporal accuracy, allow fast multi-color acquisition.

The axolotl *in-vitro* preparation was used to test the technical properties and suitability of this novel microscope for optochemical manipulations and imaging on identified vestibular networks. The accessibility of the different vestibular nuclei/axonal projections, sensory nerves and vestibular end organs together with the ideal optical properties of the axolotl brain tissue, made it possible to selectively back-fill and physiologically stimulate, specific subtypes of central vestibular neurons. Electrical (galvanic) stimulation of the intact inner ear sensory organs, which mimics natural head rotation, was applied together with calcium imaging on back-filled central vestibular neurons, glutamate and GABA uncaging at different sites of the intact vestibular network. The combination of all these techniques made it possible to understand previously unknown features of these sensory-motor computations and confirmed neuronal properties found in other vertebrates.

The sensory activation of central vestibular neurons can be modulated via different GABAergic inhibitory pathways (i.e. local feed-forward circuits, brainstem commissural pathways and cerebellar Purkinje cells) with the functional consequence of controlling the bilateral sensitivity for angular head acceleration and the gain of the vestibular ocular reflex (Shimazu and Precht, 1966; Magherini et al., 1975; Minor and Goldberg, 1991; Straka and Dieringer, 2000; Malinvaud et al., 2010). Bath or systemic application of GABA antagonists has been traditionally used to estimate the importance of the different inhibitory circuits. In contrast, the present study demonstrated the potent effect of local GABA release in shunting sensory inputs to central vestibular neurons.

Due to the possibility to limit the uncaging of excitatory and inhibitory neurotransmitters (glutamate and GABA) to different distances (up to 40 µm) from central vestibular neuron

somata, this part of the thesis revealed the prevalent somatic localization of both neurotransmitter receptors; as it was already proposed for adult frogs (Dieringer and Precht, 1979; Straka et al., 2005).

2. Manuscripts enclosed

- **Analysis of signal processing in vestibular circuits with novel a light-emitting diodes-based fluorescence microscope.**
- In this manuscript the technical novelties of the developed microscope were combined with the accessibility of the axolotl *in-vitro* preparation to understand basic computational principles of the vestibular system.
- **Locomotor corollary activation of trigeminal motor neurons: coupling of discrete motor behaviors.**
- In this study a locomotor CD is described. This intrinsic signal drives the retraction of the touch appendages (i.e. tentacles) of *Xenopus* larvae, potentially reducing the hydrodynamic drag and preventing overstimulation of the touch organs during swimming.
- **Spinal corollary discharge modulates motion detection during vertebrate locomotion.**
- In this enclosed manuscript a mixture of electrophysiological, anatomical, ablation and imaging techniques were applied to the *Xenopus in-vitro* preparation to identify and show the functional relevance of a locomotor CD acting on the vestibular and lateral line system.

Analysis of signal processing in vestibular circuits with a novel light-emitting diodes-based fluorescence microscope

Stephan Direnberger, **Roberto Banchi**, Sonja Brosel Christian Seebacher, Stefan Laimgruber, Rainer Uhl, Felix Felmy, Hans Straka, Lars Kunz

Eur J Neurosci 41:1332–1344

S.D. and **R.B**. contributed equally to this work

Contributions of R.B

- Establishment of the novel axolotl semi-intact *in-vitro* preparation.
- Morphological characterization and allocation of brainstem vestibular circuitries.
- Multicolor back-filling of brainstem sub-neuronal populations to demonstrate the advantages of the novel fluorescent microscope (i.e. multicolor imaging of spatially independently adjustable field of views, Fig. 2).
- Back filling techniques and preparations for calcium imaging experiments.
- Differential calcium responses in identified central vestibular neurons located at different distances from the glutamate uncaging site (Fig. 4).
- Application of Galvanic Vestibular Stimulation (GVS) and related characterization of the physiological responses specificity in identified central vestibular neurons by means of calcium imaging techniques (Fig. 5).
- Writing and revising, together with all other authors.

EJN European Journal of Neuroscience

FENS Federation of European Neuroscience Societies

European Journal of Neuroscience, Vol. 41, pp. 1332–1344, 2015 doi:10.1111/ejn.12907

NEUROSYSTEMS

Analysis of signal processing in vestibular circuits with a novel light-emitting diodes-based fluorescence microscope

Stephan Direnberger,[1,*] Roberto Banchi,[1,2,*] Sonja Brosel,[1] Christian Seebacher,[3] Stefan Laimgruber,[3] Rainer Uhl,[3] Felix Felmy,[1,3,†] Hans Straka[1,†] and Lars Kunz[1,†]

[1]Department Biology II, Division of Neurobiology, Ludwig-Maximilians University Munich, Grosshaderner Str. 2, Planegg-Martinsried 82152, Germany

[2]Graduate School of Systemic Neurosciences, Ludwig-Maximilians University Munich, Planegg-Martinsried, Germany

[3]Department Biology I, BioImaging Center, Ludwig-Maximilians University Munich, Planegg-Martinsried, Germany

Keywords: *Ambystoma mexicanum*, axolotl, calcium imaging, galvanic stimulation, photo-uncaging, semicircular canal

Abstract

Optical visualization of neural network activity is limited by imaging system-dependent technical tradeoffs. To overcome these constraints, we have developed a powerful low-cost and flexible imaging system with high spectral variability and unique spatio-temporal precision for simultaneous optical recording and manipulation of neural activity of large cell groups. The system comprises eight high-power light-emitting diodes, a camera with a large metal-oxide-semiconductor sensor and a high numerical aperture water-dipping objective. It allows fast and precise control of excitation and simultaneous low noise imaging at high resolution. Adjustable apertures generated two independent areas of variable size and position for simultaneous optical activation and image capture. The experimental applicability of this system was explored in semi-isolated preparations of larval axolotl (*Ambystoma mexicanum*) with intact inner ear organs and central nervous circuits. Cyclic galvanic stimulation of semicircular canals together with glutamate- and γ-aminobutyric acid (GABA)-uncaging caused a corresponding modulation of Ca^{2+} transients in central vestibular neurons. These experiments revealed specific cellular properties as well as synaptic interactions between excitatory and inhibitory inputs, responsible for spatio-temporal-specific sensory signal processing. Location-specific GABA-uncaging revealed a potent inhibitory shunt of vestibular nerve afferent input in the predominating population of tonic vestibular neurons, indicating a considerable impact of local and commissural inhibitory circuits on the processing of head/body motion-related signals. The discovery of these previously unknown properties of vestibular computations demonstrates the merits of our novel microscope system for experimental applications in the field of neurobiology.

Introduction

Signal processing in the CNS depends on the computational capacity of individual neurons as well as the emerging properties of the specific neuronal circuitry. Classical electrode recordings allow simultaneous capturing of the discharge of only one or a few neurons (Sullivan *et al.*, 2005), and thus have a limited applicability for analysing the simultaneous activity of multiple network components. Optical imaging techniques using Ca^{2+} sensors or voltage-sensitive dyes provide a solution for the visualization of neuronal activity of larger networks (Regehr *et al.*, 1989; Yuste & Katz, 1991; Fetcho & O'Malley, 1995; Stosiek *et al.*, 2003; Cossart *et al.*, 2005; Direnberger *et al.*, 2012; Grienberger & Konnerth, 2012). The ideal microscope setup for improved optical circuit analysis would therefore combine image acquisition with high temporal acuity and speed with a spatially and temporally tightly controlled light source for a great spectral excitation/absorption range. This is necessary to attain a high flexibility for the use of different fluorescent dyes and indicators, and for combining and synchronizing various imaging approaches. On the other hand, resolving network activity requires simultaneous, but independent light activation of multiple interconnected neuronal sites. In addition, maximum information would be available by employing large fields of view (FOVs) with high spatial resolution.

Current imaging systems can be configured to fulfill any of the aforementioned requirements, but not at the same time. Wide-field epifluorescence microscopes equipped with xenon or mercury arc lamps cover a broad spectral range, but filter-sliders or -wheels for switching between illumination wavelengths impair fast multi-color applications. Single-/multi-photon laser-scanning microscopes, on the other hand, lack acquisition speed at high spatial resolution (Grewe *et al.*, 2010), and the upgrade to multi-color systems requires the installation of several expensive laser lines (Piston, 1999; Combes *et al.*, 2008). Finally, all current imaging systems

Correspondence: Dr L. Kunz, as above.
E-mail: Lars.Kunz@bio.lmu.de

*S.D. and R.B. contributed equally to this work.
†F.F., H.S. and L.K. contributed equally to this work.

Received 14 November 2014, accepted 30 March 2015

lack the possibility to employ multiple, spatially separable and independently adjustable FOVs.

In the current study, we have implemented and experimentally tested a novel imaging system with multiple light-emitting diodes (LEDs), and with variable areas for fast optical excitation and image capture. The technical capacity and experimental applicability was evaluated in semi-isolated *in vitro* preparations of larval axolotl (*Ambystoma mexicanum*) with morpho-physiologically preserved inner ear sensory organs, and interconnected and optically accessible neural circuits that allowed simultaneous imaging of neuronal activity in multiple network elements. The optical access to all levels of a functionally intact vertebrate brain with the novel LED-based microscope facilitated optochemical manipulations and imaging of neuronal processing in identified vestibular networks (Straka & Dieringer, 2004), thereby revealing previously unknown aspects of sensory-motor computations.

Materials and methods

Animals

Experiments were performed on semi-isolated *in vitro* preparations of axolotl (*Ambystoma mexicanum*) larvae (developmental stages 48–54; Nye *et al.*, 2003), and complied with the Principles of Animal Care (Publication 86-23, revised 1985 by the National Institute of Health) and the German law for animal protection (Tierschutzgesetz). Permission for the *in vitro* experiments was granted by the Regierung von Oberbayern (55.2-1-54-2531.3-18-10; 55.2-1-54-2532.3-59-12). All animals were obtained from the in-house breeding facility at the Biocenter Martinsried of the Ludwig-Maximilians University Munich. The experiment using the brain of a Mongolian gerbil (*Meriones unguiculatus*) was carried out in accordance with institutional guidelines, with State (Bavarian) and German Federal laws, and with the European Communities Council Directive of 24 November 1986 (86/609/EEC). The Regierung von Oberbayern approved this experiment (55.2-1-54-2531-105-10).

Preparations

Axolotl were deeply anesthetized in 0.05% 3-aminobenzoic acid ethyl ester (MS-222; Sigma-Aldrich, Germany) dissolved in ice-cold frog Ringer's solution with a low Ca^{2+} concentration (in mM: NaCl, 75; $NaHCO_3$, 25; $CaCl_2$, 1; KCl, 2; $MgCl_2$, 2; glucose, 11; pH 7.4) and decapitated at the level of the rostral spinal cord as described in detail for *Xenopus laevis* tadpoles (Ramlochansingh *et al.*, 2014). This procedure preserved the dorsal part of the skull, including inner ear organs along with the brain and the first spinal segments. The skin covering the head was removed, the mostly cartilaginous tissue of the dorsal skull was opened, the forebrain disconnected and the optical nerves transected at the entrance into the brain to eliminate visual inputs. For the subsequent opto- and electrophysiological recordings, isolated preparations were rinsed in fresh Ringer's solution, firmly secured with insect pins to the Sylgard floor of a Petri dish, which was mounted onto the stage of the microscope. Preparations were continuously superfused at a rate of 1.3–2.1 mL/min with an oxygenated Ringer's solution (see above) that now contained an elevated Ca^{2+} concentration of 2 mM $CaCl_2$. During the experiments, the temperature of the bath solution was electronically controlled and maintained at 17.0 ± 0.2 °C. Preparations were used for experimentation up to 4 days after their isolation without any noticeable functional deterioration, and were stored overnight at 10–12 °C in oxygenated Ringer's solution (carbogen: 95% O_2, 5% CO_2; pH 7.5) as previously described for comparable semi-isolated preparations of larval and adult *Xenopus laevis* frogs (Straka & Simmers, 2012).

Identification of vestibular projection neurons

In part of the experiments, particular functional subgroups of central vestibular projection neurons were identified prior to the physiological recordings by retrograde labeling from their axonal target sites with dextran-conjugated fluorescent tracers. The tracing procedure was performed immediately after the isolation of the preparation as described for tadpoles of ranid frogs (Straka *et al.*, 2001) and *Xenopus laevis* (Lambert *et al.*, 2013). Crystals of Alexa Fluor® 488 or 594 dextran (MW 10 000; Life Technologies GmbH, Darmstadt, Germany) were melted onto the tip of an injection needle and inserted for 5 s into the rostral spinal cord or the vestibular nuclei on one side after temporary removal of the Ringer's solution from the Petri dish, in which the preparation was mechanically secured. After rinsing in fresh Ringer's solution, preparations were stored at 12 °C overnight in oxygenated Ringer's solution for retrograde transport of the tracer and complete backfilling of the cell bodies, thereby identifying hindbrain segment-specific populations of vestibulo-spinal and brainstem commissural vestibular neurons.

Electrical stimulation of vestibular end-organs

The sensory epithelium of the horizontal semicircular canal within the otic capsule of the semi-isolated preparation was electrically stimulated with a pair of Teflon®-coated silver wires (0.03″ coated; AG 25-T; Science Products, Hofheim, Germany). For specific epithelial stimulation, one of the two electrodes was placed outside the macroscopically visible ampulla of the horizontal semicircular canal, while the second electrode was located at a distance of ~2 mm from the preparation in the bath chamber. The stimuli consisted of sinusoidally modulated currents at a frequency of 0.2 Hz and amplitudes of ± 25–100 μA, and were produced by a linear stimulus waveform generator (STG4002; Multi Channel Systems, Reutlingen, Germany). This electrical stimulus modulates the spontaneous discharge in vestibular nerve afferent fibers and causes a corresponding modulation of the activity in the postsynaptic central vestibular neurons (Kaufmann *et al.*, 2013). The modulated activity in the latter neurons was optically recorded in the current study as Ca^{2+} transients following extracellular bolus or bulk loading of central vestibular neurons with synthetic Ca^{2+} dyes (see below).

Microscope specification and image acquisition control

The novel microscope for fluorescence imaging was based on a platform as shown in Fig. $1A_1$. Its conceptual innovation depended on eight high-power LEDs with seven different excitation wavelengths (Table 1; irradiance: 20–80 mW/mm^2), which were housed in two multi-LED combiners (Fig. $1A_2$). Within each LED combiner, the beam lines of individual LEDs were combined using suitable dichroic mirrors (Fig. $1A_2$), each producing its own FOV. The optical path can be seen in Fig. 1C, and more information can be found in the corresponding Zemax file (ray_trace.zmx) as Supporting Information. Exposure time and switching frequency of all LEDs were individually triggered by TTL pulses. The light intensity of each LED was independently and gradually adjustable from 10% to 100% via analog command signals. Both digital and analog commands were controlled by PatchMaster software, and produced by an EPC10 amplifier that was also used for the electrophysiological recordings. Beam-homogenizers, installed downstream of each LED

combiner, homogenized the LED light before merging the output of the two light sources with a 50 : 50 beam-splitter (Fig. 1A$_2$). The resulting excitation beam line was projected onto a 20 ×/1.0 W Plan-Apochromat water-dipping objective with the tube lens 425308 (Fig. 1A$_3$; Carl Zeiss Microscopy, Göttingen, Germany). A filter-slider, holding six slots for fluorescence filter-sets (triple-band filter-set used in this study: excitation: 390/482/587; dichroic: 395/495/610; emission: 425/527/685; AHF Analysentechnik AG, Tübingen, Germany), directed the emitted light onto a camera with metal-oxide-semiconductor sensor pco.edge 5.5 (PCO AG, Kehlheim, Germany). This arrangement allowed the production of rectangular FOVs at individual positions and with adjustable extensions (from 40 × 40 μm to 800 × 680 μm) through rectangular-shaped apertures, inserted immediately after the beam-homogenizer at the outlet of each LED combiner (Fig. 1A$_3$). The maximal size corresponds almost to the size of the entire visual field of 832 × 702 μm (2560 × 2160 pixels). The optical ray tracing is depicted in Fig. 1A$_4$, and the corresponding Zemax file is provided as Supporting Information (ray_trace.zmx). Filter-slider and objective *z*-motion were controlled by a custom-made program using LabVIEW 8.0 (National Instruments, Austin, TX, USA). For bright-field visualization of the relatively thick preparation in the current study, an oblique far-red LED illumination with a 850-nm LED, mounted on the microscope stage at an incidence angle of 20–30°, was used to facilitate identification of cellular elements (Szűcs *et al.*, 2009; Fig. 1B).

Determination of optical resolution

Fluoro-Max Green Aqueous Fluorescent Particles with a diameter of 51 nm (G50; Thermo Fisher Scientific, Braunschweig, Germany) were imaged as non-biological samples to obtain the point spread function and resolution of the system. A microsphere suspension was embedded in Norland optical adhesive (NOA) 63 (Norland Products, Cranbury, NJ, USA) and the adhesive UV-cured. Microsphere fluorescence was imaged using excitation at 470 nm. Images were taken for various *z*-positions at 1-μm intervals.

For evaluating the resolution in the mammalian brain, hippocampal slices of the Mongolian gerbil (*Meriones unguiculatus*) were imaged. Therefore, an animal was anesthetized using isoflurane, followed by 2 mg/kg body weight pentobarbital (Narcoren®; Merial GmbH, Halbergmoos, Germany; intraperitoneal). After reaching deep anesthesia as marked by complete loss of flexor reflexes at all limbs, the animal was perfused with Ringer's solution supplemented with 0.1% heparin (Meditech Vertriebs GmbH, Parchim, Germany) at a flow rate of 4 mL/min for 10 min followed by 4% paraformaldehyde solution for 20 min (Trattner *et al.*, 2013). Brains were then post-fixed for 2 h in 4% paraformaldehyde at room temperature. Using a Leica VT1200S vibratome (Leica Mikrosysteme Vertrieb GmbH, Wetzlar, Germany), 50-μm sections of the cortical area of the cerebrum containing the hippocampus were collected. The slices were stained with an antibody against the Ca^{2+}-binding protein parvalbumin (1 : 1000, PV25; Swant, Marly, Switzerland; Felmy & Schneggenburger, 2004; Ammer *et al.*, 2012), and a donkey anti-mouse IgG (H+L) secondary antibody linked to Alexa Fluor® 488 (1 : 300, A21202; Life Technologies) was used for visualization. The slices were mounted with Vectashield (Vector Laboratories, Burlingame, CA, USA) and neurons imaged with excitation at 470 nm with maximum intensity.

Neurons in the axolotl whole-mount preparation were retrogradely labeled with Alexa Fluor® 488 dextran (10 000 MW; D-22910; Life Technologies). Following incubation in oxygenated Ringer's solution at 14 °C for 24–48 h, preparations were fixed in 4% paraformaldehyde [in 0.1 M phosphate-buffered saline (PBS), pH 7.4] at 10 °C for 5–6 h and rinsed in cold 0.1 M PBS (pH 7.4). The brainstem was removed, cleaned of surrounding tissue, and mounted on slides using Vectashield (Vector Laboratories). Images were acquired with the 470-nm LED at an intensity of 1.5 V.

The intensity distribution of the fluorescence signal was analysed across the structures of interest using ImageJ (imagej.nih.gov/ij/). Intensity data were fitted with a Gaussian distribution (Origin®; OriginLab Corporation, Northampton, MA, USA) and the full width at half maximum (FWHM) was obtained. For fluorescent microspheres, the point spread function was determined.

Loading of vestibular neurons with synthetic Ca^{2+} dyes

Ca^{2+} transients in central vestibular neurons were measured following labeling of the cells with membrane-permeable acetoxymethyl ester dyes (AM-dyes; Tsien, 1981). To facilitate dye penetration, preparations were incubated with 1–2 μL of a 0.025% trypsin solution at 37 °C for 3–5 min. Subsequently, the hindbrain was rinsed twice with 2–3 mL Ringer's solution to remove any residual enzyme. After repeating this procedure, the ventricular surface above the hindbrain recording area was cleaned from remaining debris by gently blowing Ringer's solution along the IVth ventricle. For bulk loading of the target neurons, Oregon Green BAPTA-1AM (OGB-1AM; Life Technologies GmbH) was freshly dissolved in dimethylsulfoxide (DMSO) to yield a concentration of 10 μM. After adding Ringer's solution with 2% Pluronic 127 (Sigma Aldrich, St Louis, MO, USA) to the OGB-1AM solution to facilitate cellular dye uptake, a final concentration of 25 nM OGB-1AM was obtained. Immediately prior to the recording experiments, isolated preparations were incubated in OGB-1AM solution for 30–45 min at 17 °C followed by a 30-min washout with Ringer's solution. Targeted bolus injections of OGB-1AM into the vestibular nuclei at the level of the

Table 1. Characteristics of LEDs

Combiner	LED type	Denomination/ nm	Maximum/ nm	FWHM/ nm
1	Nichia NCSU033A	370	369.5	18.9
	Osa Opto Light OCU-440 UE400	405	398.2	23.5
	Osram LB W5AM-GYHY-25-Z	470	463.5	30.5
	Osram LY W5AM-HYJZ-36-Z	590	592.2	22.0
2	Osram LB W5AM-GYHY-25-Z	470	462.9	27.2
	Osram LV W5AM-JYKY-25-Z	505	500.5	28.7
	Osram LT CP7P-JYKZ-26	530	533.9	35.1
	Osram LR W5AM-HZJZ-1-Z	630	631.5	23.7

Properties were measured at a current of 500 mA (potential current range: 100–950 mA). LEDs by Nichia, Tokushima, Japan; Osa Opto Light GmbH, Berlin, Germany; Osram Opto Semiconductors, Munich, Germany. FWHM, full width at half maximum; LED, light-emitting diode.

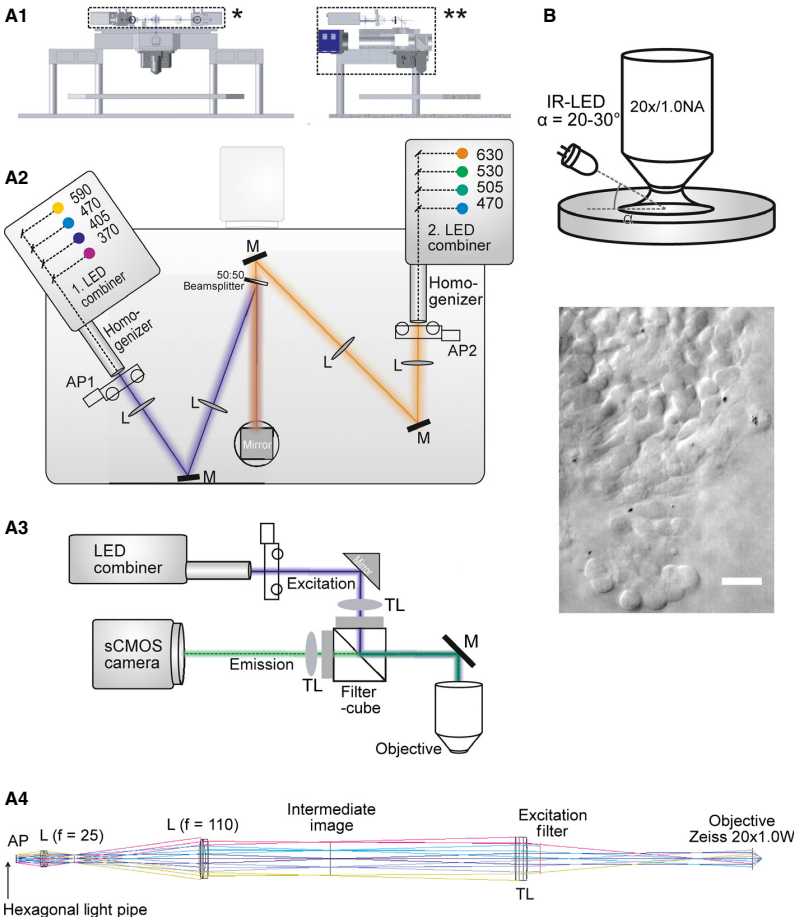

FIG. 1. Operating principle of the novel microscope. (A) Schematic frontal and lateral view of the microscope (A_1); dotted rectangles refer to schematic views of the optical components from top (*, A_2) and side (**, A_3). Blue and orange beam lines in (A_2) illustrate the excitation paths of the two LED combiners (LED wavelengths in nm are indicated). The green line in (A_3) indicates the emission path. AP, aperture; L, lens; M, mirror; TL, tube lens. (A_4) Optical path of the microscope. The corresponding Zemax file is provided as Supporting Information. (B) Illustration of the oblique bright-field illumination with an IR-LED (top) and corresponding bright-field image of a hindbrain region in the semi-isolated preparation of larval axolotl (bottom, scale bar: 30 μm).

entrance of the VIIIth nerve into the brainstem were made according to a previously described protocol (Brustein *et al.*, 2003). In brief, stock solutions of 10 μM OGB-1AM in DMSO containing 20% Pluronic 127 were diluted 1 : 10 with Ringer's solution, filtered through a syringe (0.2 μm pore size, Nalgene Syringe filter; Thermo Scientific, Waltham, MA, USA) and pressure-injected through a borosilicate glass pipette into the target area. Following injections, preparations were maintained for 30–45 min at 17 °C in a constantly Ringer's-superfused bath chamber. For Ca^{2+} imaging with Calcium Green, neurons were retrogradely labeled 24–48 h prior to the experiment by inserting crystals of Calcium Green™-1 dextran (melted to the tip of an injection needle) at several rostrocaudal positions of the contralateral vestibular nucleus (Straka *et al.*, 2001).

Ca^{2+} imaging of neuronal activity

Ca^{2+} transients in central vestibular neurons were optically recorded using OGB-1AM. Camera image acquisition and LED excitation were controlled by external TTL trigger pulses, and synchronized using PatchMaster software (see above). All experiments were conducted at a 5-Hz image capture frame rate, and a camera acquisition and light exposure time of 50 ms. Data processing and quantitative analyses of Ca^{2+} responses were performed by custom-made macros using ImageJ and respective available plug-ins (Schneider *et al.*, 2012). Graphical illustrations were made with Igor Pro 6.32A (WaveMetrics, Lake Oswego, OR, USA).

Glutamate (Glu)-/γ-aminobutyric acid (GABA)-uncaging experiments

MNI (4-methoxy-7-nitroindolinyl)-caged Glu (Tocris Bioscience, Bristol, UK) or CNB (carboxy-2-nitrobenzyl ester)-caged GABA (Life Technologies GmbH) were bath-applied at a final concentration of 250 and 500 μM, respectively, 20 min prior to the experiments. UV light uncaging was performed using a 370-nm LED with maximum light intensity (irradiance: 80 mW/mm^2) at various pulse lengths and switching cycles. MNI-caged Glu was activated by short, single pulses with a duration of 10–100 ms. CNB-caged

GABA was activated either by single long pulses (1–3 s) or by trains of short single pulses (10–100 ms) at 5 Hz for 15 s. To limit UV-induced transmitter activation to specific sites and spatial extensions, the FOV, i.e. the area of activation, was defined by a manual adjustment of the aperture. Uncaging trials were repeated after 1 min of recovery, allowing residual transmitter to diffuse out of the zone of activation.

Whole-cell patch-clamp recordings

Retrogradely labeled vestibular projection neurons as well as unlabeled neurons in close proximity to the latter were approached with patch electrodes fabricated from borosilicate glass pipettes (3–6 MΩ) and filled with internal recording solution (in mM): K-gluconate, 145; KCl, 5; HEPES, 15; Mg-ATP, 2; K-ATP, 2; Na_2-GTP, 0.3; Na_2-phosphocreatine, 7.5; and K-EGTA, 5 (pH 7.2). Current-clamp recordings were carried out with an EPC10/2 amplifier (HEKA Elektronik, Lambrecht, Germany). Data were filtered at 3 kHz and digitized at 20 kHz, and stored on computer for off-line analysis. Neuronal firing patterns were characterized by intracellular injections of short (5 ms) or long (600 ms) current steps at increasing intensity using the PatchMaster software (HEKA Elektronik).

Statistics

All results were expressed as means ± standard deviation (SD) unless stated otherwise. Statistical differences in response parameters were calculated using the Mann–Whitney *U*-test (unpaired parameters; GraphPad Prism version 6.00) or the Wilcoxon signed-rank non-parametric test (paired parameters; Igor Pro 6.32A).

Results

Optical resolution of the novel microscope

The resolution of the microscope was evaluated utilizing fluorescent microspheres (Fig. 2A), as well as two different biological preparations, mammalian hippocampus slices (Fig. 2B) and whole-mounts of axolotl brain (data not shown). Images of fluorescent microspheres were taken for different *z*-positions (1 μm intervals; Fig. 2A). The point spread function in the three spatial directions was fitted with a Gaussian distribution (Fig. $2A_1$ and A_2). Altogether, 58 microspheres were analysed, and FWHM = 1.2 ± 0.2 μm was obtained in the *xy*-plane and FWHM = 7.0 ± 1.0 μm in the *z*-direction. Values for FWHM exhibited no dependence on position in the FOV (data not shown).

In order to determine the optical resolution in mammalian brain slices, we have analysed hippocampal neurons labeled with an antibody against parvalbumin (Felmy & Schneggenburger, 2004; Ammer *et al.*, 2012) and a fluorescent secondary antibody (Fig. 2B). The image showed a large-intensity dynamic and a resolution close to that obtained with sub-resolution microspheres (Fig. 1A). The optical resolution was dependent on the overall intensity in the analysed image region. The optimal FWHM had a value of 0.8 ± 0.1 μm in a region with low overall intensity (Fig. $2B_2$). In brighter areas, the value was higher (FWHM = 1.8 ± 0.1 μm; Fig. $2B_3$), most likely due to a not sub-diffraction size of the structures.

The optical resolution was also evaluated in thicker brain samples of the axolotl as used in all other experiments. The tissue was 260 μm thick and neurons had been retrogradely labeled with a fluorescent dye (Alexa Fluor® 488 dextran) similar to the experiments presented below. In these thick samples, a FWHM = 2.4 ± 0.2 μm was still obtained, but the resolution might be even better.

Implementation of independent optical fields of interest

The working range and experimental applicability of our custom-build microscope and imaging system was evaluated by testing functional aspects of sensory-motor signal processing in axolotl central vestibular neurons located in the alar plate of the brainstem. The first step was to explore the possible range of different spatial arrangements of dual FOVs as a major technical advancement of this imaging system. The high degree of freedom introduced by the epifluorescence aperture system allowed to generate two independent FOVs that were either spatially overlapping or completely separated (see green and red rectangles in Fig. 2C, top row). The optical consequence of adjustable areas that contained various fluorescent neuronal elements in different colors is illustrated by differential optical appearance of distinct populations of ipsilateral- (green) and contralateral-projecting (red) vestibulo-spinal neurons (Fig. 2C). The independent adjustment of position and size of the multiple FOVs made it possible to activate neurons within one brain region, and to record responses in interconnected postsynaptic neurons located in the same or a topographically remote area. The flexibility in defining particular regions of interest allowed a sampling of neuronal activity at frame rates up to 100 Hz at maximum spatial resolution (2560 × 2160 pixel), and up to 900 Hz at a lower spatial resolution (320 × 240 pixel). The following opto-physiological experiments took predominantly advantage of the high spatial resolution of our imaging system.

Light-activated neuronal responses in central vestibular neurons of larval axolotl

To elucidate the technical advancement of the microscope, action potential generation in vestibular neurons was studied by a basal electrophysiological characterization of these neurons in semi-isolated axolotl preparation (Fig. $3A_{1,2}$). Stable whole-cell current-clamp recordings of the cell bodies for periods of 25–40 min were conducted on the two types of vestibular projection neurons ($n = 4$) as well as on unlabeled neurons ($n = 6$), intermingled with the identified vestibular projection neurons. The membrane potential of the vestibular neurons was clamped at the measured resting membrane potential (−55 to −60 mV). Repetitively applied current steps of constantly varying amplitude from −20 to +30 pA were used to determine action potential thresholds and firing patterns (Fig. 3B). Two neurons responded with a short, initial burst of one-three spikes at the onset of the depolarization. In eight neurons, the response consisted of repetitively generated action potentials throughout the depolarizing current step, as illustrated in Fig. 3B. The distinction into two subtypes is reminiscent of phasic and tonic vestibular neurons described in adult frogs, suggesting that axolotl central vestibular neurons also subdivide into two major functional subpopulations with firing patterns that match the general concept of frequency-tuned signaling pathways in the vertebrate vestibular system (Straka *et al.*, 2009).

Following characterization of the firing patterns of individual vestibular neurons, the opto-physiological setup was challenged with a Glu-uncaging experiment. MNI-caged Glu (MNI-Glu) was bath-applied at a final concentration of 250 μM. Uncaging experiments were limited to 45 min, as an overall, concomitant increase of excitability within the preparation, most likely because of accumulation

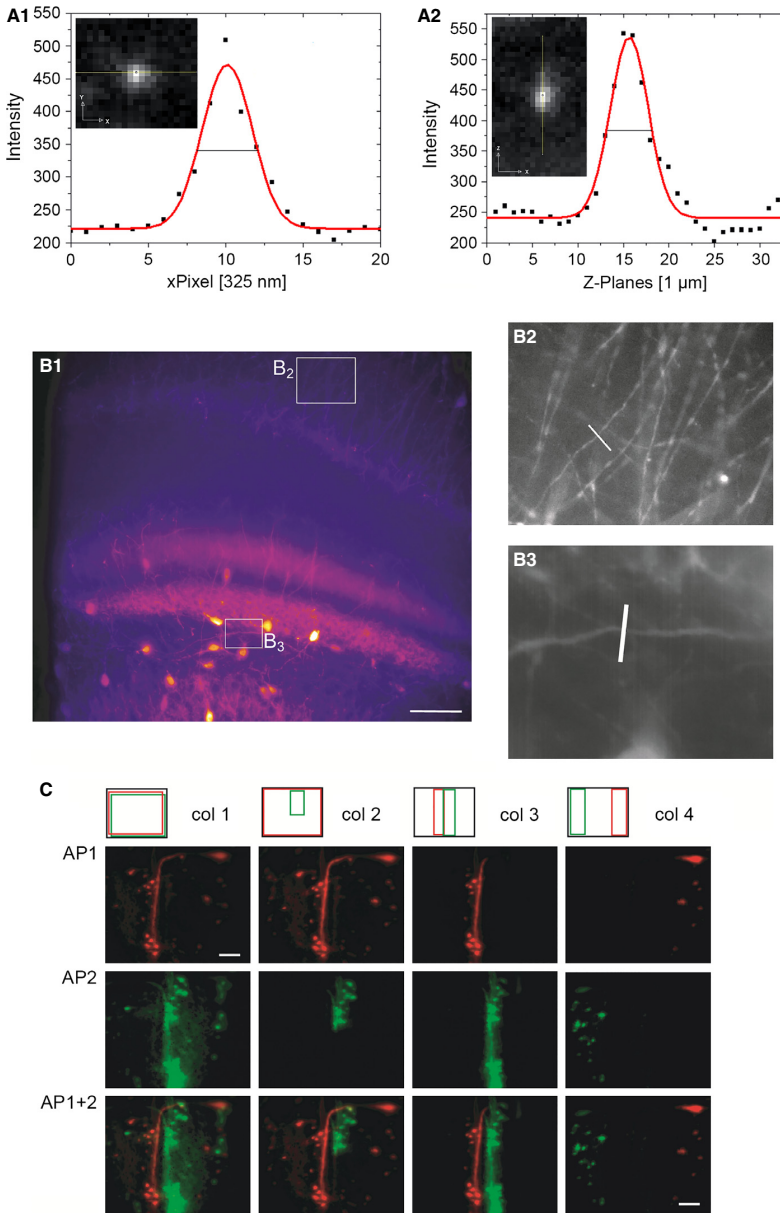

FIG. 2. Spatial features of the novel microscope. (A) Fluorescence intensity distribution and image (insets) of a typical microsphere in the *xy*-plane (A_1) and *z*-direction (A_2). Intensities were fitted with a Gaussian distribution (red line), and yielded FWHM values of 1.2 ± 0.1 µm in the *x*-direction and 4.9 ± 0.3 µm in the *z*-direction. (B) Fluorescence imaging of neurons in the rodent hippocampus (50-µm sections) labeled by means of an antibody against parvalbumin. An image stack in the *z*-direction was taken with 15 frames at 1-µm intervals (excitation at 470 nm; size: 832 × 702 µm; 0.325 µm per pixel). (B_1) Maximum projection of the image stack (scale bar: 100 µm). (B_2 and B_3) Magnification of the two marked regions in (B_1). Along the white lines, the intensity distribution had been analysed and fitted yielding FWHM = 0.8 ± 0.1 µm (B_2) and FWHM = 1.8 ± 0.1 µm (B_3), respectively. (C) Images show different aperture combinations [columns (col) 1–4; black rectangle, full FOV; red rectangle, aperture (AP) 1; green rectangle, aperture 2]. The consequences of applying different apertures are illustrated by the differential appearance of the two retrogradely labeled populations of ipsi- (green, Alexa Fluor® 488 dextran) and contralateral (red, Alexa Fluor® 594 dextran) spinal-projecting hindbrain neurons within the optical field; scale bar: 100 µm.

of uncaged Glu, was apparent. For UV activation of MNI-caged Glu, a FOV with a size of 150 × 150 µm centered on the recorded cell was generated. Sequentially applied UV light pulses of increasing duration (10–100 ms), separated by a recovery period of 1 min to allow the diffusion of released Glu, were used to evoke Glu-triggered neuronal responses (Fig. $3C_{1,2}$). The efficacy of action potential activation by Glu-uncaging was determined by quantifying the probability of triggering action potentials by UV pulses of different

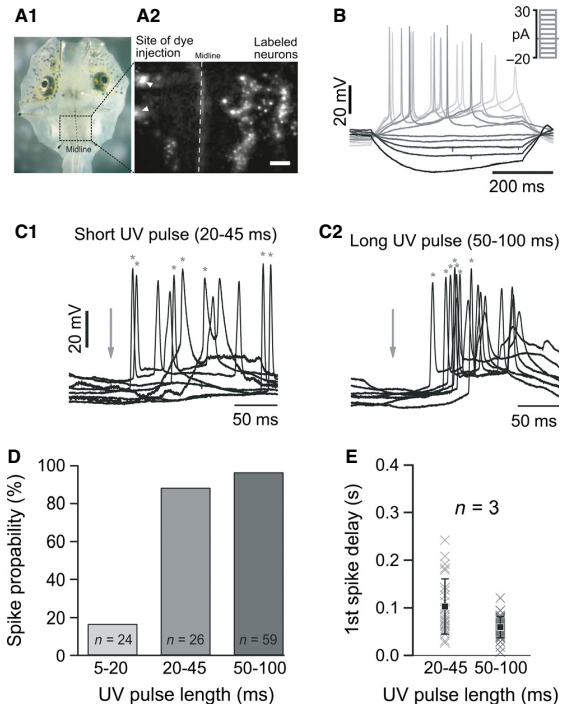

FIG. 3. Isolated preparations of larval axolotl for combined whole-cell recordings and UV light activation of MNI-caged Glu. (A) Photomicrograph depicting a semi-isolated preparation of a larval axolotl (A_1) with a dorsal view of the hindbrain ventricular surface (A_2); injection of fluorescent tracer into the left vestibular nuclei retrogradely labeled commissural neurons on the right side. (B) Patch recording of a tonic central vestibular neuron in current-clamp configuration; overlay of responses to a series of hyper- and depolarizing current steps (600 ms) from −20 to +30 pA (top right). (C) Superimposed single sweeps of evoked action potentials in a central vestibular neuron following uncaging of MNI-caged Glu with short (20–45 ms; C_1) and long UV pulses (50–100 ms; C_2); gray arrows indicate UV pulse onset; asterisks indicate the timing of the first light-evoked spike in each single sweep. (D) Dependency of spike probability on the duration of UV pulses (n = numbers of analysed single sweeps). (E) Onset latency of the first spike evoked by Glu-uncaging with short (20–45 ms) or long (50–100 ms) UV pulses.

duration (Fig. $3C_{1,2}$). UV pulses of 5–20 ms duration elicited Glu-evoked spike activity in < 20% of the 24 trials (n = 3; Fig. 3D). UV pulses of 20–45 ms duration provoked a spike discharge in almost 90% of the 26 trials (n = 3; Fig. $3C_1$ and D), while UV pulses of even longer duration (50–100 ms) evoked spikes in almost all 59 trials (n = 3; Fig. $3C_2$ and D).

The clear dependency of action potential probability on the duration of the Glu-uncaging pulse was matched by a corresponding dependency of the latency of the first action potential with the length of the uncaging pulse. The average latency of the first action potential (~100 ms) decreased significantly to ~60 ms (Wilcoxon signed-rank test; $P < 0.01$; n = 3 cells, 73 trials) with increasing UV pulse length (Fig. 3E). Moreover, the observed jitter of the first action potential (Fig. $3C_{1,2}$) indicated by the standard deviation of the latency concomitantly decreased with increasing uncaging pulse length (Fig. 3E). The significant reduction in latency of the first action potential along with the increasing reliability of action potential generation with increasing UV pulse duration gave a convenient estimate of basic parameters for reliable neuronal activation within the specific experimental setting using the implemented technical arrangement. In addition, the outcome of this set of experiments indicated that LED light activation of neuronal activity through adjustable single FOVs could be effectively combined with single-cell electrophysiology.

Light-activated Ca^{2+} transients in central vestibular neurons

The applicability of two separate and independently controllable FOVs for simultaneous optical triggering and recording of neuronal activity was experimentally tested by bath application of MNI-Glu (250 μM) to neurons that had been either bulk-loaded with OGB-1AM or retrogradely labeled with Calcium Green™-1 dextran. Glu-uncaging by UV light (LED 370 nm) within a large FOV (200 × 200 μm) was combined with the imaging of Ca^{2+} transients of central vestibular neurons (LED 470 nm) within different size-adjusted FOVs. Technically, this was achieved by defining LED combiner 1 with aperture 1 as UV activation channel (ChUV) for Glu-uncaging, and LED-combiner 2 with aperture 2 as the channel for optical recordings of Ca^{2+} responses (ChCa; Fig. $1A_{1,2}$). In the first set of experiments, Ca^{2+} transients of commissural vestibular neurons located in close proximity to the hindbrain ventricular surface were recorded within a large FOV that had the same size and position as the FOV used for Glu-uncaging (Fig. $4A_{1,2}$ and B).

MNI-Glu-uncaging elicited Ca^{2+} transients of a $\Delta F/F$ of 2–8% in optically recorded vestibular neurons (Fig. $4A_{1,2}$ and B). The magnitude of these responses depended on UV pulse duration as indicated by the increase in the average Ca^{2+} transient from 3.8% to 6.7% $\Delta F/F$, when the UV pulse length was augmented from 2.5 to 100 ms (Fig. 4E). In order to explore the spatial limitations of UV light activation, the size of the FOV for MNI-Glu-uncaging was gradually decreased to a region of ~50 × 50 μm (Fig. 4C). Comparison of the evoked Ca^{2+} responses during MNI-Glu-uncaging in large (Fig. 4B) and small fields (Fig. 4D and E) indicated very similar magnitudes independent of the size of the optically activated area. Ca^{2+} transients were consistently evoked if the neuron was located inside or at least in close proximity to the UV light-activated area, but not if the neuron was located at more remote positions (> 100 μm; Fig. 4D).

Sensory stimulus-evoked Ca^{2+} transients in central vestibular neurons

The major synaptic input to vertebrate central vestibular neurons originates from ipsilateral semicircular canal and otolith organs (Straka & Dieringer, 2004). Hair cells in these inner ear organs detect and transduce head/body motion into voltage signals, which are mediated as modulated spike trains by vestibular nerve afferent fibers onto central vestibular neurons in the hindbrain. In the current study on semi-isolated preparations, natural head rotations were experimentally simulated by galvanic vestibular stimulation (Fig. 5A) that allows a semicircular canal-specific electrical activation of hair cells/afferent fibers (Kaufmann *et al.*, 2013). Accordingly, one electrode was placed on the outside of the otic capsule in close proximity to the horizontal semicircular canal ampulla, and a second one in the bath chamber at a distance of ~2 mm from the first electrode (Fig. 5A). A continuous sequence of 12 sinusoidally modulated current cycles at a frequency of 0.2 Hz and amplitudes between ±25 and ±100 μA were applied to the pair of electrodes. Neuronal activity was monitored by imaging Ca^{2+} transients follow-

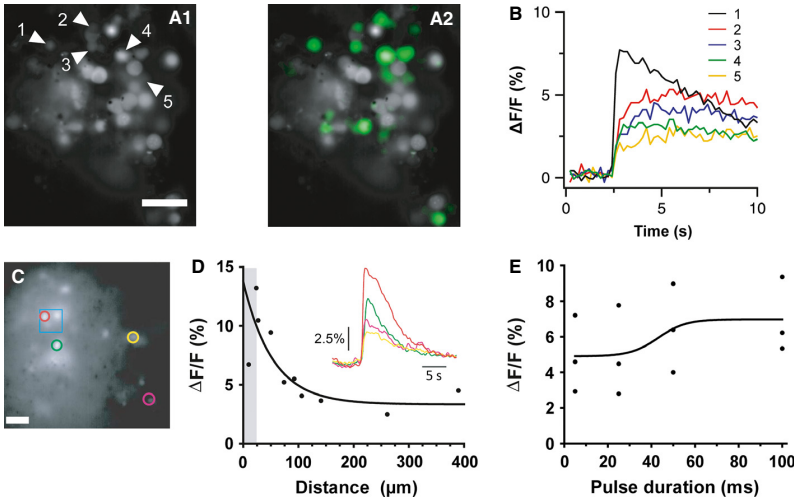

FIG. 4. Ca^{2+} responses in axolotl central vestibular neurons evoked by Glu-uncaging. Neurons labeled with either OGB-1AM ($A_{1,2}$ and B) or Calcium Green™-1 dextran (C–E) were stimulated by UV light activation of MNI-caged Glu. (B) Single sweeps of UV pulse (duration, 50 ms) evoked Ca^{2+} responses in a sample of neurons (1–5 in A_1) following irradiation of the entire FOV (200 × 250 μm). (C–E) Sample of neurons activated by Glu-uncaging within a small area of 50 × 50 μm (blue rectangle). (D) Dependence of Ca^{2+} responses on the distance from the center of UV irradiation (center of blue rectangle in C; UV pulse duration, 50 ms). The data were fitted with a one-phase exponential decay function (weight by $1/y^2$). The gray rectangle represents distances within the activation rectangle. The inset shows Ca^{2+} responses of the neurons marked with colored circles in (C). (E) Ca^{2+} transients evoked by UV pulses of varying duration. Three neurons in the irradiated area (blue rectangle in C) were analysed, and each data point represents the average of two stimulations of an individual cell. The data were fitted with a Boltzmann sigmoidal fit. Scale bars: 50 μm (in A_1; applies to A_2, as well; and C).

ing bulk loading of neurons in the vestibular nuclei with OGB-1AM (Fig. 5B).

Despite the successful labeling of many central vestibular neurons with OGB-1AM, a stimulus-related modulation of Ca^{2+} transients was only encountered in a relatively small fraction (< 5%) of neurons. This sparse activation was not unexpected and is likely due to the fact that central vestibular neurons usually receive labyrinthine afferent inputs from only one semicircular canal (Straka & Dieringer, 2004). The illustrated representative sample of neurons in a given experiment (Fig. 5B and C) with a reliable modulation of the Ca^{2+} transients depicted the range and variability of response amplitudes in different cells. The specificity of the galvanic stimulus is indicated by the activation of Ca^{2+} transients whenever the current in the stimulus electrode closer to the canal cupula depolarized the sensory periphery (black trace in Fig. $5C_2$). Common to the responses in all neurons was an initial summation with a subsequent modulation around an elevated Ca^{2+} level (Fig. $5C_1$). This elevated signal after the first cycle is likely due to the generally low dynamics of the Ca^{2+} sensor and a failure to return to baseline at a stimulus frequency of 0.2 Hz, rather than a direct correlate of the electrical signal. The population average of the Ca^{2+} response of ~6.5% $\Delta F/F$ for the illustrated sample of neurons (lower trace in Fig. $5C_1$) was very similar to that observed during UV light-released Glu (Fig. 4B, D and E), confirming an activation of central vestibular neurons within their physiological range by external Glu in the vicinity of the recorded neurons.

Inhibition of sensory stimulus-evoked Ca^{2+} responses in central vestibular neurons by GABA-uncaging

In order to explore both the technological advancement in microscopy and the axolotl preparation, the effect of GABA-uncaging on the activity of central vestibular neurons induced by galvanic stimulation was assessed. As in adult ranid frogs (Malinvaud *et al.*, 2010), in axolotl GABA is expected to mediate commissural inhibitory responses for bilateral signal amplification during head rotation as well as in shunting vestibular nerve afferent inputs through short-latency local circuits (Straka & Dieringer, 2000; Biesdorf *et al.*, 2008). Therefore, CNB-GABA was uncaged on central vestibular neurons to suppress ipsilateral semicircular canal-evoked excitatory responses recorded here by Ca^{2+} imaging.

Following bulk loading with OGB-1AM and identification of vestibular neurons by their modulated responses, CNB-GABA was bath-applied at a final concentration of 500 μM. For these experiments, two different UV light-activation protocols and different sizes of FOVs for imaging and uncaging were explored (Fig. 6A and B). In the first protocol, a continuous UV light pulse was applied for 1–3 s during a sequence of sinusoidally modulated Ca^{2+} transients in vestibular neurons (Fig. $6C_{1,2}$). Depending on the size of the FOV for uncaging of caged GABA, its position with respect to the monitored neuron and the duration of the UV pulse, modulated responses for up to three consecutive cycles were reversibly shunted after the light pulse, likely due to a marked synaptic inhibition by the optically released GABA (bottom traces in Fig. $6C_{1,2}$). Even though the response modulation recovered relatively quickly, the peak amplitude of the Ca^{2+} transients usually remained smaller, suggesting a persistence of residual GABA at the site of action.

Monitoring of Ca^{2+} transients during the uncaging period was achieved by using pulsed UV light illumination (at 5 Hz) alternating with Ca^{2+} imaging (Fig. 6D). Stepwise increase of the duration of UV light pulses (from 10 to 100 ms) yielded an increasingly more efficient suppression of the Ca^{2+} transients (Fig. 6D), likely due to larger amounts of optically liberated GABA. The precise coordination of UV pulses and image acquisition enabled a monitoring of Ca^{2+} transients with sufficient temporal resolution during CNB-

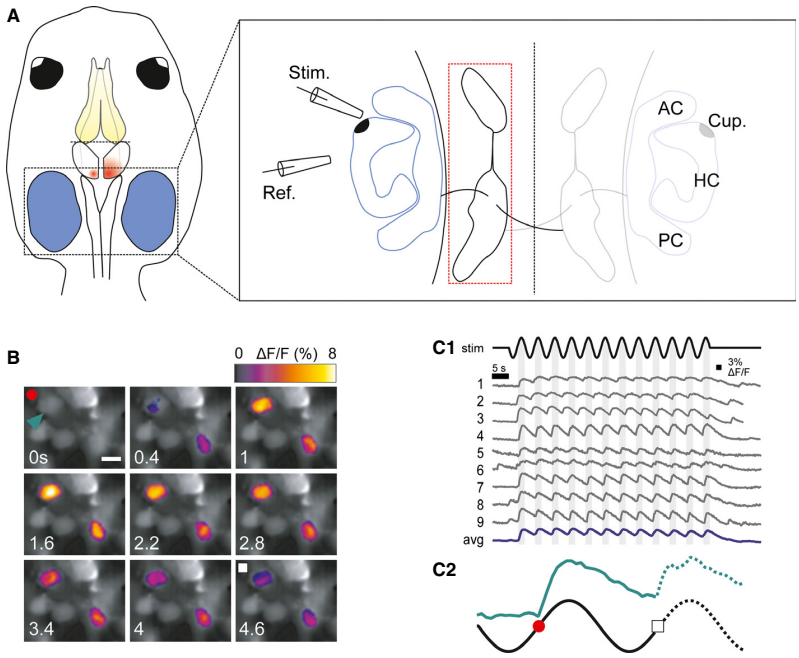

FIG. 5. Electrically evoked Ca^{2+} responses in axolotl central vestibular neurons. (A) Schematic view of the preparation and magnification of the hindbrain region (red dashed rectangle) and semicircular canal stimulus arrangement (AC, PC, anterior, posterior vertical canal; HC, horizontal canal). Stimulation (Stim.) and reference (Ref.) electrodes generate a sinusoidally oscillating electric field that cyclically activates neuronal elements in the cupula (Cup.) of the horizontal semicircular canal (HC). (B) Images of Ca^{2+} transients evoked by sinusoidally modulated currents at various intervals after stimulus onset; scale bar: 15 μm. (C) Ca^{2+} responses over several stimulus cycles in multiple neurons. (C_1) Black, stimulus protocol; light gray bar, positive current phase at the electrode close to the cupula; dark gray, single cell; blue, average Ca^{2+} response (avg). (C_2) Ca^{2+} transient of a typical neuron during two cycles of sinusoidal galvanic stimulation (black sinusoid). The blue trace corresponds to the neuron marked by an arrowhead in (B) (upper left image). The red circle aligns with the first image (B; top, left), the white square marks the last image (B; bottom, right).

GABA-uncaging, but likely also of other, so far untested caged neuroactive compounds.

Taking advantage of independently adjustable FOVs used for UV activation further allowed identifying those area(s) in which uncaged GABA (Fig. 7) most effectively blocked Ca^{2+} signals. FOVs of different size and relative location with respect to OGB-1AM-labeled central vestibular neurons (cells 1–4 in Fig. 7A) were generated by the aperture system (Fig. 7A). Ca^{2+} transients, triggered by sinusoidal galvanic stimulation, were differentially reduced or suppressed depending on the location and/or size of the FOV used to uncage CNB-GABA (see responses of neurons in Fig. $7B_2$ and $C_{1–3}$). Compared with control responses (Fig. $7B_1$), global pulsed UV illumination of the entire optical field temporarily suppressed the modulated Ca^{2+} transients in all four tested neurons (Fig. $7B_2$). Smaller FOVs, overlapping with the optically recorded cell, completely blocked the Ca^{2+} transients (cell 1 in Fig. $7C_1$), whereas the responses of more distantly located cells (e.g. cell 4) remained rather unaffected. Thus, the possibility to generate FOVs of flexible size and position for uncaging neuroactive compounds will provide substantial insight into the local neuronal connectivity of functionally intact vertebrate brains.

Discussion

A novel, highly flexible and inexpensive LED-based fluorescence microscope has been developed, suitable for simultaneous optical manipulation of functionally identified neuronal subgroups and monitoring of neural responses. The system is characterized by eight high-power LEDs with seven different excitation wavelengths within two multi-LED combiners, and by two separate FOVs adjusted by rectangular-shaped apertures. As a major advance of the novel system, the position and size of the FOVs as well as their illumination wavelength and timing can be easily and independently controlled. The computer control of camera and LEDs offers the possibility of light exposure and image acquisition with high temporal accuracy as well as rapid switching between excitation wavelengths. In mammalian brain slices of 50 μm thickness, we could resolve structures with a size of 1 μm in the *xy*-plane, i.e. obtained a resolution similar to that with 50 nm fluorescent microspheres. The fluorescence intensity exhibited a large dynamic. In thicker brain samples (e.g. 260 μm), the resolution was inferior, but still in the range of 2–3 μm.

Advantages and limitations of the novel imaging system

For standard arc lamp-equipped fluorescence microscopes, the switching between excitation filters for illumination with specific wavelengths and the use of mechanical shutters for the control of light exposure pose critical technical limitations on acquisition rates of multi-color imaging. The incorporation of state-of-the-art LED technology in our imaging setup facilitates handling of multiple wavelengths with a simple control of light intensity and exposure time in the microsecond range. This technical arrangement is suitable to analyse fast processes such as neuronal coding. By alternat-

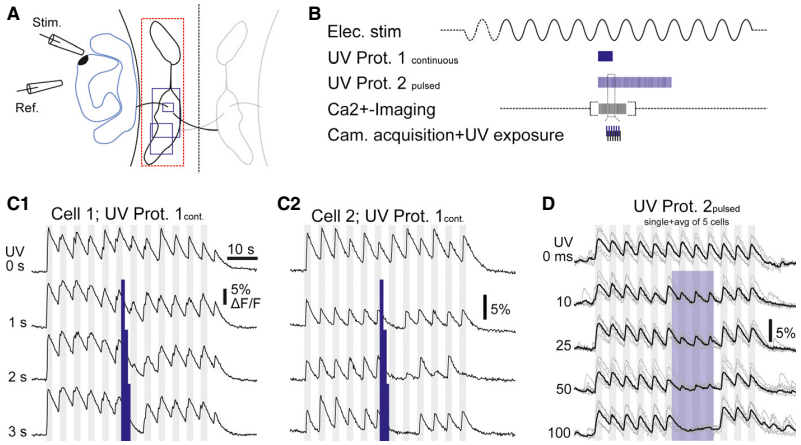

FIG. 6. GABAergic modulation of labyrinthine nerve afferent-evoked neuronal responses. (A) Schematic view of the experimental paradigm; blue rectangles indicate the regions of UV uncaging, and the red dashed rectangle shows the area of Ca^{2+} imaging. (B) Electrical and photo-stimulation protocols, illustrating the timing of image capture and UV light exposure; protocol 1: continuous UV pulse for 1–3 s; protocol 2: trains of short UV pulses (10–100 ms) at 5 Hz for 15 s alternating with image acquisition (black, electric stimulation; blue, UV pulse; red, camera acquisition). (C and D) Ca^{2+} responses in three different OGB-1AM-labeled central vestibular neurons were transiently blocked by CNB-caged GABA following activation by either continuous UV irradiation (UV Prot. 1; $C_{1,2}$) or trains of UV pulses (UV Prot. 2; D). The impact of uncaged GABA on the Ca^{2+} responses in two individual neurons ($C_{1,2}$) using different durations of UV irradiation. Individual (light blue traces; D) and averaged Ca^{2+} transients (black trace) of five cells irradiated by the discontinuous UV protocol with different durations of single UV pulses (0–100 ms).

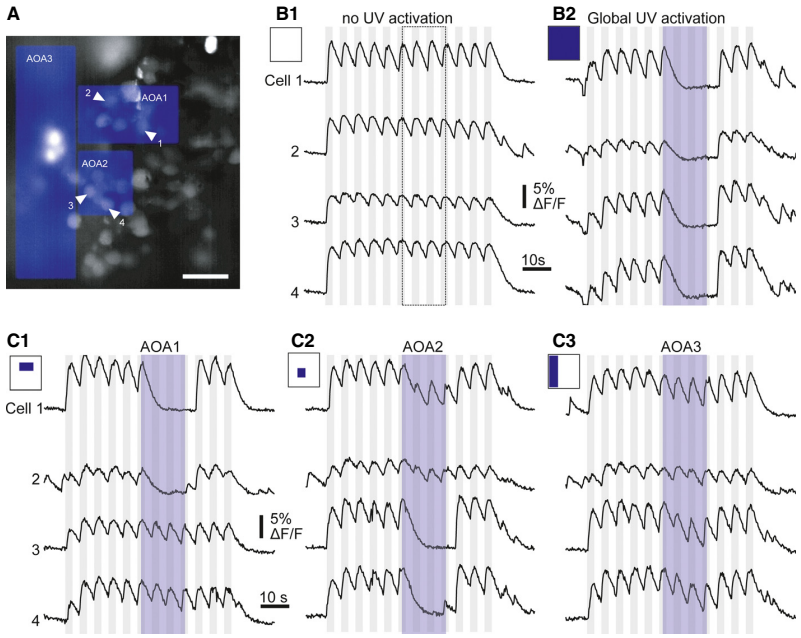

FIG. 7. Spatially specific inhibitory modulation of labyrinthine nerve afferent-evoked neuronal responses. (A) Fluorescence image of OGB-1AM-labeled central vestibular neurons superimposed by blue rectangles illustrating the different UV activation areas. Arrowheads and numbers mark cells analysed in (B) and (C) (scale bar: 50 μm). (B) Ca^{2+} responses for cells 1–4 indicated in (A) without (B_1) and with UV irradiation of the entire field of view (B_2), or of three (C_{1-3}) distinct areas (AOA 1–3) highlighted by the position of the corresponding blue rectangles on the upper left in (C_{1-3}) and in (A) of the visual field.

ing LED exposure for recording (Ca^{2+} imaging) and activating (GABA-uncaging) with high frequency, it was possible to monitor the neuronal activity with adequate temporal resolution during GABA-uncaging for several seconds. Furthermore, the regulation of the UV pulse length enabled the control of the uncaged GABA concentration, and as a consequence allowed a graded suppression of labyrinthine nerve-evoked neuronal responses of vestibular neurons in the current experimental model.

The separation of the light source into distinct units and the integration into individually adjustable apertures generated independently controllable FOVs. Thereby, the described setup permits recordings of multiple imaging tasks at various wavelengths and with overlapping or completely segregated regions of interest, as illustrated by our series of Ca^{2+} imaging and uncaging experiments. Thus, this setup is particularly suited for optical manipulations of either overlapping or spatially segregated neural circuits and neuronal subpopulations. The minimal aperture size of 40 × 40 μm allows limiting photo-stimulation to only few or even single cells. While in the present microscope prototype, size and position adjustments of the apertures are accomplished manually, the next step would implement a motorized aperture control to further simplify experimental procedures.

High-power UV LEDs in contrast to UV lasers are an inexpensive and a sufficiently efficient light source for activating caged compounds (Bernardinelli *et al.*, 2005; Venkataramani *et al.*, 2007). This is indicated in the present study by demonstrating that UV LED uncaging of MNI-caged Glu reliably elicited action potentials and Ca^{2+} transients of central vestibular neurons in semi-isolated *in vitro* preparations of axolotl larvae. Even though UV LEDs were able to consistently evoke Glu responses in all trials, the required pulses, however, were relatively long (20–100 ms) and the onset of action potentials was considerably variable (Fig. 3C and D). These observations might be caused by several parameters, but need further clarification, which extend the scope of the current study. Briefly, the UV irradiation intensity might be too low for two potential reasons: a 50 : 50 reflection transmission beam splitter is used, which accordingly reduces the light intensity at the focal plane by 50%, and purchasable multi-band excitation filter-sets are not yet optimized for LED spectra. Installing a variable reflection transmission beam splitter in an advanced version of the imaging setup as well as optimizing the respective filter-sets will improve these current technical limitations. Furthermore, the low recording temperature of 17 °C, even though representing physiological conditions for amphibian species, limits the dynamics of synaptic transmission compared with classical mammalian preparations at higher recording temperatures.

Optical analysis of sensory signal processing in central vestibular neurons

Vertebrate central vestibular neurons fall into two categories that differ in several intrinsic and synaptic properties (Straka *et al.*, 2005). In adult frogs, the majority of these neurons (phasic vestibular neurons: ~80%) have highly dynamic response properties, while a smaller portion of neurons (tonic vestibular neurons: ~20%) exhibit characteristics that make these cells ideally suited to transform and encode low-dynamic sensory signals (Straka *et al.*, 2004; Beraneck *et al.*, 2007; Pfanzelt *et al.*, 2008). In larval axolotl, more neurons appear to have tonic response properties as indicated by the predominance of recorded vestibular neurons with a continuous discharge during depolarizing current pulses (Fig. 3B). This notion is supported by the repetitive synaptic firing in virtually all recorded neurons following Glu-uncaging (Fig. 3C). The difference in proportion of the two subtypes between adult frog and larval axolotl might reflect eco-physiological adaptations of vestibular neurons for encoding of head/body motion in animals with different lifestyles or locomotor patterns as suggested earlier (Straka *et al.*, 2005). In fact, a pilot study in larval *Xenopus* also described a predominance of vestibular neurons with continuous firing patterns upon depolarization (Beraneck *et al.*, 2008), very reminiscent to those described here and at variance with the predominant pattern in adult frogs.

The magnitude of Ca^{2+} transients triggered by MNI-Glu-uncaging was similar in all vestibular neurons independent of FOV size used for uncaging, as long as the cell body was located within or in close proximity to the illuminated area (Fig. 4). This observation is consistent with the fact that the predominant termination of the major excitatory input that derives from ipsilateral semicircular and otolith afferent fibers on central vestibular neurons is on the soma (and the proximal dendrite) and, therefore, most Glu receptors are located in this region (Dieringer & Precht, 1979; Straka *et al.*, 2005). The small Ca^{2+} transients activated at more remote sites with respect to the cell bodies might concur with the weak and slow commissural excitatory inputs at distal parts of the large dendritic tree of vestibular neurons (Dieringer & Precht, 1979; Malinvaud *et al.*, 2010). Thus, the differential efficacy of activating Ca^{2+} transients in vestibular neurons by Glu-uncaging at different distances relative to the cell body coincides with the functional differentiation of the major glutamatergic inputs in these neurons, provided the observed effect of the uncaged transmitter in the current experimental setting is only direct and not mediated in addition by unknown numbers of local interneurons.

The amplitude and dynamics of Ca^{2+} transients evoked by Glu-uncaging close to the soma are comparable to the responses following electrical stimulation of vestibular end-organs (Figs 5–7), suggesting an excitation of similar numbers of synapses at similar sites of central vestibular neurons. The employed sinusoidal galvanic stimulation allows a spatially specific activation of individual semicircular canals and thus offers the possibility to imitate head rotations in different planes by applying modulated currents (Kaufmann *et al.*, 2013). Whereas the evoked Ca^{2+} responses correlate with each depolarizing half-wave of the sinusoid and thus comply with theoretical considerations of this method (Goldberg *et al.*, 1984), it remains so far unclear if the applied current recruits vestibular hair cells and/or afferent fibers at the sensory periphery. However, irrespective of the actually stimulated structural element(s) at the vestibular sensory periphery, the induced Ca^{2+} transient is an excellent estimate of vestibular neuronal activity. In combination with the advantages of the novel imaging system, it allows simultaneous visualization of larger neuronal populations in deep brainstem nuclei as in the current experimental animal model. The responsiveness of only a few vestibular neurons to galvanic stimulation of the ipsilateral horizontal semicircular canal in the illustrated example is not due to functional restrictions of the experimental setting, but complies with the end-organ-specific monosynaptic activation of central vestibular neurons and the limited convergence of excitatory inputs from multiple vestibular end-organs in individual neurons (Straka *et al.*, 2002).

Sensory vestibular activation of central vestibular neurons is controlled by inhibitory inputs mediated by local feed-forward circuits (Minor & Goldberg, 1991; Straka & Dieringer, 2000), brainstem commissural pathways (Shimazu & Precht, 1966; Malinvaud *et al.*, 2010) or cerebellar Purkinje cells (Magherini *et al.*, 1975; Babalian & Vidal, 2000). The local disynaptic inhibition with its short latency has been shown to effectively shunt the sensory-driven monosynaptic excitation and, thereby, to terminate the afferent activation after the first few action potentials (Biesdorf *et al.*, 2008). The functional consequence is a flexible control of different dynamic signal components during head/body motion. While semicircular canal plane-specific commissural inhibitory connections improve the bilateral sensitivity for angular head acceleration, Purkinje cell-mediated inhibition controls the gain of vestibulo-ocular reflexes (Straka &

Dieringer, 2004). Common to all these inhibitory inputs is a GABA-mediated reduction of the ipsilateral vestibular sensory-driven excitation. While bath application or systemic administration of GABA antagonists was previously used to estimate the impact of the different inhibitory circuits, the current study directly demonstrated the potency of GABA on shunting vestibular nerve afferent activity (Figs 6 and 7). The effect of GABA-uncaging on Ca^{2+} transients was remarkably profound during the entire period of the uncaging pulse in different vestibular neurons, provided the area for the optical release included the soma of the recorded neuron. This is in accordance with the assumption that uncaged GABA activates somatic receptors, a condition that is particularly effective in shunting excitatory somatic inputs in close proximity to the inhibitory synapses. The complete block of afferent excitation by local GABA-uncaging is likely the result of an activation of all accessible receptors at variance with a more fractional recruitment of these inputs following separate activation of the different inhibitory circuits. Nonetheless, it clearly demonstrates the considerable impact of inhibitory signals on the processing of head/body motion-related sensory-motor transformation in central vestibular neurons. Based on the outcome of these first explorative sets of experiments, the novel microscope allows employing numerous optical manipulations that help deciphering the connectivity between larger groups of identifiable neuronal elements along the hierarchical structure of specific functional circuitries in *in vivo*-like semi-isolated preparations.

Supporting Information

Additional supporting information can be found in the online version of this article:
Data S1. Zemax file of optical path (ray_trace.zmx).

Acknowledgements

The authors thank the Collaborative Research Center 870 (CRC 870, DFG), the Munich Center for Neurosciences – Brain & Mind (MCN, Ludwig-Maximilians University Munich), the Graduate School of Systemic Neurosciences (GSN, Ludwig-Maximilians University Munich) and the GRK 1373 of the German Science Foundation for financial support. The authors appreciate funding of S.D. by the MCN (Ludwig-Maximilians University Munich), and of S.B. by Benedikt Grothe. F.F. was supported by the Elisabeth and Helmut Uhl Foundation. All authors declare to have no conflict of interest.

Abbreviations

CNB, carboxy-2-nitrobenzyl ester; DMSO, dimethylsulfoxide; FOV, field of view; FWHM, full width at half maximum; GABA, γ-aminobutyric acid; Glu, glutamate; LED, light-emitting diode; MNI, 4-methoxy-7-nitroindolinyl; OGB-1AM, Oregon Green BAPTA-1AM; PBS, phosphate-buffered saline.

References

Ammer, J.J., Grothe, B. & Felmy, F. (2012) Late postnatal development of intrinsic and synaptic properties promotes fast and precise signaling in the dorsal nucleus of the lateral lemniscus. *J. Neurophysiol.*, **107**, 1172–1185.

Babalian, A.L. & Vidal, P.P. (2000) Floccular modulation of vestibuloocular pathways and cerebellum-related plasticity: an in vitro whole brain study. *J. Neurophysiol.*, **84**, 2514–2528.

Beraneck, M., Pfanzelt, S., Vassias, I., Rohregger, M., Vibert, N., Vidal, P.P., Moore, L.E. & Straka, H. (2007) Differential intrinsic response dynamics determine synaptic signal processing in frog vestibular neurons. *J. Neurosci.*, **27**, 4283–4296.

Beraneck, M., Lambert, F.M. & Straka, H. (2008) Membrane properties of central vestibular neurons in larval Xenopus: eco-physiological adaptations to locomotor strategy. 34th Annual Meeting of the Society for Neuroscience 2008, *Soc. Neurosci. Abstr.*, **34**, 169.12.

Bernardinelli, Y., Haeberli, C. & Chatton, J.-Y. (2005) Flash photolysis using a light emitting diode: an efficient, compact, and affordable solution. *Cell Calcium*, **37**, 565–572.

Biesdorf, S., Malinvaud, D., Reichenberger, I., Pfanzelt, S. & Straka, H. (2008) Differential inhibitory control of semicircular canal nerve afferent-evoked inputs in second-order vestibular neurons by glycinergic and GAB-Aergic circuits. *J. Neurophysiol.*, **99**, 1758–1769.

Brustein, E., Marandi, N., Kovalchuk, Y., Drapeau, P. & Konnerth, A. (2003) "In vivo" monitoring of neuronal network activity in zebrafish by two-photon Ca^{2+} imaging. *Pflug. Arch. Eur. J. Phy.*, **446**, 766–773.

Combes, D., Le Ray, D., Lambert, F.M., Simmers, J. & Straka, H. (2008) An intrinsic feed-forward mechanism for vertebrate gaze stabilization. *Curr. Biol.*, **18**, R241–R243.

Cossart, R., Ikegaya, Y. & Yuste, R. (2005) Calcium imaging of cortical networks dynamics. *Cell Calcium*, **37**, 451–457.

Dieringer, N. & Precht, W. (1979) Mechanisms of compensation for vestibular deficits in the frog. I. Modification of the excitatory commissural system. *Exp. Brain Res.*, **36**, 311–328.

Direnberger, S., Mues, M., Micale, V., Wotjak, C.T., Dietzel, S., Schubert, M., Scharr, A., Hassan, S., Wahl-Schott, C., Biel, M., Krishnamoorthy, G. & Griesbeck, O. (2012) Biocompatibility of a genetically encoded calcium indicator in a transgenic mouse model. *Nat. Commun.*, **3**, 1031.

Felmy, F. & Schneggenburger, R. (2004) Developmental expression of the Ca^{2+}-binding proteins calretinin and parvalbumin at the calyx of held of rats and mice. *Eur. J. Neurosci.*, **20**, 1473–1482.

Fetcho, J.R. & O'Malley, D.M. (1995) Visualization of active neural circuitry in the spinal cord of intact zebrafish. *J. Neurophysiol.*, **73**, 399–406.

Goldberg, J.M., Smith, C.E. & Fernández, C. (1984) Relation between discharge regularity and responses to externally applied galvanic currents in vestibular nerve afferents of the squirrel monkey. *J. Neurophysiol.*, **51**, 1236–1256.

Grewe, B.F., Langer, D., Kasper, H., Kampa, B.M. & Helmchen, F. (2010) High-speed in vivo calcium imaging reveals neuronal network activity with near-millisecond precision. *Nat. Methods*, **7**, 399–405.

Grienberger, C. & Konnerth, A. (2012) Imaging calcium in neurons. *Neuron*, **73**, 862–885.

Kaufmann, A.K., Gensberger, K., Dietrich, H., Branoner, F., Banchi, R., Chagnaud, B.P. & Straka, H. (2013) Mechanistic basis and spatio-temporal specificity of galvanic vestibular stimulation in *Xenopus laevis*. 39th Annual Meeting of the Society for Neuroscience. *Soc. Neurosci. Abstr.*, **39**, 164.04.

Lambert, F.M., Malinvaud, D., Gratacap, M., Straka, H. & Vidal, P.P. (2013) Restricted neural plasticity in vestibulo-spinal pathways after unilateral labyrinthectomy as the origin for scoliotic deformations. *J. Neurosci.*, **33**, 6845–6856.

Magherini, P.C., Giretti, M.L. & Precht, W. (1975) Cerebellar control of vestibular neurons of the frog. *Pflug. Arch. Eur. J. Phy.*, **356**, 99–109.

Malinvaud, D., Vassias, I., Reichenberger, I., Rössert, C. & Straka, H. (2010) Functional organization of vestibular commissural connections in frog. *J. Neurosci.*, **30**, 3310–3325.

Minor, L.B. & Goldberg, J.M. (1991) Vestibular nerve inputs to the vestibulo-ocular reflex: a functional ablation study in the squirrel monkey. *J. Neurosci.*, **11**, 1636–1648.

Nye, H.L., Cameron, J.A., Chernoff, E.A. & Stocum, D.L. (2003) Extending the table of stages of normal development of the axolotl: limb development. *Dev. Dynam.*, **226**, 555–560.

Pfanzelt, S., Rössert, C., Rohregger, M., Glasauer, S., Moore, L.E. & Straka, H. (2008) Differential dynamic processing of afferent signals in frog tonic and phasic second-order vestibular neurons. *J. Neurosci.*, **28**, 10349–10362.

Piston, D.W. (1999) Imaging living cells and tissues by two-photon excitation microscopy. *Trends Cell Biol.*, **9**, 66–69.

Ramlochansingh, C., Branoner, F., Chagnaud, B.P. & Straka, H. (2014) Tricaine methanesulfonate (MS-222) as an effective anesthetic agent for blocking sensory-motor responses in Xenopus laevis tadpoles. *PLoS One*, **9**, e101606.

Regehr, W.G., Connor, J.A. & Tank, D.W. (1989) Optical imaging of calcium accumulation in hippocampal pyramidal cells during synaptic activation. *Nature*, **341**, 533–536.

Schneider, C.A., Rasband, W.S. & Eliceiri, K.W. (2012) NIH Image to ImageJ: 25 years of image analysis. *Nat. Methods*, **9**, 671–675.

Shimazu, H. & Precht, W. (1966) Inhibition of central vestibular neurons from the contralateral labyrinth and its mediating pathway. *J. Neurophysiol.*, **29**, 467–492.

Stosiek, C., Garaschuk, O., Holthoff, K. & Konnerth, A. (2003) In vivo two-photon calcium imaging of neuronal networks. *Proc. Natl. Acad. Sci. USA*, **100**, 7319–7324.

Straka, H. & Dieringer, N. (2000) Convergence pattern of uncrossed excitatory and inhibitory semicircular canal-specific inputs onto second-order vestibular neurons of frogs. *Exp. Brain Res.*, **135**, 462–473.
Straka, H. & Dieringer, N. (2004) Basic organization principles of the VOR: lessons from frogs. *Prog. Neurobiol.*, **73**, 259–309.
Straka, H. & Simmers, J. (2012) Xenopus laevis: an ideal experimental model for studying the developmental dynamics of neural assembly and sensory motor computations. *Dev. Neurobiol.*, **72**, 649–663.
Straka, H., Baker, R. & Gilland, E. (2001) Rhombomeric organization of vestibular pathways in larval frogs. *J. Comp. Neurol.*, **437**, 42–55.
Straka, H., Holler, S. & Goto, F. (2002) Patterns of canal and otolith afferent input convergence in frog second order vestibular neurons. *J. Neurophysiol.*, **88**, 2287–2301.
Straka, H., Beraneck, M., Rohregger, M., Moore, L.E., Vidal, P.P. & Vibert, N. (2004) Second-order vestibular neurons form separate populations with different membrane and discharge properties. *J. Neurophysiol.*, **92**, 845–861.
Straka, H., Vibert, N., Vidal, P.P., Moore, L.E. & Dutia, M.B. (2005) Intrinsic properties of vertebrate vestibular neurons: function, development and plasticity. *Prog. Neurobiol.*, **76**, 349–392.
Straka, H., Lambert, F.M., Pfanzelt, S. & Beraneck, M. (2009) Vestibulo-ocular signal transformation in frequency-tuned channels. *Ann. NY Acad. Sci.*, **1164**, 37–44.
Sullivan, M.R., Nimmerjahn, A., Sarkisov, D.V., Helmchen, F. & Wang, S.S.-H. (2005) In vivo calcium imaging of circuit activity in cerebellar cortex. *J. Neurophysiol.*, **94**, 1636–1644.
Szűcs, P., Pinto, V. & Safronov, B.V. (2009) Advanced technique of infrared LED imaging of unstained cells and intracellular structures in isolated spinal cord, brainstem, ganglia and cerebellum. *J. Neurosci. Meth.*, **177**, 369–380.
Trattner, B., Gravot, C.M., Grothe, B. & Kunz, L. (2013) Metabolic maturation of auditory neurones in the superior olivary complex. *PLoS One*, **8**, e67351.
Tsien, R.Y. (1981) A non-disruptive technique for loading calcium buffers and indicators into cells. *Nature*, **290**, 527–528.
Venkataramani, S., Davitt, K.M., Xu, H., Zhang, J., Song, Y.-K., Connors, B.W. & Nurmikko, A.V. (2007) Semiconductor ultra-violet light-emitting diodes for flash photolysis. *J. Neurosci. Meth.*, **160**, 5–9.
Yuste, R. & Katz, L.C. (1991) Control of postsynaptic Ca2+ influx in developing neocortex by excitatory and inhibitory neurotransmitters. *Neuron*, **6**, 333–344.

Locomotor corollary activation of trigeminal motor neurons: coupling of discrete motor behaviors

Sara Hänzi, **Roberto Banchi**, Hans Straka and Boris P. Chagnaud

J Exp Biol 218:1748–1758

S.H. and **R.B**. contributed equally to the present study

Contributions of RB

- Preliminary experiments and design of the study, together with BPC.
- All experiments and analyses required for the anatomical part of the study including the visualization of rhombomeric domains (Fig. 2).
- Back-filling method for use in calcium imaging.
- All experiments and analyses involved in the calcium imaging of tentacle motoneurons during fictive swimming (Fig. 3).
- Analysis of the duration of the tentacle nerve discharge compared to the duration of fictive swimming (Fig. 5 A, B).
- Writing and revising, together with all other authors.

© 2015. Published by The Company of Biologists Ltd | The Journal of Experimental Biology (2015) 00, 1-11 doi:10.1242/jeb.120824

RESEARCH ARTICLE

Locomotor corollary activation of trigeminal motoneurons: coupling of discrete motor behaviors

Sara Hänzi[1,2,*], Roberto Banchi[1,2,*], Hans Straka[1,‡] and Boris P. Chagnaud[1,‡,§]

ABSTRACT

During motor behavior, corollary discharges of the underlying motor commands inform sensory-motor systems about impending or ongoing movements. These signals generally limit the impact of self-generated sensory stimuli but also induce motor reactions that stabilize sensory perception. Here, we demonstrate in isolated preparations of *Xenopus laevis* tadpoles that locomotor corollary discharge provokes a retraction of the mechanoreceptive tentacles during fictive swimming. In the absence of sensory feedback, these signals activate a cluster of trigeminal motoneurons that cause a contraction of the tentacle muscle. This corollary discharge encodes duration and strength of locomotor activity, thereby ensuring a reliable coupling between locomotion and tentacle motion. The strict phase coupling between the trigeminal and spinal motor activity, present in many cases, suggests that the respective corollary discharge is causally related to the ongoing locomotor output and derives at least in part from the spinal central pattern generator; however, additional contributions from midbrain and/or hindbrain locomotor centers are likely. The swimming-related retraction might protect the touch-receptive Merkel cells on the tentacle from sensory over-stimulation and damage and/or reduce the hydrodynamic drag. The intrinsic nature of the coupling of tentacle retraction to locomotion is an excellent example of a context-dependent, direct link between otherwise discrete motor behaviors.

KEY WORDS: Corollary discharge, Efference copy, Spinal locomotion, Trigeminal nerve, *Xenopus laevis*

INTRODUCTION

During rhythmic locomotion, a number of otherwise independent movements are influenced by the rhythm of the motor commands. In vertebrates, such coupling is observed for respiration (Bramble and Carrier, 1983), eye movements (Lambert et al., 2012), tail motion (Wada et al., 1993) or phase-locked arm and trunk motor adjustments (Earhart, 2013). While some coupled motor behaviors such as tail motion, e.g. in dogs, improve locomotor performance (Wada et al., 1993), others improve sensory acquisition and processing as observed for retinal image stabilization (Chagnaud et al., 2012a; Lambert et al., 2012). One possibility for coupling otherwise unrelated motor behaviors to locomotion is via corollary discharge that derives from spinal or supraspinal locomotor centers. These signals allow fast and reliable phase locking of the respective motor behavior to the locomotor rhythm (Chagnaud et al., 2012a). Corollary discharges are independent of locomotor style and occur during rhythmic limb-based locomotion in terrestrial vertebrates as well as during body/tail-based swimming in aquatic vertebrates (Chagnaud et al., 2012a). Traditionally, motor corollary discharges have been described as mechanisms to differentiate between environmental and self-generated sensory inputs (Crapse and Sommer, 2008; Cullen, 2004, 2011; von Holst and Mittelstaedt, 1950; Poulet and Hedwig, 2007; Sommer and Wurtz, 2008). In contrast, the impact of motor corollary discharges on motor systems and the indirect effects on the sensory encoding have been less well investigated. Some studies have shown that corollary discharge can cause reflex inhibition during swimming in *Xenopus* embryos (Sillar and Roberts, 1988), suppress withdrawal responses in gastropods during feeding behavior (Davis et al., 1974; Kovac and Davis, 1980) and drive compensatory eye movements during swimming in larval *Xenopus* (Lambert et al., 2012). However, attempts to decipher the mechanisms underlying the effects of corollary discharge on motor behaviors are often constrained by the complexity of the central nervous system and the limb-based locomotion. In contrast, tail-based swimming in amphibians (Wassersug and Hoff, 1985) and fishes represents a simple, stereotyped locomotor pattern with correspondingly simpler spatio-temporal profiles of corollary discharges.

A number of aquatic anamniotes possess various numbers of mobile appendages on the head that contain several types of sensors (see Fox, 1999). One example is the pair of rostrally protruding tentacles in *Xenopus laevis* Daudin tadpoles that are equipped with Merkel cells (Ovalle, 1979). The mechanosensory nature of these cells (Maricich et al., 2009) suggests an important role for touch discrimination and surface structure recognition. Because of the location of the tentacles on the head and the tadpole's undulatory swimming style with prominent horizontal head oscillations, the tactile function of these appendages might be impaired during locomotor behavior. Given the previously reported spinal efference copy-driven compensatory eye motion in *Xenopus* tadpoles during swimming (Combes et al., 2008; Lambert et al., 2012), a protection of the sensor and a potential improvement of propulsive efficacy could be achieved by a similar spinal locomotor corollary discharge that causes a tentacle retraction.

Here, we provide direct evidence that locomotor corollary discharges during rhythmic swimming in *X. laevis* tadpoles initiate a bilateral tentacle retraction. Fluorescent tract tracing, Ca^{2+} imaging, electrophysiological recordings and video analysis of tentacle motor behavior during fictive locomotion in semi-intact *in vitro* preparations outline the underlying trigeminal motoneuronal populations, their firing pattern and their link to ongoing locomotor commands. The observed coupling of tentacle retraction to swimming is an excellent example of intrinsic control of a particular motor behavior that is otherwise unrelated to locomotion.

[1]Department Biology II, Ludwig-Maximilians-University Munich, 82152 Planegg, Germany. [2]Graduate School of Systemic Neurosciences, Ludwig-Maximilians-University Munich, 82152 Planegg, Germany.
*These authors contributed equally to this work
‡These authors contributed equally to this work

§Author for correspondence (b.chagnaud@lmu.de)

Received 16 February 2015; Accepted 30 March 2015

The Journal of Experimental Biology (2015) 00, 1-11 doi:10.1242/jeb.120824

RESULTS

Locomotion-coupled tentacle motion

Xenopus laevis tadpoles are equipped with a bilateral, mobile pair of tentacles (Cannone and Kelly, 1977; Ovalle, 1979) that are attached to the upper jaw at the lateral aspect of the mouth. At rest, these appendages extend rostro-laterally (Fig. 1Ai,B) at an angle of 19±10 deg (mean±s.d., 61 tentacles) relative to the longitudinal body axis. During fictive locomotion, indicated by rhythmic bursts in spinal ventral roots (VRs) in isolated tadpole preparations (Combes et al., 2004; see below for details), video recordings revealed that the tentacles were concurrently retracted (Fig. 1Aii). The maximal retraction angle during swimming was 115±24 deg (61 tentacles, n=41 swimming episodes in N=7 preparations; Fig. 1B). During locomotor activity, the tentacles essentially remained in a lateral position interspersed by variably timed and sized oscillations (Fig. 1C). As the locomotor activity ceased, the tentacles protracted towards the initial resting position (Fig. 1Aiii, Aiv, Ci).

Simultaneous video recordings of the tentacles on both sides (n=20 episodes in N=4 preparations) yielded very similar motion dynamics and trajectories of both tentacles during a given locomotor episode (see red and blue traces in Fig. 1Ci). The close coupling of onset, duration and motion pattern of the left and right tentacle was verified by correlating the respective motion trajectories (Fig. 1Cii). The distribution of the correlation coefficients (median: 0.81; Fig. 1D) was significantly different from zero (P<0.0001; Wilcoxon signed-rank test) indicating that both tentacles move symmetrically. This close match of the bilateral motor activity was exploited in subsequent experiments by combined recordings of the motion pattern of one tentacle and the neuronal commands of the trigeminal motor nerve that innervates the tentacle on the other side. Moreover, the presence of tentacle movements during locomotion in completely isolated and immobile *Xenopus* tadpole preparations and thus in the absence of tail motion-related sensory signals suggests that the motor commands derive from a locomotor corollary discharge that activates the tentacle motor system.

Anatomical organization of the tentacle motor system

Tentacle movements in *Xenopus* tadpoles are produced by a single muscle (m. levator mandibulae pars lateralis) that retracts the tentacle (Nieuwkoop and Faber, 1994); in contrast, protraction of the tentacle occurs in the absence of a respective muscle but likely involves the mechanics of a cartilaginous spring (Ovalle et al., 1998). The tentacle muscle, responsible for the retraction, has a joint proximal origin with the jaw closing muscles (m. levator mandibulae pars intermedius and medialis) but remains otherwise separate (dashed line in Fig. 2B), and attaches distally at the cartilaginous base of the tentacle (Fig. 2A,B). The exclusive control of tentacle movements by the lateral portion of the m. levator mandibulae was demonstrated by a set of differential muscle lesions. A specific transection (three preparations) of the m. levator mandibulae pars lateralis, which left the other two portions of the m. levator mandibulae intact, abolished all tentacle movements. In contrast, a reciprocal surgical intervention (three preparations), that preserved the lateral portion, left tentacle movements unaffected. The sensory-motor innervation of the tentacle and its muscle is formed by the trigeminal ophthalmic (rOP) and mandibular branches (rMA) as illustrated by the pattern of labeled peripheral nerves following application of biocytin to the trigeminal nerve root close to the hindbrain (Fig. 2A). The motor innervation of the tentacle muscle, however, originates exclusively from the smaller branch (tentacle nerve, TN) after ramification of the rMA into two branches at the level of the m. levator mandibulae (red asterisk in Fig. 2B).

Apart from innervating the tentacle muscle, the TN branch also innervates the jaw closing muscle (Fig. 2A,B). This branch exclusively contains motor axons as indicated by the absence of sensory hindbrain projections following tracer application to this particular nerve (left side in Fig. 2C). This differs from the observed pattern after labeling of the second rMA branch (blue arrowhead in Fig. 2B) or the trigeminal nerve root, where

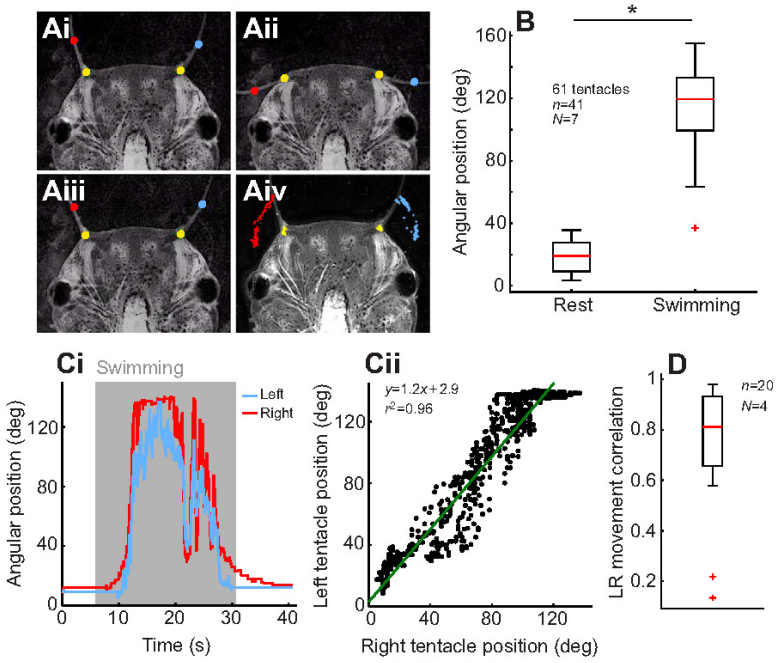

Fig. 1. Bilaterally coordinated tentacle movements during fictive swimming in an isolated *in vitro* *Xenopus laevis* tadpole preparation. (A) Representative frames from a video recording before (Ai), during (Aii) and after (Aiii) an episode of fictive swimming; positions of the left and right tentacle and their proximal insertions (yellow) are superimposed on an image overlay (Aiv) visualizing the trajectories during the entire locomotor event. (B) Boxplots of angular tentacle positions at rest and at maximal eccentricity (relative to the longitudinal body axis) during fictive swimming (61 tracked tentacles, obtained from n=41 locomotor episodes in N=7 preparations). (Ci) Angular trajectory of the left and right tentacle during an episode of fictive swimming (gray area); (Cii) scatter plot and linear regression correlating the angular positions of the two tentacles during the locomotor episode shown in Ci. (D) Boxplot of correlation coefficients between angular positions of the left and right (LR) tentacles during n=20 swimming episodes in N=4 preparations with a median coefficient of 0.81 (P<0.0001; Wilcoxon signed-rank test).

The Journal of Experimental Biology (2015) 00, 1-11 doi:10.1242/jeb.120824

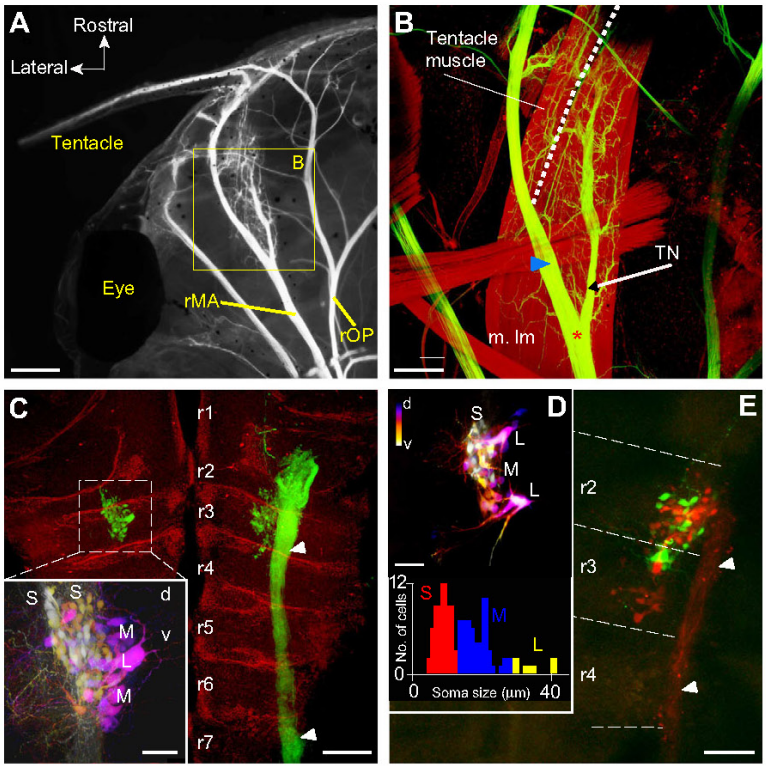

Fig. 2. Anatomical organization of the tentacle motor system. (A) Wide-field fluorescence image, depicting the left tentacle and its biocytin/streptavidin-Cy2-labeled (in white) neuronal innervation by the ophthalmic (rOP) and mandibular branch (rMA) of the trigeminal nerve. (B) Confocal reconstruction of the area outlined in A, illustrating the tentacle muscle – lateral portion (dashed line) of the m. levator mandibulae (m. lm) – and the tentacle nerve (TN) that branches off (red asterisk) from the main rMA (blue arrowhead); confocal scanning at 488 and 633 nm visualized biocytin/streptavidin-Cy2-labeled trigeminal nerve branches (green) and muscle tissue (red). (C–E) Confocal reconstruction of trigeminal motoneurons and afferent projections in the hindbrain (white arrowheads in C, E), labeled with biocytin/streptavidin-Cy2 or Alexa Fluor dextran 488/546 from the TN (left side in C, D; green neurons in E), the trigeminal nerve root (right side in C) or the main rMA (red neurons in E) distal to the TN branching (blue arrowhead in B); rhombomere (r1–7) boundaries (C) were visualized with 633 nm illumination; tentacle motoneurons, color coded according to their position along the *z*-axis (inset in C, D), subdivide into dorso-medially located large (L) and medium-sized (M) elongated cells and ventro-laterally located small, round cells (S); the dorso-ventral extension of the *z*-stack is 74 µm in the inset in C and 128 µm in D. The histogram in the lower part of D displays the distribution of soma diameters across preparations. Color code: d, dorsal; v, ventral. Scale bars are 0.5 mm in A, 0.2 mm in B, C and E, and 50 µm in C inset and D. Arrows in A indicating the rostral and lateral direction apply to all other panels.

additional dense afferent terminations were observed in the dorsal hindbrain throughout r1–r7 (arrowheads on the right side in Fig. 2C,E), indicating the presence of sensory fibers in the respective nerves.

The hindbrain location of motoneurons innervating the tentacle muscle was compared with the entire population of trigeminal motoneurons following application of biocytin to the TN at its entrance into the muscle or to the trigeminal nerve close to the hindbrain (cell groups on the left and right side, respectively, in Fig. 2C). Tracer application to the TN consistently labeled a group of motoneurons in hindbrain segments r2 and r3 (left side in Fig. 2C–E). This bi-segmental location coincides with that of the entire population of trigeminal motoneurons, labeled from the trigeminal nerve root (right side in Fig. 2C). The number of retrogradely labeled tentacle motoneurons was variable and ranged from 9 to 87 neurons in different experiments (median: 27 cells, N=10 preparations). These motoneurons only innervated the m. levator mandibulae because labeling of the TN and the second rMA branch (blue arrowhead in Fig. 2B) in different colors (Alexa Fluor dextran 488 and 546; N=4 preparations) did not yield double-labeled neurons (see absence of yellow cells in r2 and r3 in Fig. 2E). However, tentacle motoneurons were intermingled with other rMA motoneurons (green and red cells in r2 and r3 in Fig. 2E) within the trigeminal nucleus.

Tentacle motoneurons form a heterogeneous population with respect to soma size and shape (inset in Fig. 2C,D). A histogram of soma diameters (120 cells in N=6 preparations) revealed that cell size extends over a large range that suggests the presence of up to three groups of neurons with a tendency for a size-related dorso-ventral separation (see Fig. 2C,D inset for *z*-axis color-coded confocal reconstruction). Neurons were categorized as either small (<12 µm) and mostly round (group 1: S) or medium sized (≥12 and <30 µm) with oval somata (group 2: M) with the consistent exception of one to two very large (≥30 µm) neurons with elongated cell bodies (group 3: L), located at the most dorso-medial aspect of the labeled cell group (L in Fig. 2C,D inset). Medium-sized neurons were located at more medial and dorsal positions relative to the smaller cells (Fig. 2C,D inset). The mean size of the neurons was 8.3±1.9 µm (56 cells) for small neurons, 18.1±3.8 µm (58 cells) for medium neurons and 34.6±4.4 µm (six cells) for large neurons. Accordingly, tentacle motoneurons form a morphologically diverse and dispersed cell group within the trigeminal motor nucleus in r2 and r3 with a size-related dorso-ventral arrangement.

Activity of tentacle motoneurons during locomotion

The morphological diversity of tentacle motoneurons prompted us to test whether all or only a particular subpopulation of motoneurons become active during swimming and cause the observed tentacle retraction. Neuronal activity was measured as Ca^{2+} transients in the entire tentacle motor nucleus or in individual motoneurons, following unilateral or bilateral application of Calcium Green-1 dextran to the peripheral motor target(s) and retrograde transport to the cell bodies (Fig. 3Ai inset, Bii, Cii). During episodes of fictive locomotor activity, visible as rhythmic bursting in the spinal VR (green trace in Fig. 3Ai), the population of tentacle motoneurons showed fluorescence changes that were timed to the VR bursting (Fig. 3Ai). Simultaneous Ca^{2+} imaging of the bilateral tentacle motor nuclei (red and blue outline in Fig. 3Ai inset) yielded almost identical dynamics of the transients (red and blue traces in Fig. 3Ai), matching the symmetric motion profiles of the two appendages (Fig. 1Ci,D). The duration of these population responses (n=15 swimming episodes in N=8 preparations), measured as half-width of the Ca^{2+} transients (Fig. 3Ai), was highly correlated with the

The Journal of Experimental Biology (2015) 00, 1-11 doi:10.1242/jeb.120824

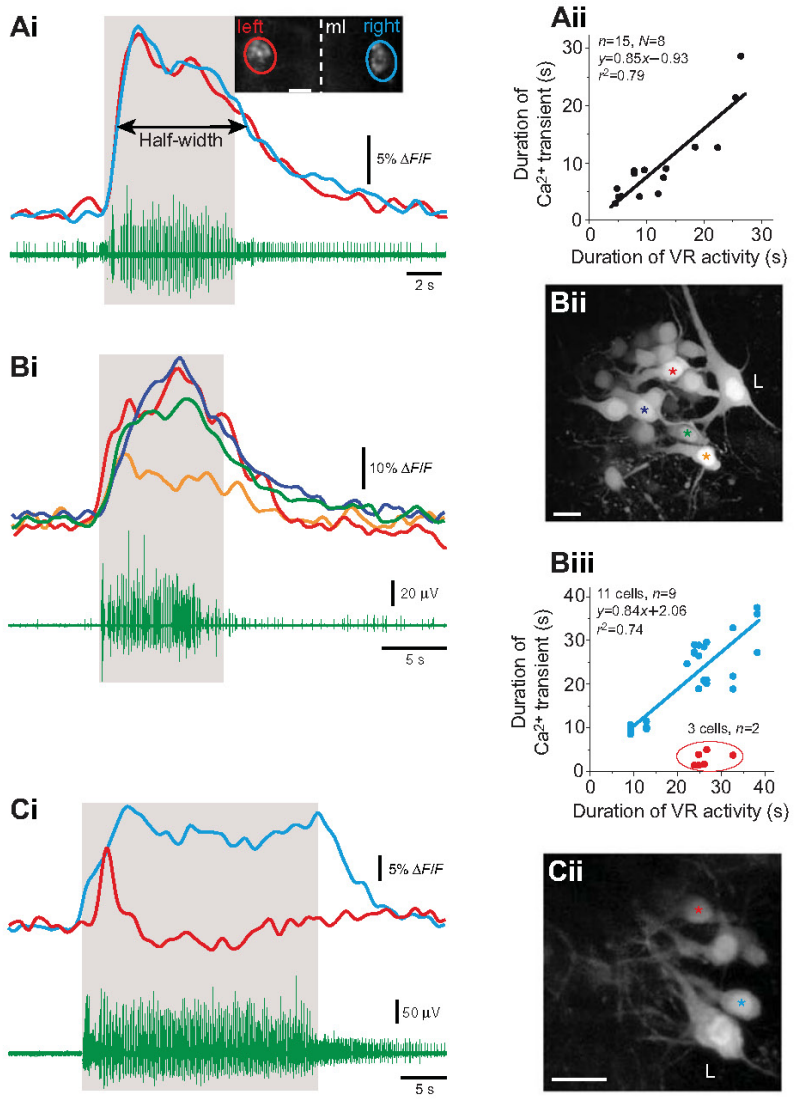

Fig. 3. Calcium dynamics in tentacle motoneurons during fictive locomotion. (Ai) Population Ca^{2+} transients (red and blue traces) of the tentacle motor nuclei on both sides (red and blue encircled areas in inset) during an episode of fictive swimming (gray area), indicated by the spinal ventral root (VR) burst discharge (green trace); motoneurons were retrogradely labeled with the Ca^{2+} sensor (Calcium Green-1 dextran) from the target muscle. (Aii) Scatter plot and linear regression of population Ca^{2+} response duration (half-width) as a function of the duration of rhythmic VR activity during n=15 swimming episodes in N=8 preparations (r^2=0.79, P<0.0001, Wilcoxon signed-rank test). (B,C) Ca^{2+} transients (color-coded traces in Bi, Ci) of individual tentacle motoneurons (color-matched asterisks in Bii, Cii) during episodes of fictive swimming (gray areas in Bi, Ci). (Biii) Scatter plot and linear regression of the Ca^{2+} response half-width in single neurons (blue dots) as a function of the duration of rhythmic VR activity (r^2=0.74, P<0.0001, Wilcoxon signed-rank test); note the small group of motoneurons (red dots) with highly phasic Ca^{2+} transients (red trace in Ci) during fictive swimming (no significant correlation, P>0.05). Data in B and C are from 14 cells during n=9 swimming episodes in N=3 preparations (31 data points). ml, midline. Scale bars are 100 µm in inset of Ai, 20 µm in Bii and Cii.

duration of the fictive swimming episodes (Fig. 3Aii). Thus, the duration of Ca^{2+} responses in the tentacle motor nuclei closely matches the duration of a swimming episode.

In a separate set of experiments, we determined the fraction and morphology of the activated tentacle motoneurons by recording Ca^{2+} responses of individual motoneurons (34 cells; n=9 swimming episodes in N=3 preparations; Fig. 3Bii,Cii). Ca^{2+} transients were encountered in 14 out of 34 retrogradely identified motoneurons during fictive swimming episodes (Fig. 3Bi,Ci). Responses were observed only in the population of medium-sized motoneurons with oval cell bodies (16.1±1.6 µm, 14 cells), whereas neither the subgroup of small motoneurons nor the one to two very large motoneurons displayed any locomotion-related responses (Fig. 3B,C). Based on the dynamics of the Ca^{2+} responses, the 14 responsive neurons could be separated into a majority of cells (11 cells; color-coded traces in Fig. 3Bi and blue trace in Fig. 3Ci) with a half-width of the transients that significantly correlated with the duration of the corresponding swimming episode (blue dots in Fig. 3Biii). In contrast, a few motoneurons (two swimming episodes in three neurons) exhibited Ca^{2+} responses that were highly transient and only present at the beginning of a swimming episode (red trace in Fig. 3Ci; red dots in Fig. 3Biii). However, the morphology of these neurons was indistinguishable and the size not significantly different from the size of those with the predominant response pattern. Thus, motoneurons responsible for tentacle motion during tadpole swimming appear to form a morphologically homogeneous group with Ca^{2+} response profiles that suggest the presence of either transient or sustained activity during locomotor episodes.

Dynamics of tentacle motor commands

To reveal the discharge profile of the motor commands that provoke tentacle movements during locomotor CPG activity, we made simultaneous recordings of a VR on one or both sides of the spinal cord, the TN on one side and the motion of the tentacle on the other side (Fig. 4A). During fictive swimming, indicated by an episode of burst activity in VRs (green and gray traces in Fig. 4B), the otherwise silent TN became active (black trace and firing rate

The Journal of Experimental Biology (2015) 00, 1-11 doi:10.1242/jeb.120824

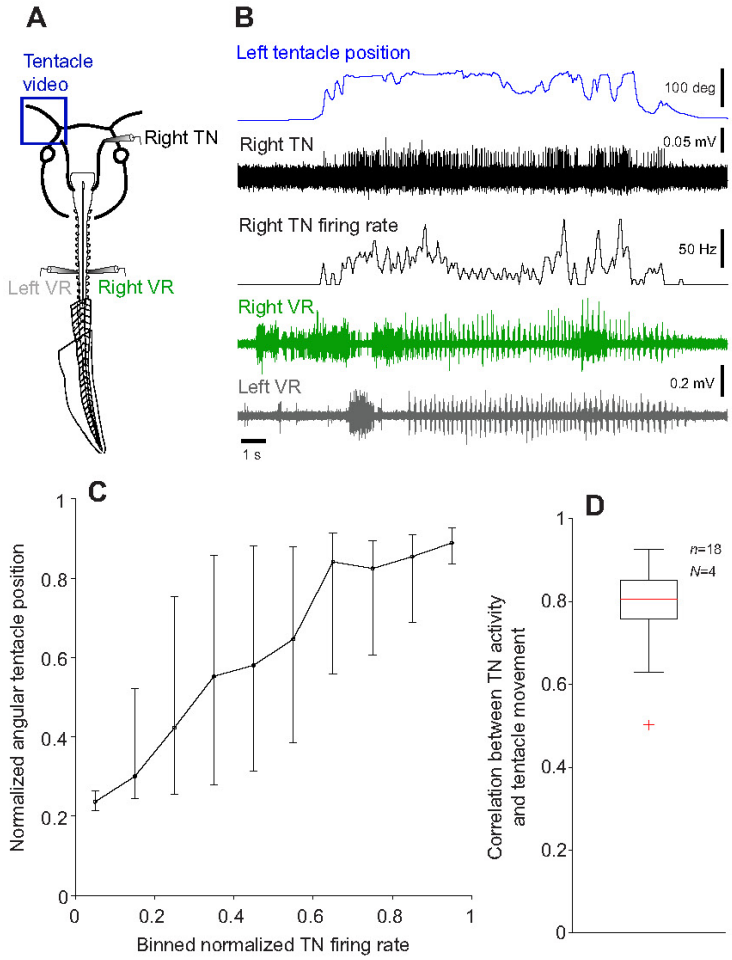

Fig. 4. Correlation between TN motoneuronal activity and tentacle movement during fictive locomotion. (A) Sketch depicting simultaneous video imaging of the left tentacle and electrophysiological recording of the right TN and bilateral spinal VRs in a semi-intact tadpole preparation. (B) Tentacle motion (blue trace), TN spike activity and instantaneous firing rate (black traces) and bilateral VR discharge (green and gray traces) during fictive swimming. (C) Median and 25th and 75th percentiles of normalized tentacle position plotted against normalized and binned TN firing rate of n=18 swimming episodes in N=4 preparations. (D) Boxplot illustrating the distribution of the correlation coefficients between the firing rate of the TN on one side and the movement of the tentacle on the other side (red cross indicates outliers) for the swimming episodes in C with a median of 0.81 (the distribution is significantly different from zero, P<0.001; Wilcoxon signed-rank test).

in Fig. 4B). In addition, the intact tentacle contralateral to the recorded TN was simultaneously retracted (blue trace in Fig. 4B). The similarity of tentacle motion and tentacle motor profiles (blue and black traces in Fig. 4B) was quantified by correlating the normalized position of the tentacle with the normalized firing rate of the contralateral TN (Fig. 4C). Normalized tentacle motion and contralateral TN firing rates were correlated with a coefficient ranging between 0.50 and 0.93 (median: 0.81; n=18 swim episodes in N=4 preparations; Fig. 4D). The distribution of correlation coefficients was significantly different from zero (P<0.001; Wilcoxon signed-rank test). Despite the variability in the movements of both tentacles (Fig. 1Ci), the distribution of correlation coefficients indicates that the firing pattern of the TN on one side faithfully predicts the motion profile of the tentacle on the other side.

Coupling properties of locomotor and tentacle motor activity

Locomotor influence on tentacle motion was studied by analyzing the coupling pattern between spinal and tentacle motor activity. Tadpole swimming is a fluctuating motor behavior in terms of duration and strength/speed, which is reflected during fictive locomotion by variable episode durations, burst frequencies and amplitudes (Combes et al., 2004). By comparing spinal VR and TN activity, we identified those parameters of the locomotor commands that are transmitted to the tentacle motor system. The most obvious of these parameters was the duration of the fictive swimming episode: the discharge in spinal VRs and in the TN closely matched in time (compare black with green traces in Fig. 5A), as indicated by the significant linear regression with a slope close to unity (Fig. 5B; r^2=0.94, P<0.0001, Wilcoxon signed-rank test, n=57 swim episodes in N=10 preparations). This agrees with the behavioral observation that the tentacles are retracted during the entire swimming event.

Alterations in swimming strength *in vivo* essentially derive from changes in the magnitude and frequency of tail excursions that in turn are represented *in vitro* by variations in the cycle frequency of the VR bursts and in the intra-burst firing rate (Combes et al., 2004). A spontaneous increase in spinal VR intra-burst discharge, represented by a larger integral of the firing rate (green traces in Fig. 5C) was accompanied by a similar increase in retraction angle of the tentacle (blue trace in Fig. 5C). With increasing locomotor strength from low to medium to high swimming amplitudes (Fig. 5D), the tentacle reached progressively more eccentric positions. In fact, the tentacle positions for the three levels of swimming strength were significantly different from each other (P<0.0001, Kruskal–Wallis test and *post hoc* comparisons; n=4 swimming episodes in N=3 preparations). The variation of position with swimming strength prompted us to compare the swimming

The Journal of Experimental Biology (2015) 00, 1-11 doi:10.1242/jeb.120824

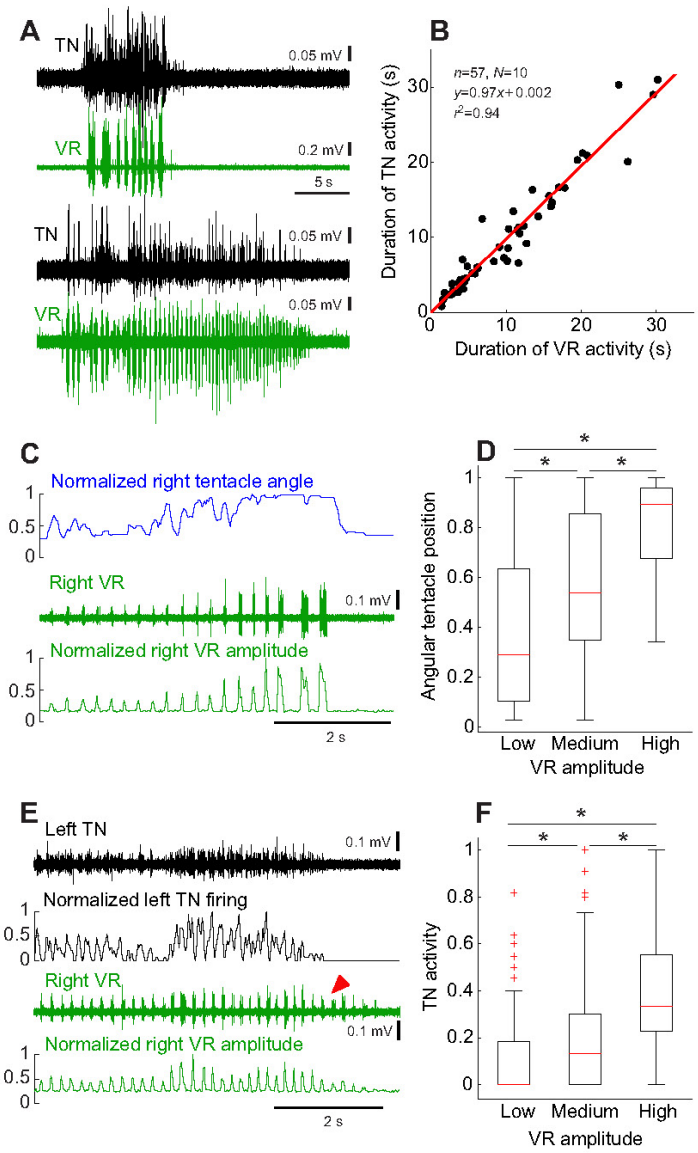

Fig. 5. Tentacle motor commands contain information about fictive swimming duration and amplitude. (A) TN discharge (black traces) and VR burst activity (green traces) during two fictive swimming episodes of different length in the same preparation. (B) Scatterplot and linear regression of TN discharge duration as a function of the duration of VR activity during n=57 swimming episodes in N=10 preparations (r^2=0.94). (C) Angular trajectory of the tentacle (normalized to maximal excursion, blue trace), ipsilateral VR activity with increasing burst amplitude (upper green trace) and integrated burst amplitudes (normalized to maximal value, lower green trace) during an episode of fictive swimming. (D) Boxplot of tentacle angular position as a function of VR burst amplitude; normalized VR burst amplitudes were binned into three levels (low, medium and high); normalized tentacle angular positions, obtained from n=4 swimming episodes in N=3 preparations, were significantly different between the three groups (P<0.0001; Kruskal–Wallis test and *post hoc* comparisons). (E) TN discharge (upper black trace), contralateral VR burst activity (upper green trace) and normalized TN and VR firing rate amplitudes (to maximal magnitude; lower black and green traces, respectively) during fictive swimming with modulated VR burst amplitudes. (F) Boxplot (red crosses indicate outliers) of TN firing rate as a function of VR burst amplitude; normalized VR burst amplitudes were binned into three levels (low, medium and high); normalized TN firing rate amplitudes – obtained from n=4 swimming episodes in N=3 preparations – were significantly different between the three groups (P<0.0001, Kruskal–Wallis test and *post hoc* comparisons).

strength (green traces in Fig. 5E) during a given locomotor episode with the rate of TN firing (black traces in Fig. 5E). Spontaneous alterations of VR burst amplitude caused a comparable modulation of the TN firing rates, with the latter discharge ceasing as soon as the VR bursting decreased below a particular level (red arrowhead in Fig. 5E). Pooling the data from four different swimming episodes in three preparations where the VR burst discharge frequency displayed a spontaneous modulation showed that the TN activities at the three levels of swimming strength were also significantly different from each other (Fig. 5F; P<0.0001, Kruskal–Wallis test with *post hoc* comparisons), with a more pronounced TN activity during stronger swimming.

While the previously described corollary discharge in extraocular motoneurons during rhythmic locomotion in *Xenopus* tadpoles is strictly phase coupled to the VR bursting in a 1:1 fashion (Lambert et al., 2012), the dynamics of tentacle motor commands appears to be more variable and temporally more complex (Fig. 6). To assess the coupling of TN spiking during episodes of fictive swimming as a function of the timing of VR bursts, we generated VR burst-triggered cumulative spike time histograms (see Materials and methods). Based on entropy statistics (Kajikawa and Hackett, 2005), recordings from 18 out of 31 swimming episodes in N=7 preparations (58%) showed significant phase coupling between spinal VR and TN discharge (Fig. 6A,B,D), while the TN discharge during 13 swim cycles displayed no coupling to the VR burst rhythm (Fig. 6C). In the group of phase-coupled recordings, a mono-phasic coupling (four out of 18; Fig. 6A) could be clearly distinguished from a bi-phasic pattern (five out of 18; arrowhead in Fig. 6Bii inset), while the remainder (nine out of 18) exhibited a phase coupling that could not be unambiguously distinguished as one or the other. The different coupling patterns during individual swimming bouts were summarized as circular plots, emphasizing the variability among the different coupling categories (Fig. 6Aiii–Ciii). Functionally, the mono- or bi-phasic timing of TN bursts (Fig. 6Aiii, Biii) suggests that

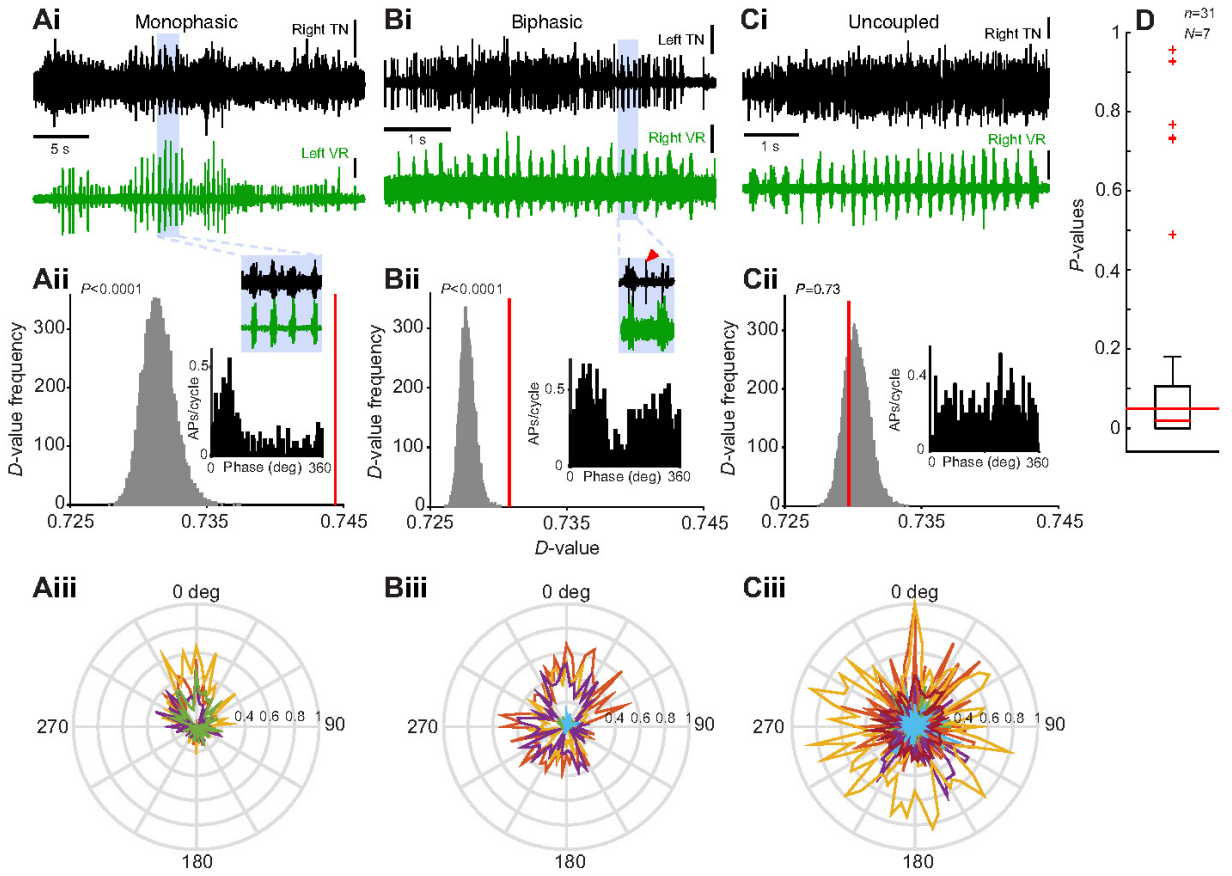

Fig. 6. Phase coupling between TN and VR activity during fictive locomotion. (A–C) TN discharge (black traces) and contralateral (Ai, Bi) or ipsilateral (Ci) VR burst activity (green traces); VR–TN coupling subdivides into mono-phasic (Ai), bi-phasic (red arrowhead in Bi) and uncoupled patterns (Ci) as indicated by the insets on an extended time scale (blue background); distribution of *D*-values (Aii, Bii, Cii) from re-shuffled inter-spike intervals (see Materials and methods) in the TN recording from the three examples (Ai, Bi, Ci) assessed the significance of phase coupling; the *D*-value from the original trace is indicated by the red vertical line; insets in Aii, Bii and Cii show the spike histograms of the TN discharge relative to the swimming phase. Circular plots in Aiii, Biii and Ciii summarize the distribution of TN spikes across VR cycles for individual swimming bouts (color coded). (D) Boxplot of the *P*-value distribution obtained from $n=31$ swimming episodes in $N=7$ preparations to assess the significance of phase coupling based on the *D*-value. Scale bars: Ai TN, 0.05 mV; VR, 0.2 mV, Bi TN, 0.2 mV; VR, 0.05 mV, Ci TN, 0.05 mV; VR, 0.1 mV.

the inputs to trigeminal motoneurons originate from one or both sides of the spinal cord during a particular recording. This might also explain the difficulty of assigning a particular phase relation to the coupling pattern in most cases (mono- versus bi-phasic), assuming a continuum between unilateral and bilateral locomotor corollary drive to tentacle motoneurons.

DISCUSSION

During fictive swimming in *Xenopus* tadpoles, a corollary discharge informs the tentacle motor system about ongoing locomotor activity. This intrinsic locomotor signal activates a discrete set of trigeminal motoneurons on each side of the rostral hindbrain that causes a symmetrical retraction of the appendages. The motor command encodes both duration and magnitude of the locomotor activity, thereby ensuring a reliable coupling between propulsive locomotion and tentacle motion. Given the phase coupling between trigeminal nerve discharge and spinal motor rhythm, the locomotor corollary discharge derives at least in part from the spinal central pattern generator (CPG) circuitry.

Function of tentacles

Xenopus laevis tadpoles possess a pair of mobile appendages between developmental stage 47 and 61 (Nieuwkoop and Faber, 1994), which contain Merkel cells and thus were suggested to play a role in touch reception (Ovalle, 1979; Ovalle et al., 1998). These tentacles are usually protruded forward but can be actively retracted into a lateral position (Fig. 1A). The use of appendages for mechanoreceptive exploration of the environment in these animals is useful for near-field orientation and navigation in the mostly murky aquatic environment in which these animals naturally live (Nieuwkoop and Faber, 1994). A similar mechanoreceptive role in mammals is performed by mechanoreceptive facial hairs – whiskers. Rodents use whisker movements for tactile exploration of the environment, for instance while walking along the wall of a cage (Hartmann, 2011). Similarly, tadpoles drift slowly with their tentacles touching the walls and floor of the tank (S.H., R.B., H.S. and B.P.C., unpublished observation), potentially collecting tactile information. However, several differences between the two structures exist: tentacles are formed by a single protrusion located on each side of the head, while whiskers are usually arranged in

groups (Berg and Kleinfeld, 2003). Moreover, whisker movements in rodents are controlled by multiple muscles (Berg and Kleinfeld, 2003), while tentacle motion in *Xenopus* tadpoles is exerted by a single muscle and a spring-like antagonistic mechanism (Ovalle et al., 1998). For tactile exploration, whiskers are actively moved ('whisking'), while tentacles are kept in an extended position. However, despite these morphological differences, amphibian tentacles appear to be similar, yet simpler versions of touch-receptive mammalian appendages.

Potential function of tentacle retraction

The presence of Merkel cells at a relatively high density in *Xenopus* tentacles (Ovalle, 1979) indicates a particular sensitivity of these structures to touch. Because of the hydrodynamic drag between the appendages and water, permanently extended tentacles could rhythmically stimulate these touch receptors during swimming-related head undulations. A tonic retraction of the tentacles during locomotor episodes might considerably reduce excessive stimulation of the sensory cells, in particular during strong and fast swimming. Under this assumption, locomotor corollary discharge-mediated tentacle retraction would minimize self-generated stimulation of the Merkel cells during swimming by reducing the water flow/pressure impinging on the tentacles. In a number of other sensory systems, corollary discharge similarly reduces or even suppresses self-generated sensory inputs (for review, see Crapse and Sommer, 2008); this also complies with the classical role of motor efference copies or corollary activity (von Holst and Mittelstaedt, 1950; Sperry, 1950). As a side effect, tentacle retraction during locomotion reduces the likelihood of mechanical damage to the tentacles that can reach a maximal length of 1 cm (~20% of larval body length).

In addition to this putative protective function, tentacle retraction might also improve the hydrodynamics of the tadpole. Appendage retraction streamlines the body shape, thereby facilitating energetically more efficient swimming (Crespi et al., 2013; Liu et al., 1997). This is particularly important during strong swimming, when protruded tentacles would cause a considerable drag and impair the sinusoidal motion of the head during swimming, specifically at those larval stages where these appendages are at their maximal length. In fact, a similar streamlining of the body shape is observed during tail-based swimming in other amphibians such as salamanders, where both forelimbs and hindlimbs are aligned to the body (Delvolvé et al., 1997) or in axolotl, where the external gills are retracted (D'Août and Aerts, 1997). Thus, locomotor-coupled head appendage or limb retractions in amphibians represent distinct behavioral reactions that improve the hydrodynamic signature and, in the case of retracted limbs during tail-based swimming, considerably enhance locomotor performance (Crespi et al., 2013). Such a strategy is not restricted to amphibians but occurs also during swimming in alligators (Manter, 1940; Fish, 1984) and 'terrestrial swimming' in sandfish lizards (Maladen et al., 2009) where the tail-based propulsion is accompanied by similar limb adductions as in salamanders (Delvolvé et al., 1997).

Origin of corollary discharge in trigeminal/tentacle motoneurons

The absence of propulsive movements and movement-related sensory feedback in semi-intact *Xenopus* preparations (Straka and Simmers, 2012) demonstrates that the coupling between locomotion and tentacle motion relies exclusively on intrinsic signals, i.e. corollary discharge from locomotor areas. Theoretically, these signals could derive from midbrain locomotor centers (Cabelguen et al., 2003; Saitoh et al., 2007) or from CPGs in the rostral spinal cord or from a combination of the two.

A spinal contribution of the corollary activity in tentacle motoneurons is supported by the presence of strict phase coupling of the TN burst discharge with the burst rhythm of the spinal VR on one (mono-phasic) or on both sides (bi-phasic; Fig. 6A,B) along with the highly correlated amplitudes of spinal VR and TN firing or tentacle motion. The absence of a clear VR–TN burst coupling in a number of experiments (Fig. 6C) might reflect the consequence of signal integration in a particular motoneuronal population that only becomes apparent in some experiments depending on the number and variety of recorded TN axons. Alternatively, or in addition, the ascending spinal locomotor corollary discharge in tentacle motoneurons, unlike in extraocular motoneurons (Lambert et al., 2012) might be supplemented by tonic signals from locomotor centers in the midbrain and/or hindbrain. In fact, midbrain neurons in the salamander *Notophthalmus viridescens*, for instance, display tonic activity during locomotion (Cabelguen et al., 2003), similar to that seen in the TN nerve during locomotor episodes. Even though the relative contributions of midbrain locomotor regions and spinal CPGs to the tentacle motor corollary discharge remain unclear, we hypothesize that both neuronal structures contribute to the trigeminal activation during locomotor activity.

Evolutionary origin of spinal–hindbrain coupling

While locomotion-related tentacle retraction potentially serves several distinct, not mutually exclusive purposes (see above), the coupling could be a vestige of the rostro-caudally distributed activity in the spinal cord-like nervous system of vertebrate ancestors during undulatory swimming (Fetcho, 1992; Wada, 1998). However, given the rather specialized structure and function of these rostral appendages, this notion appears too simplistic. The inherent linkage between the two motor systems rather suggests a particular functional role of tentacle retraction during swimming, which is not necessarily exclusive or in opposition with a pre-existing vestigial signaling pathway. Accordingly, ascending locomotor corollary discharges from the spinal CPG circuitry might represent a widely distributed signaling component within the brain during rhythmic locomotion and might influence numerous sensory and/or motor systems. Among the hindbrain motor systems currently known to receive spinal inputs are the extraocular system (Combes et al., 2008; Lambert et al., 2012; von Uckermann et al., 2013) and the trigeminal motor component (this study). Evidence for an even more widespread function arises from studies on spiny dogfish (Russell and Roberts, 1974) and larval *Xenopus* (Chagnaud et al., 2012b), in which connections from the spinal cord locomotor CPG to mechanosensory efferent neurons were demonstrated. Further hindbrain targets might include hindbrain nuclei in axolotl that cause a retraction of the gills during swimming (D'Août and Aerts, 1997).

Based on the various examples, we hypothesize that appendage retraction (e.g. limbs, tentacles, gills) during undulatory swimming is generally caused by locomotor corollary activity, which allows a fast and reliable coupling of independent motor behaviors with locomotion. Such a functional role expands the traditional concept of motor efference copies/corollary discharge in simply differentiating between external and self-generated sensory signals (Cullen, 2004, 2011). Accordingly, corollary discharge during locomotor activity appears to influence a large number of both sensory and motor systems throughout the brain, including the

trigeminal system, potentially optimizing locomotor performance and sensory perception (Chagnaud et al., 2012a). Depending on the type of motor behavior (rhythmic, task oriented), the effect of corollary activity might vary considerably (Crapse and Sommer, 2008; Cullen, 2014; King, 2013). Nonetheless, intrinsic coupling offers a convenient substrate for a context-dependent, direct linkage between otherwise discrete motor behaviors.

MATERIALS AND METHODS

Experiments were performed on semi-intact *in vitro* preparations of 33 larval *Xenopus* at stages 51–55 (Nieuwkoop and Faber, 1994) in compliance with the 'Principles of Animal Care' publication by the National Institutes of Health and the German law for animal protection (Tierschutzgesetz). Permission for the experiments was granted by the Regierung von Oberbayern (55.2-1-54-2531.3-18-10). All animals were obtained from the in-house breeding facility at the Biocenter-Martinsried of the LMU Munich.

Preparations

In all experiments, animals were first anesthetized in 0.02% 3-aminobenzoic acid ethyl ester (MS-222; Sigma-Aldrich Pharma Ltd, UK) in ice-cold frog Ringer solution (composition in mmol l^{-1}: NaCl, 75; KCl, 2; $CaCl_2$, 2; $MgCl_2$, 0.5; $NaHCO_3$, 25; glucose, 11: pH 7.4). The ventral part of the head/body, including the lower jaw and visceral organs, was carefully removed, leaving the tail attached to the head and the sensory-motor innervation of the tentacles intact. The skin covering the dorsal portion of the head was removed, the soft skull tissue opened and the forebrain disconnected. Preparations were transferred to a Petri dish (volume 5 ml) and fixed dorsal-side up to the Sylgard floor with insect pins. In some cases the spinal cord was exposed up to segment 20 and the VRs were transected bilaterally. The remaining, caudal part of the tail was firmly secured on both sides to the Sylgard floor with insect pins at the level of segments 21–25, with the remainder of the tail left free to perform undulatory swimming movements. After repeated rinsing in fresh Ringer solution, preparations were continuously superfused with oxygenated Ringer solution at a rate of 1.3–2.1 ml min^{-1}. The temperature of the bath solution was maintained at 17±0.5°C. Recordings lasted up to 5 h.

Tentacle motor behavior during spinal VR activity (i.e. fictive swimming, hereafter referred to as swimming) in these isolated preparations was quantified by video analyses of tentacle motion and/or recording the respective motor nerve discharge. For monitoring tentacle movements during fictive swimming, one or both tentacle(s) remained attached and innervated by the respective trigeminal nerve branch. Motor commands for tentacle movements were captured after further unilateral or bilateral isolation of the trigeminal motor nerve branch that innervates the tentacle muscle.

Behavioral analysis of tentacle motion

Movements of one or both tentacles during spinal locomotor activity (see below) were video-captured from the top in isolated preparations (n=8) with a CCD camera (Axiocam, Zeiss, Germany) with a resolution of 272×208 pixels at a rate of 20–50 frames s^{-1} either separately or in combination with the spike activity of the contralateral tentacle motor nerve. The motion trajectory of the tentacle was analyzed offline by manually tracking the distal yet still straight portion of the tentacle with respect to the base using the Vidana software (courtesy of Dr M. Hofmann). From the position coordinates, the angle of the tentacle relative to the longitudinal body axis was calculated in Matlab (MathWorks, Natick, MA, USA) and plotted as motion trajectory over time.

Electrophysiological recordings

Spontaneous or evoked locomotion in isolated tadpole preparations was recorded as bilaterally alternating rhythmic burst discharge in spinal VRs, termed fictive swimming (e.g. Combes et al., 2004). Multi-unit activity from one or two spinal VRs of segments 10–15 along with the discharge of one or both tentacle motor nerves (N=12) were recorded with individually adjusted glass suction electrodes, fabricated with a horizontal puller (P-97 Brown/Flaming, Sutter Instruments, Novato, CA, USA). The recorded neuronal activity was amplified (EXT 10-2F; npi electronics, Tamm, Germany), digitized at 10 kHz (CED 1401, Cambridge Electronic Design, Cambridge, UK), processed with commercial software (Spike 2, Cambridge Electronic Design), stored on a PC and analyzed off-line with custom-written scripts using Igor Pro (Wavemetrics, Tigard, OR, USA) or Matlab.

Data analysis

To compare the tentacle retraction on one side with the TN firing on the other side, we calculated the correlation coefficient after normalizing the angular tentacle position and the TN firing rate to their maximum for each swimming bout. The temporal relationship between rhythmic spinal VR and trigeminal motor activity was evaluated by comparing the duration of the concurrent discharge episodes, obtained from multi-unit recordings of at least one VR and one TN. These data were extracted from n=57 individual swimming episodes (these included only rhythmic alternating activity and no escape) in N=10 preparations and compared using a scatter plot and linear regression.

The degree and variation of swimming strength during fictive locomotion were estimated from integrals of the VR bursting in recordings of those locomotor episodes that showed a modulation of the swimming strength. In these traces, the swimming amplitude was calculated from integrals of VR bursts with a bin width of 30 ms (N=2 preparations) or with a bin width that matched the frame rate of simultaneously video-recorded tentacle motion (21 ms, N=3 preparations; 71 ms, N=1 preparation). Integrated and binned VR burst amplitudes were normalized to the maximal magnitude within a given swimming episode and were grouped according to amplitude into three categories (low, medium, high) indicating weak, medium and strong swimming. These three different levels were used to plot the normalized firing rate of the simultaneously recorded TN or the video-recorded tentacle position. Significance between the three levels was tested using a Kruskal–Wallis test, followed by *post hoc* multiple sample comparisons (Wilcoxon signed-rank tests).

To determine potential phase correlations between swimming (i.e. VR activity) and TN activity, the instantaneous firing rate of the VR bursts was calculated from recordings of 31 locomotor episodes in N=7 preparations. The phase relationship between the TN discharge and VR bursts was calculated and plotted as a histogram of spikes with a bin size of 5 deg (one burst cycle=360 deg). The histogram was normalized by dividing the spike count by the number of swimming cycles. Histogram data were displayed as circular plots, with their maxima aligned at 0 deg. To assess whether the distribution of spikes in the TN was phase coupled to unilateral or bilateral VR activity, a previously described procedure was employed (Kajikawa and Hackett, 2005). Briefly, the entropy (D score) of the plotted spike time histogram was calculated as the difference between unity and a normalized entropy measure (D=1−E/E_{max}). D may vary from 0 to 1, with 0 being no phase coupling (probability of firing is equally distributed over the entire swimming cycle) and 1 being maximal phase coupling, independent of the underlying spike time distribution. In order to determine the significance of D, the inter-spike intervals were reshuffled 10,000 times for each swimming episode and a D-value was calculated for each repetition (Kajikawa and Hackett, 2005). The D-value from the initial analysis was then compared with this distribution of reshuffled D-values by calculating the proportion of those that were equally large or larger than the original value. Phase coupling was considered significant if this proportion was smaller than 0.05 (i.e. one-tailed probability with α=0.05).

Anatomical identification of tentacle motoneurons

To assess the location and spatial arrangement of tentacle motoneurons in the hindbrain, fluorescent tracers (Alexa Fluor dextran 488, 546; Life Technologies, Carlsbad, CA, USA) and biocytin (Sigma-Aldrich) were applied to different portions of the trigeminal nerve in isolated *in vitro* preparations (Straka et al., 2001). Crystals of the respective tracer, melted

to the tip of an injection needle, were inserted into various trigeminal nerve branches or the main trigeminal nerve root. After overnight incubation in oxygenated Ringer solution at 14°C, preparations were fixed in 4% paraformaldehyde in 0.1 mol l^{-1} phosphate buffer (PB, pH 7.4) at 10°C for 5–12 h and rinsed (3×10 min) in cold 0.1 mol l^{-1} phosphate-buffered saline (PBS, pH 7.4). In experiments where biocytin was applied, preparations were fixed and rinsed as described above and kept in Dent's solution [80% methanol, 20% dimethylsulfoxide (DMSO)] at room temperature for 12–14 h, transferred into 100% methanol and stored at −80°C for at least 1 h. Then, preparations were rehydrated at room temperature in 70%, 50% and 35% methanol solutions in distilled water for 1 h each, followed by 0.1 mol l^{-1} PBS (3×30 min), incubated in a 1:200 solution of streptavidin-Cy2 (Dianova, Germany) in 0.1 mol l^{-1} PBS for 2 h and rinsed in PBS (3×30 min). The brainstem of all preparations was removed, cleaned of surrounding tissue, mounted on slides and coverslipped with Vectashield (Vector Laboratories, Burlingame, CA, USA). Retrogradely labeled neurons and afferent nerve terminations were reconstructed from stacks of optical sections (1.5–3 µm) obtained from a confocal microscope (SP5, Leica, Germany). In order to map the position of retrogradely labeled motoneurons onto the rhombomeric scaffold, preparations were additionally scanned with an illumination wavelength of 633 nm, outlining the spatial arrangement of the rhombomeres (r). *Z*-axis projections, image processing and quantification of neuronal numbers were carried out using the Fiji software package (http://fiji.sc/wiki/index.php/Fiji).

Imaging of Ca^{2+} transients in tentacle motoneurons

Tentacle motoneurons were retrogradely labeled 1–2 days prior to the experiment with Calcium Green-1 dextran (Life Technologies) by applying crystals of this Ca^{2+} sensor to the peripheral part of the tentacle motor nerve. Imaging of Ca^{2+} transients was performed with a confocal scanning microscope (LSM 700, Carl Zeiss, Germany) in the presence and absence of fictive locomotor activity. To prevent potential movement artifacts during imaging, all residual muscular elements of the isolated preparation were removed, except for the most caudal portion of the tail, which was left free to perform swimming movements (see above). Images were acquired at a rate of 5–10 frames s^{-1} (ZEN black, Carl Zeiss, Germany), stored and analyzed *post hoc*. Image analysis was performed off-line using the Fiji software package and custom-written scripts in Igor Pro. Background fluorescence was subtracted and bleaching was corrected using a linear regression algorithm. All data are presented as relative changes in fluorescence ($\Delta F/F$). The duration of Ca^{2+} transients were determined as the time at half-maximal amplitude of the fluorescence change (half-width) during a given swimming episode.

Acknowledgements

The authors thank Dr M. Hofmann for the Vidana software and D. Wickmaier for contributions to initial experiments.

Competing interests

The authors declare no competing or financial interests.

Author contributions

S.H., R.B., H.S. and B.P.C. planned the experiments, S.H., R.B. and B.P.C. acquired and analyzed the data, S.H., R.B., H.S. and B.P.C. wrote the manuscript.

Funding

Financial support was provided by the German Science Foundation [CRC870 to B.P.C. and H.S.; RTG1373 to R.B.] and the Graduate School of Systemic Neurosciences [to S.H.].

References

Berg, R. W. and Kleinfeld, D. (2003). Rhythmic whisking by rat: retraction as well as protraction of the vibrissae is under active muscular control. *J. Neurophysiol.* **89**, 104-117.

Bramble, D. and Carrier, D. (1983). Running and breathing in mammals. *Science* **219**, 251-256.

Cabelguen, J.-M., Bourcier-Lucas, C. and Dubuc, R. (2003). Bimodal locomotion elicited by electrical stimulation of the midbrain in the salamander *Notophthalmus viridescens*. *J. Neurosci.* **23**, 2434-2439.

Cannone, A. and Kelly, P. (1977). The tentacles of *Xenopus laevis* tadpoles - evidence for a mechanoreceptive role. *S. Afr. Med. J.* **52**, 407.

Chagnaud, B. P., Simmers, J. and Straka, H. (2012a). Predictability of visual perturbation during locomotion: implications for corrective efference copy signaling. *Biol. Cybern.* **106**, 669-679.

Chagnaud, B. P., Banchi, R. and Straka, H. (2012b). Spinal corollary discharge informs mechanoreceptor organs about frequency and duration of locomotor activity. In *Neuroscience 2012 Abstracts* (ed. S. F. Neuroscience). New Orleans: online, 470.01.

Combes, D., Merrywest, S. D., Simmers, J. and Sillar, K. T. (2004). Developmental segregation of spinal networks driving axial- and hindlimb-based locomotion in metamorphosing *Xenopus laevis*. *J. Physiol.* **559**, 17-24.

Combes, D., Le Ray, D., Lambert, F. M., Simmers, J. and Straka, H. (2008). An intrinsic feed-forward mechanism for vertebrate gaze stabilization. *Curr. Biol.* **18**, R241-R243.

Crapse, T. B. and Sommer, M. A. (2008). Corollary discharge across the animal kingdom. *Nat. Rev. Neurosci.* **9**, 587-600.

Crespi, A., Karakasiliotis, K., Guignard, A. and Ijspeert, A. J. (2013). Salamandra robotica II: an amphibious robot to study salamander-like swimming and walking gaits. *IEEE Trans. Robotic.* **29**, 308-320.

Cullen, K. E. (2004). Sensory signals during active versus passive movement. *Curr. Opin. Neurobiol.* **14**, 698-706.

Cullen, K. E. (2011). The neural encoding of self-motion. *Curr. Opin. Neurobiol.* **21**, 587-595.

Cullen, K. E. (2014). The neural encoding of self-generated and externally applied movement: implications for the perception of self-motion and spatial memory. *Front. Integr. Neurosci.* **7**, 108.

D'Août, K. and Aerts, P. (1997). Kinematics and efficiency of steady swimming in adult axolotls (*Ambystoma mexicanum*). *J. Exp. Biol.* **200**, 1863-1871.

Davis, W. J., Mpitsos, G. J. and Pinneo, J. M. (1974). The behavioral hierarchy of the mollusk *Pleurobranchaea*. *J. Comp. Physiol. A* **90**, 225-243.

Delvolvé, I., Bem, T. and Cabelguen, J.-M. (1997). Epaxial and limb muscle activity during swimming and terrestrial stepping in the adult newt, *Pleurodeles waltl*. *J. Neurophysiol.* **78**, 638-650.

Earhart, G. M. (2013). Dynamic control of posture across locomotor tasks. *Mov. Disord.* **28**, 1501-1508.

Fetcho, J. R. (1992). The spinal motor system in early vertebrates and some of its evolutionary changes. *Brain Behav. Evol.* **40**, 82-97.

Fish, F. E. (1984). Kinematics of undulatory swimming in the American alligator. *Copeia* **1984**, 839-843.

Fox, H. (1999). Barbels and barbel-like tentacular structures in sub-mammalian vertebrates: a review. *Hydrobiologia* **403**, 153-193.

Hartmann, M. J. Z. (2011). A night in the life of a rat: vibrissal mechanics and tactile exploration. *Ann. N. Y. Acad. Sci.* **1225**, 110-118.

Kajikawa, Y. and Hackett, T. A. (2005). Entropy analysis of neuronal spike train synchrony. *J. Neurosci. Methods* **149**, 90-93.

King, W. M. (2013). Getting ahead of oneself: anticipation and the vestibulo-ocular reflex. *Neuroscience* **236**, 210-219.

Kovac, M. P. and Davis, W. J. (1980). Neural mechanism underlying behavioral choice in *Pleurobranchaea*. *J. Neurophysiol.* **43**, 469-487.

Lambert, F. M., Combes, D., Simmers, J. and Straka, H. (2012). Gaze stabilization by efference copy signaling without sensory feedback during vertebrate locomotion. *Curr. Biol.* **22**, 1649-1658.

Liu, H., Wassersug, R. and Kawachi, K. (1997). The three-dimensional hydrodynamics of tadpole locomotion. *J. Exp. Biol.* **200**, 2807-2819.

Maladen, R. D., Ding, Y., Li, C. and Goldman, D. I. (2009). Undulatory swimming in sand: subsurface locomotion of the sandfish lizard. *Science* **325**, 314-318.

Manter, J. T. (1940). The mechanics of swimming in the alligator. *J. Exp. Zool.* **83**, 345-358.

Maricich, S. M., Wellnitz, S. A., Nelson, A. M., Lesniak, D. R., Gerling, G. J., Lumpkin, E. A. and Zoghbi, H. Y. (2009). Merkel cells are essential for light-touch responses. *Science* **324**, 1580-1582.

Nieuwkoop, P. D. and Faber, J. (1994). *Normal Table of Xenopus laevis (Daudin). A Systematical and Chronological Survey of the Development from the Fertilized Egg till the End of Metamorphosis*. New York: Garland Publishing.

Ovalle, W. K. (1979). Neurite complexes with Merkel cells in larval tentacles of *Xenopus laevis*. *Cell Tissue Res.* **204**, 233-241.

Ovalle, W. K., Shinn, S. L. and Nahirney, P. C. (1998). Ultrastructure of the larval tentacle and its skeletal muscle in *Xenopus laevis*. *Tissue Cell* **30**, 216-225.

Poulet, J. F. A. and Hedwig, B. (2007). New insights into corollary discharges mediated by identified neural pathways. *Trends Neurosci.* **30**, 14-21.

Russell, I. J. and Roberts, B. L. (1974). Active reduction of lateral-line sensitivity in swimming dogfish. *J. Comp. Physiol.* **94**, 7-15.

Saitoh, K., Ménard, A. and Grillner, S. (2007). Tectal control of locomotion, steering, and eye movements in lamprey. *J. Neurophysiol.* **97**, 3093-3108.
Sillar, K. T. and Roberts, A. (1988). A neuronal mechanism for sensory gating during locomotion in a vertebrate. *Nature* **331**, 262-265.
Sommer, M. A. and Wurtz, R. H. (2008). Brain circuits for the internal monitoring of movements. *Annu. Rev. Neurosci.* **31**, 317-338.
Sperry, R. W. (1950). Neural basis of the spontaneous optokinetic response produced by visual inversion. *J. Comp. Physiol. Psychol.* **43**, 482-489.
Straka, H. and Simmers, J. (2012). *Xenopus laevis*: An ideal experimental model for studying the developmental dynamics of neural network assembly and sensory-motor computations. *Dev. Neurobiol.* **72**, 649-663.
Straka, H., Baker, R. and Gilland, E. (2001). Rhombomeric organization of vestibular pathways in larval frogs. *J. Comp. Neurol.* **437**, 42-55.
von Holst, E. and Mittelstaedt, H. (1950). Das Reafferenzprinzip. *Naturwissenschaften* **37**, 464-476.
von Uckermann, G., Le Ray, D., Combes, D., Straka, H. and Simmers, J. (2013). Spinal efference copy signaling and gaze stabilization during locomotion in juvenile *Xenopus* frogs. *J. Neurosci.* **33**, 4253-4264.
Wada, H. (1998). Evolutionary history of free-swimming and sessile lifestyles in urochordates as deduced from 18S rDNA molecular phylogeny. *Mol. Biol. Evol.* **15**, 1189-1194.
Wada, N., Hori, H. and Tokuriki, M. (1993). Electromyographic and kinematic studies of tail movements in dogs during treadmill locomotion. *J. Morphol.* **217**, 105-113.
Wassersug, R. J. and Hoff, K. (1985). The kinematics of swimming in anuran larvae. *J. Exp. Biol.* **119**, 1-30.

Highlighted Article: During swimming in *Xenopus* tadpoles, a locomotor corollary discharge is transmitted to the trigeminal nucleus, which causes retraction of the tentacles to streamline body shape and/or prevent sensory reafference.

Spinal corollary discharge modulates motion sensing during vertebrate locomotion

Boris P. Chagnaud, **Roberto Banchi**, John Simmers and Hans Straka
B.P.C and **R.B** contributed equally to this work

This manuscript was submitted to *Nature Communication* and it is currently under revision in this journal.

Contributions of R.B

- Design of the experiments together with BPC.
- Anatomical part of the study (Fig. 2)
- Establishment of the *in-vitro* preparation for calcium imaging during fictive swimming and techniques for backfilling of efferent neurons of the vestibular and lateral line system.
- Calcium imaging of efferent neurons during fictive swimming (Fig. 2).
- Duration encoding in the locomotor corollary discharge to the efferent nucleus (Fig. 3A).
- Swimming intensity and effects on the spinal corollary discharge (Fig. 3G).
- Ablation studies and sequential spinal cord activity recordings to reveal the origin of the locomotor corollary discharge together with BPC (Fig. 4).
- Developing of the *en-passant* electrophysiological technique for recordings of afferent-efferent activity in the intact vestibular-lateral line system.
- Corollary discharge induced lateral line peripheral adaptation during locomotion (Fig. 5).
- Writing and revising, together with all other authors.

Spinal corollary discharge modulates motion sensing during vertebrate locomotion

Boris P. Chagnaud[1,*,+], **Roberto Banchi**[1,2,*], John Simmers[3] and Hans Straka[1]

[1]Department Biology II, Ludwig-Maximilians-University Munich, Planegg-Martinsried, Germany

[2]Graduate School of Systemic Neurosciences, Ludwig-Maximilians-University Munich, Planegg-Martinsried, Germany

[3]Université de Bordeaux, Institut de Neurosciences Cognitives et Intégratives d'Aquitaine, CNRS UMR 5287, 33076 Bordeaux, France

[*] BPC and RB contributed equally to this work

Key words: spinal corollary discharge, efference copy, mechanosensory efferent innervation, sensory-motor integration, hair cell systems, inner ear, lateral line, locomotion

Acknowledgments:

The authors thank Haike Dietrich for critically reading and three anonymous reviewers for comments and suggestions that significantly improved the manuscript. RB received support from the GRK 1373 of the German Science Foundation. Research support was provided by the German Science Foundation (CRC 870 to BPC and HS) and the Bayerisch-Französisches Hochschulzentrum (HS and JS).

Author contributions:

BPC and RB conducted experiments. BPC and RB analyzed the data. BPC, RB, JS and HS wrote the paper.

Abstract

During active movements, neural replicas of the underlying motor commands may assist in adapting motion-detecting sensory systems to an animal's own behavior. The transmission of such motor efference copies to the mechanosensory periphery offers a potential predictive substrate for diminishing sensory responsiveness to self-motion during vertebrate locomotion. Here, we demonstrate that shared efferent neural pathways to hair cells of vestibular endorgans and lateral line neuromasts in larval *Xenopus* express cyclic impulse bursts during swimming activity that are directly driven by spinal cord locomotor circuitry. Despite common efferent innervation and discharge patterns, afferent signal encoding at the two mechanosensory peripheries is influenced differentially by the efference copy signal, reflecting the different organization of body/water motion detecting processes in the vestibular and lateral line systems. The resultant overall gain reduction in sensory signal encoding in both cases, which likely prevents overstimulation, constitutes a dynamic adjustment to the altered stimulus statistics during locomotion.

Introduction

The efficient encoding of sensory stimuli requires matching the sensitivity of neural coding processes to ongoing variations in stimulus statistics [1-3]. A particularly relevant example of a sensory system that experiences a wide range of constantly altering stimulus amplitudes and frequencies is the vestibular system, the major sensor of body motion in vertebrates [4]. Vestibular endorgans decompose an animal's movement into spatio-temporal vector components as a prerequisite for correct visual orientation, postural control and spatial navigation [5]. Accordingly, the accurate sensing of body motion-derived stimuli and their processing within the CNS depends critically on neuronal computations that ensure the optimal encoding of static and changing head/body positions in space during both passive and active movement [6]. Locomotor activity thus poses a particular challenge for the vestibular system given the necessity to detect and encode a wide dynamic range of body motion to which the coding process must adapt.

A convenient way for mechanosensory encoding to be adaptively adjusted during self-motion is through the employment of corollary discharge or efference copies originating from the locomotor neural centers themselves. The predictive nature of these intrinsic feed-forward signals is well suited to inform associated sensory systems at various levels of the nervous system about impending and/or ongoing motor activity [7-10]. In this context, vertebrates possess a highly suitable neuronal substrate for a peripheral gain control mechanism that can tune hair cell sensitivity and adapt afferent encoding in the movement-detecting periphery of both the vestibular and lateral line sensory systems [11,12]. Populations of hindbrain efferent neurons innervate the hair cells and primary afferent fibers of vestibular endorgans, and exclusively the hair cells of lateral line neuromasts [11,13-15]. Moreover, for lateral line neuromasts - the sensors of water displacement in fish and aquatic amphibians - the efferent innervation is already known to affect afferent neuron discharge during locomotion-related behavior [16-19], although the origin and precise nature of the transmitted efferent signal thus far remain unknown.

Although various aspects of vestibular efferent pathway activity and its influence on inner ear endorgan receptors have been described in both anamniote [20-24] and amniote vertebrates [25-29], the findings have been divergent and even contradictory when compared across different experimental approaches or species. For instance, the effect of direct vestibular efferent activation on vestibular afferents has been reported to be exclusively excitatory in monkeys and fish, both excitatory and inhibitory in frogs [30], and at variance with

the consistently reported inhibitory efferent influence on afferent fiber discharge in the lateral line system [18,19]. Furthermore, although vestibular efferents have been postulated to convey signals related to anticipated head/body motion, emotional states or ongoing sensory stimulation [31,32], there has hitherto been no conclusive demonstration of a clear causal relationship between vestibular efferent firing patterns and altered afferent signaling during an identified natural behavior. Thus, despite a prolonged accumulation of disparate morpho-physiological evidence, a general functional picture of the vestibular efferent system and its impact on mechanosensory encoding has remained obscure.

Here, we provide direct evidence in larval *Xenopus* frogs that ascending corollary discharge signals originating from CPG circuitry in the spinal cord are conveyed to mechanosensory efferent neurons of both the vestibular and lateral line systems during rhythmic locomotor activity. The phase-coupled discharge of these efferent pathways transmits the temporal structure of the locomotor CPG pattern and causes an overall gain reduction in afferent encoding of concomitant sensory inputs to both systems.

Results

Mechanoreceptor efferent neurons are rhythmically active during locomotion

The neural correlate of undulatory tail-based swimming in *Xenopus* tadpoles is expressed as spontaneous, left-right alternating impulse bursts in spinal ventral roots (vr) of semi-isolated *in vitro* preparations (Fig. 1a-e). Such episodes of so-called 'fictive locomotion' typically consist of an initial irregular discharge at episode onset (black traces in Fig. 1b,c) followed by a more regular, bilaterally symmetrical vr burst rhythmicity (Fig. 1b,d) that persists for up to tens of seconds at a frequency of 2 to 8 Hz[33].

Single- and multi-unit recordings of the central severed ends of the anterior (AVN) or posterior branch (PVN) of the vestibular (VIIIth cranial) nerve (Fig. 1a) revealed the occurrence of locomotor activity-timed discharge in both of these otherwise silent mechanosensory nerves (Fig. 1b-e; Supplemental Fig. 1b,c). Following a short tonic firing at swim episode onset (red traces in Fig. 1b,c), the two vestibular nerve branches displayed sustained rhythmic discharge that was closely timed with spinal vr motor bursting on the same side of the cord (dashed vertical lines in Fig. 1d,e; Supplemental Fig. 1b,c). The strict in-phase coordination of AVN and PVN discharge with ipsilateral vr burst activity and their out-of-phase relationship with contralateral vr bursts was confirmed by circular plot analysis

of instantaneous vr firing relative to spiking in both vestibular nerves recorded on the same (PVN, blue in Fig. 1f) or opposite (AVN, red in Fig. 1f and Supplemental Fig. 1d,e) side. It is noteworthy, however, that in many preparations the predominant ipsilateral coupling between spinal vr and vestibular/lateral line nerve activity could be transiently replaced by a bi-phasic pattern where mechanosensory nerve discharge occurred in phase with the rhythmic vr bursts on both cord sides (see AVN recording in Fig. 1d and Supplemental Fig. 1b).

An identical coupling relationship with spinal vr bursting was also observed for the anterior (ALLN) and posterior nerves (PLLN) of the neighboring lateral line system during fictive locomotion (Supplemental Fig. 1f-j), consistent with earlier reports on the activation of lateral line efferent fibers during swimming in both *Xenopus* and dogfish [16,17,19]. Significantly, however, the coupling of lateral line (as well as vestibular) nerve activity with spinal vr bursts observed in our motionless semi-isolated preparations extends on these previous studies by excluding sensory feedback signals as a potential source of the rhythmic efferent signal during locomotion. Moreover, this common locomotor influence provided us with the unique opportunity to explore in parallel and directly compare the efferent control of the two co-existing mechanosensory systems under the same experimental conditions within the same animal.

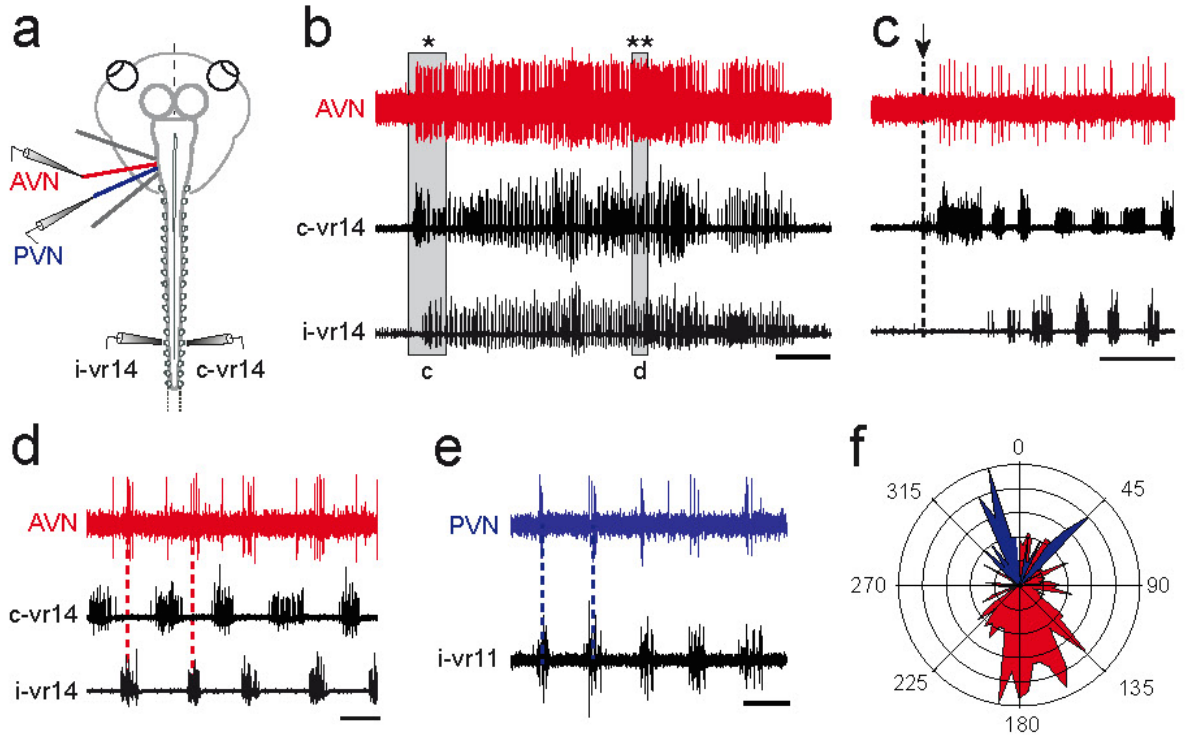

Figure 1. Locomotor-related neural activity in vestibular nerve efferent neurons in *Xenopus* tadpoles. a-d, Episodes of spontaneous fictive swimming in semi-isolated *in vitro* preparations (a), recorded as multiple-unit impulse discharge (b-d) in the left (ipsilateral) and right (contralateral) ventral roots (i-vr and c-vr, respectively; black traces) of spinal segment 14 together with the central cut portion of the left anterior vestibular (VIIIth) nerve branch (AVN, red trace). The initial discharge at episode onset (*) and subsequent regular (**) vr bursting (shaded areas in b) are shown on an extended time scale in c and d, respectively. After mostly tonic firing at swim episode onset (c), the AVN activity develops into rhythmic bursting occuring in phase with locomotor bursts in the ipsilateral vr (red dashed lines in d). e, Different preparation showing coincident burst coupling between ipsilateral vr11 and the posterior vestibular nerve (PVN) branch (blue dashed lines) during an episode of fictive swimming. f, Polar plot quantifying the phase relationship between the c-vr/AVN and i-vr/PVN activity shown in d,e; AVN (red area) and PVN bursts (blue area) are respectively approximately out-of-phase (i.e., angle towards 180°) or in phase (angle towards 0°) with the i-vr burst rhythm. Calibration bars: 5 s in b, 1 s in c, 0.2 s in d,e.

Although mechanosensory afferent axons considerably outnumber the relatively small efferent fiber population in the vestibular and lateral line nerves [15], the rhythmic bursting observed in these cranial nerves during fictive swimming could be directly established to reflect a central activation of individual efferent neurons (ENs) by locomotor-related signals. Support for this conclusion derived from simultaneous recordings of the central and peripheral regions of the vestibular and lateral line nerves after an intervening transection close to their exit from the brainstem (for example, see configuration for PLLN recordings in Supplemental Fig. 2a). Axons in the central stump displayed rhythmic burst discharge in phase with fictive swimming (blue trace in Supplemental Fig. 2b) but otherwise remained silent at rest or during hydrodynamic stimulation of the skin (red trace in Supplemental Fig. 2b). In contrast, spontaneous firing occurred in the detached distal nerve segment at rest as well as during fictive locomotion, but was strongly sensitive to mechanical skin stimulation (green trace in Supplemental Fig. 2b). These separate discharges recorded peripherally and centrally from vestibular and lateral line nerves thus corresponded to the dissociated activities of mechanoreceptor afferent and efferent axons, respectively.

In a next step, the central nervous location and relative positions of vestibular and lateral line ENs was determined by double retrograde labeling with fluorescent tracers (Alexa Fluor 488 and 546 dextran) applied to different combinations of the two VIIIth nerve branches and the two lateral line nerves in individual preparations (Fig. 2a-d). Whereas vestibular and lateral line afferent axons terminated separately in adjacent areas of the hindbrain (red and green labeled fibers respectively in Fig. 2a,b), the somata of conjointly labeled ENs formed overlapping subgroups of 5-12 cells/preparation (AVN: 7.8 ± 4.6, n = 20; PVN: 7.7 ± 1.5, n = 3; ALLN: 7.8 ± 2.8, n = 10; PLLN: 9.2 ± 3.4, n = 6) aligned ipsilaterally in rhombomeres (r) 4 and 6 (Fig. 2a-d). The dendritic tree of this bipartite cell population extended predominantly into the ipsilateral reticular formation, although a few branches were found to cross the midline (arrow heads in Fig. 2d). While ENs with axonal projections in the two vestibular nerve branches and the PLLN were confined to single segments (r4 and r6, respectively), ALLN efferents form a larger subgroup (~70%) in r4 and a smaller population in r6, wherein they intermingled with PLLN efferent neuron somata. Moreover, the majority (~80%) of the ENs in r4 expressed double-labeling (see arrowheads in Fig. 2c) after combined tracer application to different combinations of the AVN, PVN and ALLN. The extent of this double-labeling was unrelated to mechanosensory nerve branch identity,

complying with a previous proposal that individual ENs project to multiple hair cell targets [15,34].

To determine the proportion of neurons within the combined mechanosensory efferent population that become activated during locomotion, we used multi-cellular Ca^{2+}-imaging to monitor intrasomatic Ca^{2+}-fluctuations associated with electrophysiologically recorded fictive swimming (Fig. 2e). EN cell bodies in r4 were retrogradely loaded with a Ca^{2+}-sensor (Calcium Green-1 dextran) from the AVN (Fig. 2f; see Methods). During episodes of both evoked and spontaneous fictive swimming (red and green * in Fig. 2f), all backfilled cells (32 ENs in 7 preparations) exhibited coincident fluorescence changes with onsets that were strictly timed to the onset of rhythmic spinal vr bursting (Fig. 2f,g). The duration of these responses, measured as the half-width of the overall Ca^{2+}-signal (Fig. 2g), was also closely correlated with the duration of the corresponding fictive swimming episode (Fig. 2h). Moreover, the dynamics of the Ca^{2+}-responses of different EN pairs (n = 20 from a total of 25 cells) during a given episode were very similar and highly correlated (Fig. 2i), suggesting a common underlying synaptic drive. Given the projection of individual ENs to multiple peripheral targets, and the close similarities of their Ca^{2+}-transients (Fig. 2f,i) and firing patterns during rhythmic vr bursting (Fig. 1d,e; Supplemental fig. 1b,c,i,j), it is probable that the entire efferent population participates in conveying a copy of spinal CPG activity to the inner ear and lateral line sensory periphery during swimming.

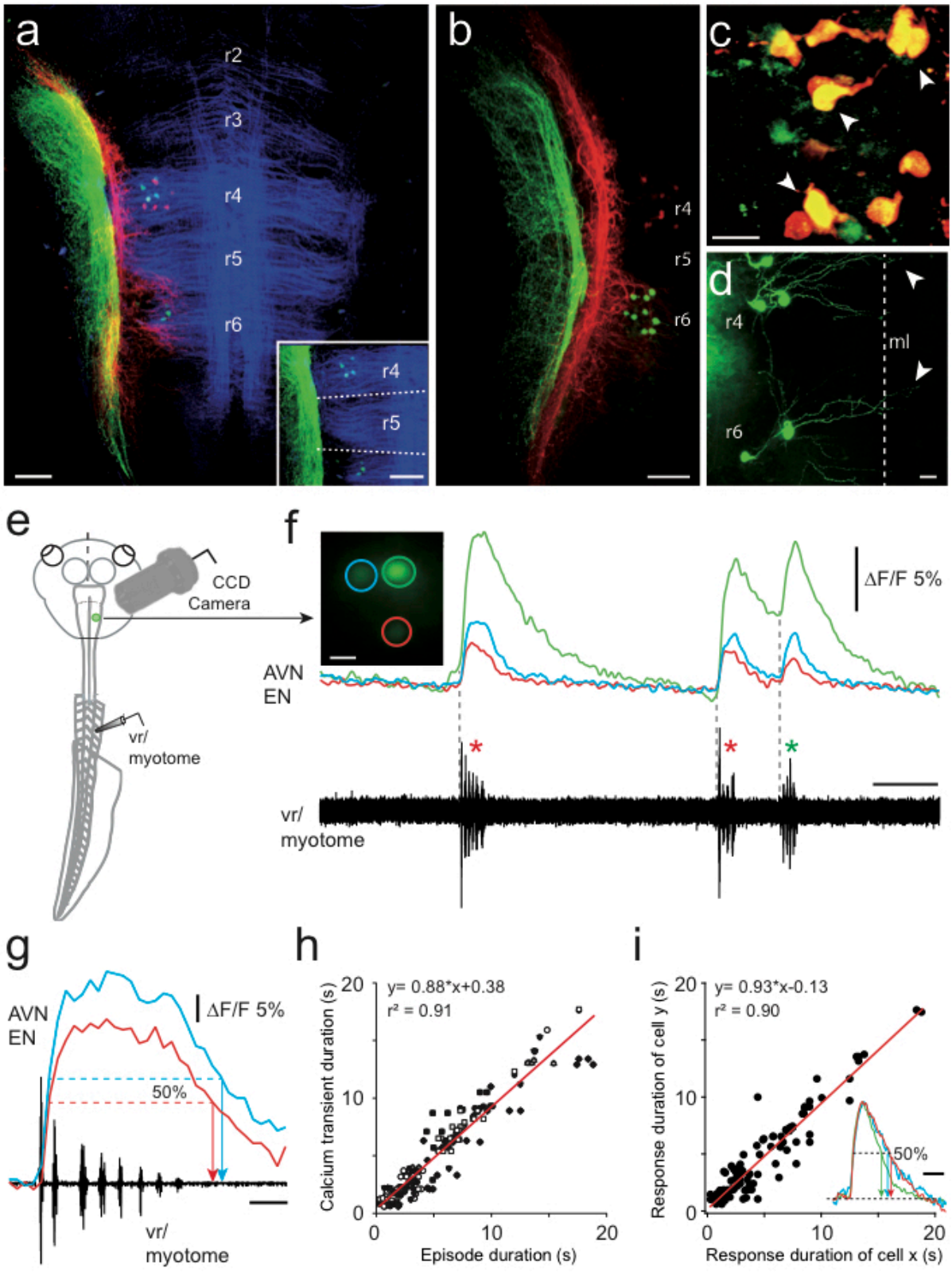

Figure 2. Ca^{2+}-imaging of morphologically identified mechanosensory efferent neurons (ENs) during fictive locomotion. a-d, Confocal reconstructions of hindbrain whole mounts after combined application of Alexa Fluor 546 (red) and 488 (green) dextran to the AVN and ALLN (a,c,d), and to the AVN and PLLN, respectively (b), showing afferent axonal projections and locations of EN somata in rhombomeres (r) 4 and 6. Note that the

longitudinal and rhombomere-specific transverse fibers (blue in a) were visualized by 612 nm illumination. The inset in (a) shows r4 and r6 ALLN efferent neurons (green) in relation to segmental boundaries (dashed lines). c, AVN (red) and ALLN (green) efferent neurons in r4 at higher magnification; note the double-labeled neurons in yellow (arrow heads). d, ALLN ENs in r4 and r6 that extend dendrites (arrow heads) across the midline (ml). e,f, Imaging of Ca^{2+}-transients in ENs of semi-isolated preparations (e) following retrograde loading of cell bodies with Calcium Green-1 dextran from the anterior vestibular nerve (AVN). Ca^{2+}-transients (f) were recorded simultaneously in several ENs (color coded cells and traces) during episodes of evoked (red *) and spontaneous (green *) ventral root/myotomal locomotor burst activity (black traces). g,h, Correlation between Ca^{2+}-dynamics, measured as the overall response half-width (g), and corresponding locomotor episode duration (h) in 32 cells during 4-7 swimming episodes per monitored cell (n = 160). i, Plot of Ca^{2+}-response durations (measured as half-width; see color-coded, normalized transients in inset) of pairs of ENs (25 pairs) during 4-7 locomotor episodes/cell (n = 114). Red lines in h,i represent linear regression. Calibration bars: 0.1 mm in a,b and inset in a; 25 μm in c,d; 15 μm in f; 5 s for traces in f and inset in i; 0.2 s in g.

Information content of the locomotor signal in ENs

The corollary discharge activation of mechanosensory ENs offers the possibility of transmitting information about a range of different features of the propulsive motor commands to the vestibular and lateral line sensory peripheries. Moreover, given the communal projections of most ENs to both systems, it is predictable that equivalent efferent information is conveyed in the nerve branches to the two peripheral targets. As typified by the AVN recordings in Fig. 3a, spinal vr and vestibular (red) or lateral line EN activity (blue) during fictive swimming revealed a close temporal match (r^2 = 0.99) in their overall discharge durations in each episode (Fig. 3a,b; see also Fig. 2h). Alterations in the strength of actual swimming *in vivo* derive from changes in the amplitude and frequency of horizontal tail excursions that in turn are represented *in vitro* by variations in the discharge intensity and cycle frequency of underlying vr bursts [33]. Spontaneous changes in vr intra-burst firing rates (see shaded c-vr14 bursts in Fig. 3c) and burst frequency (see i-vr13 bursts in Fig. 3e) during fictive swimming were also accompanied by similarly graded alterations in burst magnitude and cycle rate of associated vestibular EN activity (AVN in Fig. 3c and 3e, respectively). The strong linear correlations for both discharge intensity (Fig. 3d) and burst frequency (Fig. 3f) - obtained from vestibular (red) and lateral line (blue) nerve recordings - indicate that swimming strength is faithfully represented on a cycle-to-cycle basis within the efferent activity to the vestibular and lateral line peripheries.

Changes in swimming strength are also inscribed in a further parameter of the corollary discharge of mechanosensory ENs. During vr bursts at lower cycle frequencies and/or lower burst amplitudes (green highlighted areas in Fig. 3c,g), vr/EN coupling consisted predominantly of an ipsilateral, single-phase pattern. However, when vr burst frequency or amplitude (blue shadings in Fig. 3c,g) was relatively high, the coupling pattern was typically a bi-phasic relationship in which the ENs were now activated along with vr bursts on both cord sides (red and blue * in Fig. 3c,g). Concomitant with this bi-phasic pattern, the ipsilateral vr/EN coupling became stronger and more pronounced and was correlated with an increase in the relative magnitude of vr burst amplitudes ($p \leq 0.01$, Mann-Whitney *U*-test; Fig. 3h). Thus, during stronger swimming, the corollary signature expressed by mechanosensory ENs during each cycle represented the sum of the combined bilateral vr burst activity. However, even when bi-phasic coupling occurred during a given locomotor episode, the dominant ipsilateral phase relationship between vr and EN burst discharge was strictly maintained, and independent of rhythm frequency. Together, therefore, the above findings show that during tadpole swimming, the efference copy encoded in both vestibular as well as lateral line ENs conveys information about the duration, frequency and amplitude of locomotor activity to the mechanosensory periphery of the inner ear and lateral line systems.

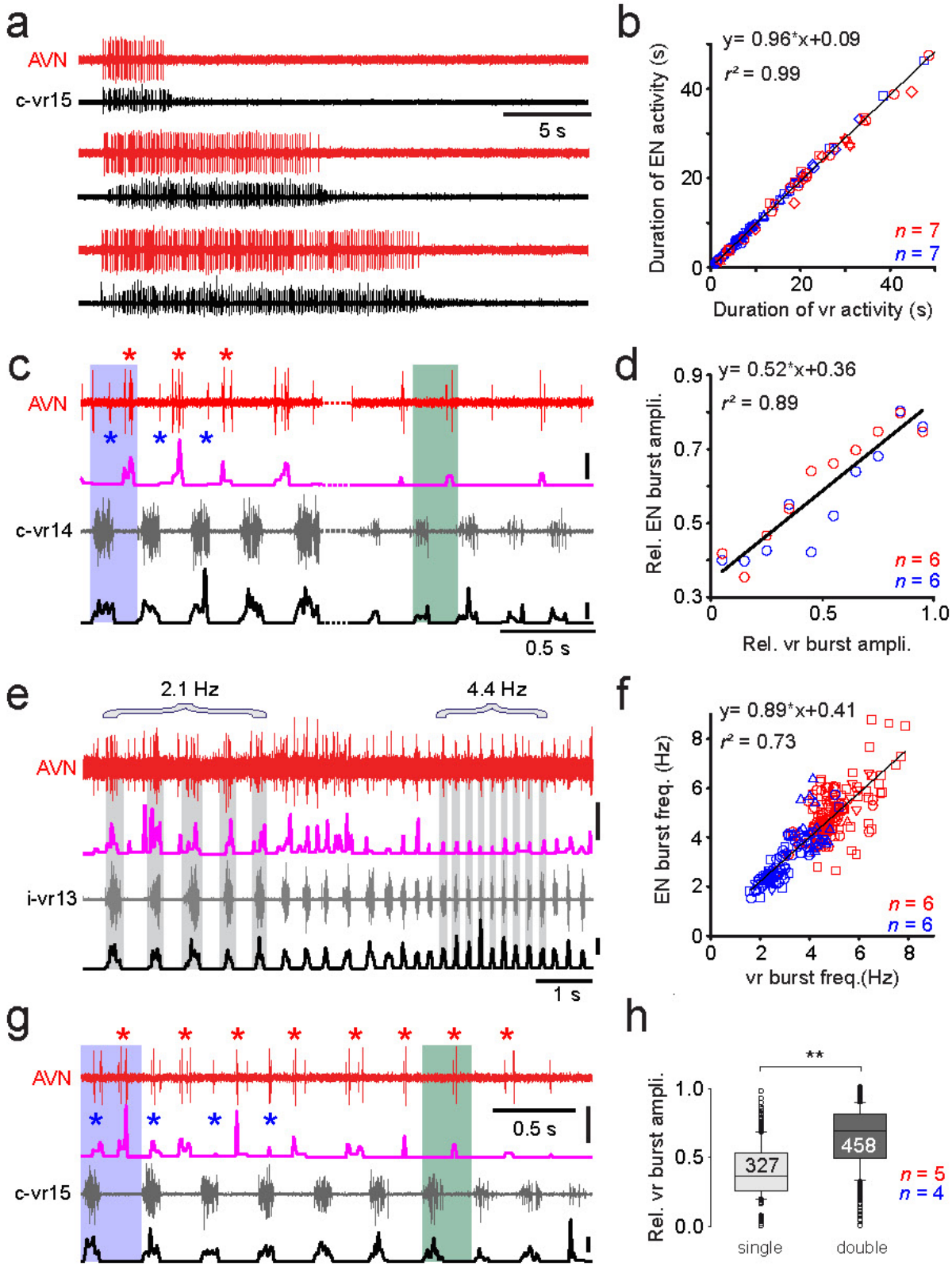

Figure 3. Parameter representation of locomotor activity in mechanosensory efferent neuron discharge. a, Recordings of AVN (red traces) and c-vr15 activity (black traces) during three swimming episodes of increasing length in the same preparation. b, Pooled data plot showing closely matching episode durations of vestibular (red open symbols, *n* = 7 preparations) and

lateral line (blue symbols, n = 7 different preparations) efferent (EN) versus vr discharge (68 swim episodes). Linear regression is indicated by black line. c, Recordings of AVN (red trace) and c-vr14 activity (grey trace) with corresponding integrals of intra-burst firing rates (pink and black traces) during sequences of strong (left) and weak fictive swimming (right) within the same episode (compare color shaded areas). During strong swimming (left), additional spikes occurred in the AVN (blue *) in phase with the contralateral vr. d, Group data plot showing a close correlation between the magnitudes of vestibular (red circles, n = 6 preparations) and lateral line (blue circles, n = 6) EN versus vr burst integrals (313 burst cycles). Linear regression is indicated by black line. e, Recording of AVN (red trace) and i-vr13 activity (grey trace) with respective integrals of intra-burst firing rates (pink and black traces) during a swim episode where vr bursting changed spontaneously from a slower (2.1 Hz) to a faster (4.4 Hz) rhythm. f, Group plot showing a close correlation between vestibular (red symbols, n = 6) and lateral line (blue symbols, n = 6) EN versus vr burst frequencies (101 cycles of 5-10 bursts/episode). Note that any bi-phasic EN burst patterns were omitted from this analysis. Linear regression is indicated by black line. g, Recording of AVN (red trace) and c-vr15 activity (grey trace) with corresponding firing rate integrals (pink and black traces) during a swimming episode in which the single-phase vr-EN coupling (red * in g) followed a pattern of EN activity occurring in time with the vr bursts on both sides (red and blue * in g). h, Box and whisker plots showing that the bi-phasic EN activity (blue) occurred with vr bursts of significantly larger relative magnitude ($p \leq 0.001$; Mann-Whitney U-test) than during mono-phasic EN-vr coupling. Number (n) of preparations is indicated in b,d,f,h. Vertical calibration bars in c,e,g indicate a discharge rate of 100 spikes/s.

Origin of locomotor corollary discharge in ENs

In theory, the locomotor-timed influence on mechanosensory ENs, as illustrated in Fig. 4a-c, could originate from the spinal CPG circuitry itself or from supraspinal levels, such as midbrain [35,36] (Cabelguen et al., 2003; Saitoh et al., 2007)(Cabelguen et al., 2003; Saitoh et al., 2007)or hindbrain reticular centers [17] known to control locomotor behavior. A midbrain contribution was excluded by surgical removal of the midbrain in isolated brainstem/spinal cord preparations (blue arrow in Fig. 4d; n = 7). Despite the midbrain ablation, the rhythmic activation of both vestibular as well as lateral line ENs persisted during fictive swimming (e.g. AVN in Fig. 4e). Moreover, neither the magnitude of locomotor-related EN firing nor the bi-phasic relationship with left/right vr bursting was affected by this lesion (Fig. 4e,f; *cf.* 4b,c), compatible with an exclusive spinal origin of the corollary signal. Significantly, however, following an additional spinal cord hemisection at the level of the obex (Fig. 4g), any bi-phasic EN firing (Fig. 4b,e) was immediately replaced by a single-phase pattern (n = 10) in which EN/vr coupling remained uniquely ipsilateral as indicated in Fig. 4h,I (*cf.* e,f) by the remaining EN activity occurring in phase-opposition with the contralateral vr. The suppression of EN activation in phase with contralateral vr bursts by this hemisection (see arrow heads and pink shaded segment in Fig. 4h,i; *cf.* 4f) thus suggests that ascending spinal

signals reach contralateral efferent neurons after traversing the midline above the obex in the brainstem, thus excluding a previously suggested contribution of the hindbrain reticular formation. Interestingly, a potential anatomical substrate for this contralateral input could include the midline-crossing dendrites of the mechanosensory efferent neurons themselves (see Fig. 2d).

The origin and coupling dynamics between spinal CPG circuitry and the ENs were further assessed by recording spinal vr activity at different segmental levels during spontaneous episodes of *in vitro* fictive swimming (n = 5). Robust phase-coupled cyclic bursts occurred in efferent fibers (e.g. PLLN in Fig. 4j,k) whenever rhythmic locomotor activity was uniformly expressed along the cord (see vr3, vr10, vr16 in Fig. 4j). However, locomotor corollary firing in ENs disappeared in all preparations (red * in Fig. 4l; n = 5) whenever bursting in the most rostral vrs (segments 1-10) occasionally ceased (vr3 and vr10 in Fig. 4l), although bursting in more caudal roots persisted (vr16 in Fig. 4l). Moreover, in preparations expressing typical axially-distributed CPG activity (as in Fig. 4k), the stepwise surgical removal of spinal segments, starting at the level of vr20 and continuing rostrally up to vr5, resulted in a gradual reduction of EN burst magnitudes during fictive swimming. Together these findings thus confirm for the first time that the locomotor efference copy drive to both lateral line and vestibular efferent neurons principally derives from CPG circuitry in the rostral cord region.

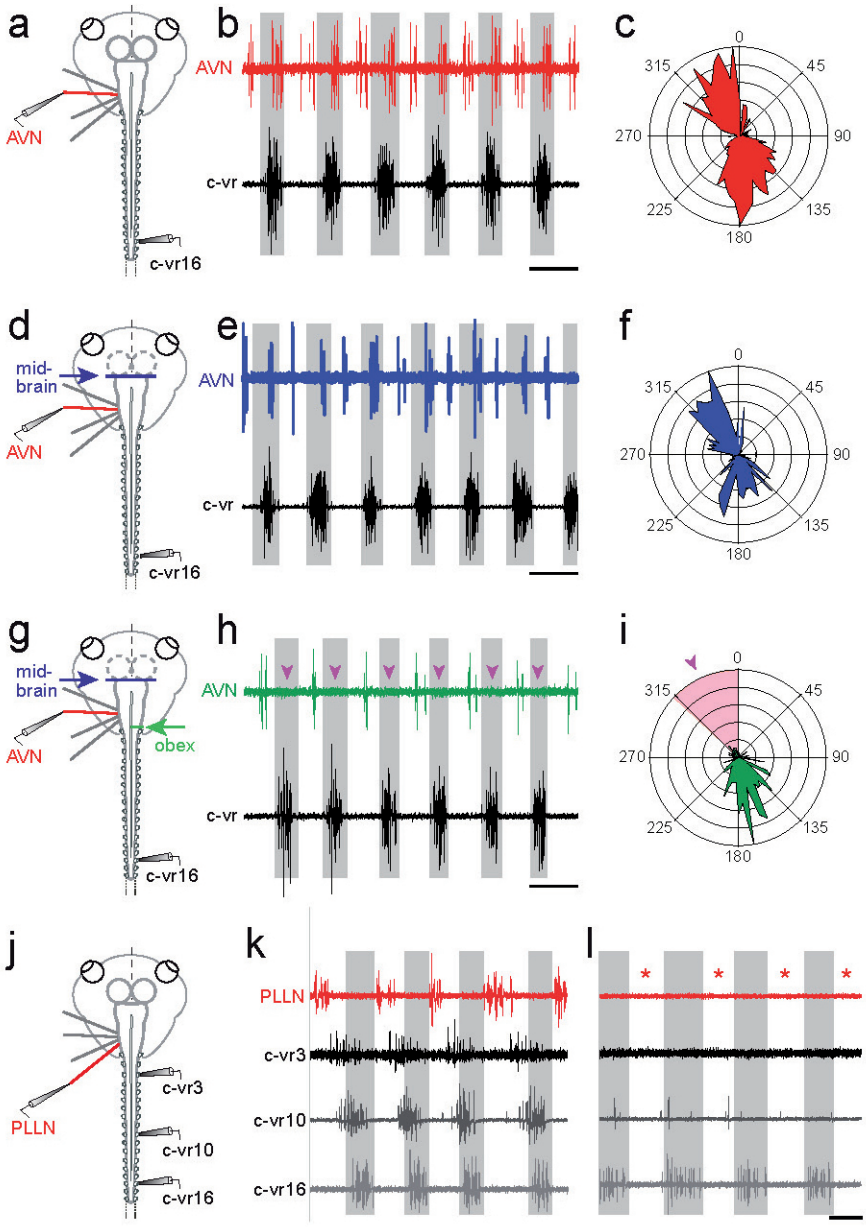

Figure 4. Spinal origin and trajectory of ascending pathways mediating locomotor corollary discharge signaling to mechanosensory efferent neurons. a-i, Episodes of spontaneous fictive swimming in the same *in vitro* preparation (a,d,g) recorded from the right (contralateral, c) vr16 (black trace) and the central stump of the left AVN (b,e,h; red, blue, green traces, respectively) in control (a-c), after midbrain removal (d-f) and then after a right obex hemisection (g-i). The corresponding polar plots in c,f,i show that the out-of-phase (contralaterally-timed) vr-EN coupling remained largely unaffected by the two lesions. However, although the additional synchronous (ipsilaterally-timed) EN activity (b,c) persisted after midbrain removal (e,f), it disappeared after obex hemisection (pink arrow heads in h and pink area/arrow head in i). j-l, Episodes of spontaneous swimming activity in a different semi-isolated preparation (j) recorded simultaneously from right vrs 3, 10 and 16 (respectively black, dark gray, light gray traces) and the central stump of the left PLLN (red trace). PLLN bursting coupled with locomotor bursts in all three cord segments (k)

disappeared (l; red *) when CPG burst activity ceased spontaneously in vr3 and vr10 but persisted in vr16. Calibration bars: 0.2 s in b,e,h,k,l.

Impact of locomotor corollary discharge on mechanosensory encoding

The functional consequences of EN locomotor efference copy for sensory signal processing by lateral line neuromasts and vestibular endorgans were explored by making *en passant* recordings from afferent fibers in the PLLN and AVN. For this, the peripheral connectivity of ENs with lateral line/inner ear hair cells and their afferent innervation were left physically intact (Figs. 5a,g, 6a,e), in contrast to the experimental conditions described so far (Figs. 1-4) where the endorgans were disconnected. Consequently, the effect of spinal CPG corollary discharge on the transduction and encoding of natural motion-driven afferent activity during fictive locomotion could be directly assessed.

Lateral line system. Previous *in vivo* studies on adult *Xenopus* [17] and dogfish [16,19] provided qualitative evidence for an attenuating role of EN activity on lateral line afferent signal encoding [16,17,19]. In order to extend these earlier observations and directly compare the consequences of locomotor efference copies on vestibular and lateral line primary afferent signaling, we first quantified the EN influence in the latter mechanosensory system. In the absence of locomotor activity, intact PLLN afferent fibers fired spontaneously at overall rates varying from 3 to 50 Hz, depending on the number of afferents recorded in a given experiment (red traces in Fig. 5b,c). During a bout of fictive swimming (see black vr trace in Fig. 5b,c), the discharge of most recorded lateral line afferent neurons (n = 22/33) became substantially reduced or even ceased completely (* in Fig. 5b,c). The afferent firing rate decrease (Fig. 5d), which was most pronounced immediately after swimming onset (see bar I in Fig. 5f) when rhythmic vr bursting was typically at its strongest, generally persisted for most of the ensuing episode (see bar E in Fig. 5f). A return to control discharge levels often occurred as vr burst amplitudes gradually declined towards episode termination (see Fig. 5c). In contrast to their dependence on the strength of swimming activity (as reflected in the intensity of vr bursting), afferent fiber firing rates were similarly reduced in the absence (Fig. 5b) or presence (Fig. 5c) of a concomitant flow of Ringer solution across the skin surface. While a smaller group of lateral line afferent recordings (n = 11/33) exhibited no or minimal (< 10%) change in spontaneous discharge during fictive swimming (Fig. 5e), an actual increase in afferent cell firing during rhythmic vr bursting was never encountered, consistent

with the results of previous studies in which lateral line efferent axons were stimulated electrically [19]. Consequently, the average firing rate of the entire recorded population of lateral line afferents (n = 33) displayed a significant reduction ($p \leq 0.001$; Wilcoxon signed-rank test) throughout episodes of locomotor CPG activity (bar E in Fig. 5f).

Simultaneous recordings of lateral line afferent and efferent fibers with intact central and peripheral synaptic connectivity further substantiated the suppressive influence of EN locomotor corollary discharge on mechanosensory afferent neuron firing (Fig. 5g). Very occasionally in such experiments (n = 3), it was possible to record the activity of pairs of afferent and efferent axons in the same lateral line nerve recording. In the very rare example shown in Fig. 5h, simultaneous recordings were made from two branches of the same PLLN; an afferent and efferent fiber were recorded *en passant* in the still intact branch (red trace, $PLLN_1$ in Fig. 5h) and several ENs alone were recorded with a different electrode placed on a second, severed branch of the same PLLN (blue trace, $PLLN_2$ in Fig. 5h). During an episode of EN activity, visible as a barrage of rhythmic discharge in $PLLN_2$ (blue trace in Fig. 5h), the firing of an individual lateral line afferent fiber recorded in $PLLN_1$ (large spikes in the $PLLN_1$ trace in Fig. 5h) was reversibly suppressed. The close temporal correlation between this suppression of afferent firing and the efferent corollary volley (*cf*. $PLLN_1$ and $PLLN_2$ traces in Fig. 5h) was especially evident from the activity profile of a single efferent fiber (small spikes in the $PLLN_1$ trace in Fig. 5h; blue arrow) that accompanied the afferent axon in the *en passant* electrode recording. These reciprocating firing patterns of afferent and efferent axons within the same PLLN branch therefore further support the conclusion that locomotor corollary discharge in mechanosensory ENs is responsible for attenuating sensory signaling in lateral line afferent pathways.

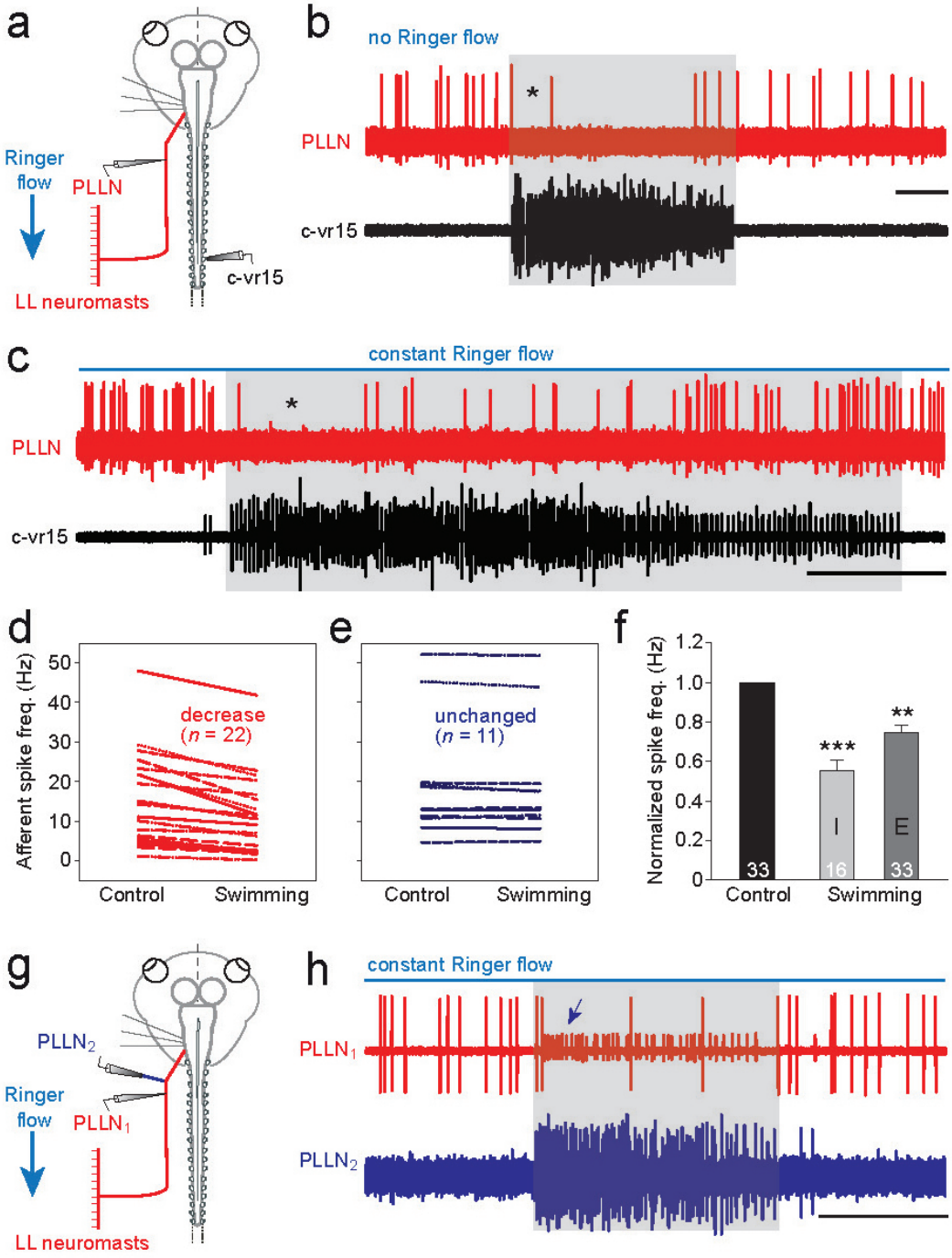

Figure 5. Locomotor corollary discharge influence on lateral line sensory encoding. a-c, Simultaneous recordings of right vr15 (black traces) and *en passant* recordings of afferent fibers in the left PLLN (red traces) of semi-isolated preparations with intact neuromast-lateral line nerve connectivity (a), in the absence (b) and presence (c) of constant sensory stimulation by Ringer flow along the skin surface. During episodes of fictive swimming (shaded areas in b,c; see black vr trace), tonic PLLN activity was initially abolished (* in b,c), but regained lower levels of firing as the locomotor activity progressed and eventually returned to resting discharge levels before episode termination. d,e, Plots illustrating a decrease (d, red) or absence of locomotor influence (e, blue) on the firing of individual lateral line afferents during CPG activity. f, Histograms showing significant average decreases in firing rates of the recorded afferent population (number indicated in each bar) during the

initial (I) and throughout the entire (E) duration of fictive swimming episodes. ** $p \leq 0.001$; *** $p \leq 0.0001$ (Wilcoxon signed-rank test). g,h, Distinguishable afferent and efferent fiber activity in a single PLLN (g) recorded *en passant* from one branch ($PLLN_1$, red trace) connected to lateral line hair cells and from a second transected branch ($PLLN_2$, blue trace) of the same nerve (h). During locomotor-related efferent activity (shaded area; indicated by the multiple-unit discharge in $PLLN_2$ and spiking in the single small unit (arrow) in $PLLN_1$), ongoing afferent firing (large spikes in $PLLN_1$) was virtually suppressed throughout the swim episode. Horizontal calibration bars: 5 s in b,c and 1 s in h.

Vestibular system. The shared projections of individual ENs to both the lateral line and vestibular sensory periphery (see Fig. 2c) also strongly suggested an action of locomotor efference copy on the encoding of motion-related signals in vestibular nerve afferent fibers. This possibility was tested by mounting semi-isolated preparations with still functional vestibular endorgans on a two-axis turntable for the application of rotational stimuli in different spatial planes [37] (Fig. 6a,e). *En passant* recorded afferent fibers in the AVN fired spontaneously at rest with rates of 2 to 20 Hz in different experiments (Supplemental Fig. 3a,c,e). Imposed sinusoidal vertical roll motion (upper trace in Fig. 6b) or horizontal left-right oscillations (upper trace in Fig. 6f) caused a corresponding cyclic modulation of the discharge in all recorded AVN afferent fibers. The peak firing rates of individual recordings during this natural stimulation ranged from 10 to 35 Hz (Fig. 6c,g).

During an episode of fictive swimming in the absence of motion stimulation, the spontaneous firing of vestibular afferents was variably affected, with the discharge rates of some fibers increasing while in others spiking decreased relative to resting levels (see red traces in Supplemental Fig. 3a,b and 3c,d, respectively). Consequently, when averaged over all recordings, neither the frequency ($p = 0.067$; Wilcoxon signed-rank test) nor the regularity (cv^2; $p = 0.57$; Wilcoxon signed-rank test) of spontaneous discharge was significantly altered during locomotor activity (S' in Supplemental Fig. 3e,f) compared to the respective controls (C and C' in Supplemental Fig. 3e,f).

Compatible with a variable impact of spinal CPG corollary activity on afferent fiber resting discharge, a similarly disparate influence of locomotor activity was observed in response to coincident, motion-induced vestibular activation. During a bout of fictive swimming, evidenced by an episode of rhythmic vr bursting (black traces in Fig. 6b,f) and/or associated corollary activity in mechanosensory ENs (ALLN, green trace in Fig. 6f), the ongoing modulation of afferent fiber discharge by sinusoidal rotational stimulation was affected differently in different recordings (shaded areas in Fig. 6b,f). As a first estimate, we

calculated the mean firing rate during table motion in the absence and presence of a fictive swimming event; the mean afferent firing rate (red line in Fig. 6c,d,g,h) throughout a given swim episode either decreased (n = 10; Fig. 6c,d), increased (n = 7; Fig. 6g,h) or remained unaffected (change < 10%; n = 5). Again, because of this variable influence of locomotor activity during rotational stimulation (color-coded plots in Fig. 6i), the mean firing rates of the overall afferent population (black and red box plots in Fig. 6i) during (11.0 ± 1.6 Hz; n = 22) and in the absence of fictive swimming (11.8 ± 2.1 Hz; n = 22) were not significantly different (p = 0.434; Wilcoxon signed-rank test). However, irrespective of the diverse spinal CPG influences on individual afferent fibers, any firing rate alteration was always strictly associated with corollary activation of lateral line and vestibular ENs (see ALLN green trace in Fig. 6f, for example), further pointing to the causality between vestibular/lateral line efferent firing and changes in mechanosensory afferent encoding.

Assuming representivity of the sampled vestibular afferent population, the overall alteration in stimulus-induced discharge modulation observed in our experiments provided a reasonable estimate of the global impact of locomotor corollary discharge on vestibular system movement encoding (Fig. 6j). This became particularly obvious from calculating the average peak-to-peak discharge modulation for a single motion cycle (Fig. 6c,d,g,h,j). Significantly, although mean firing rate levels were variably affected in different fibers by locomotor corollary activity (Fig. 6i), the peak-to-peak amplitudes of the motion-induced modulation were consistently diminished in all recordings compared to controls (compare red and black lines in Fig. 6j). Indeed, the average magnitude of discharge modulation during swimming was significantly reduced by ~45% ($p \leq 0.05$; Wilcoxon signed-rank test) with respect to controls (Fig. 6j,k), thereby revealing a considerable reduction in the gain of afferent fiber sensory responsiveness during spinal CPG activity. Thus, together with a comparable impact on the lateral line system, this finding leads to the conclusion that locomotor corollary discharge conveyed by efferent pathways to the mechanosensory periphery causes a substantial attenuation of stimulus encoding in vestibular and lateral line afferent pathways during self-motion.

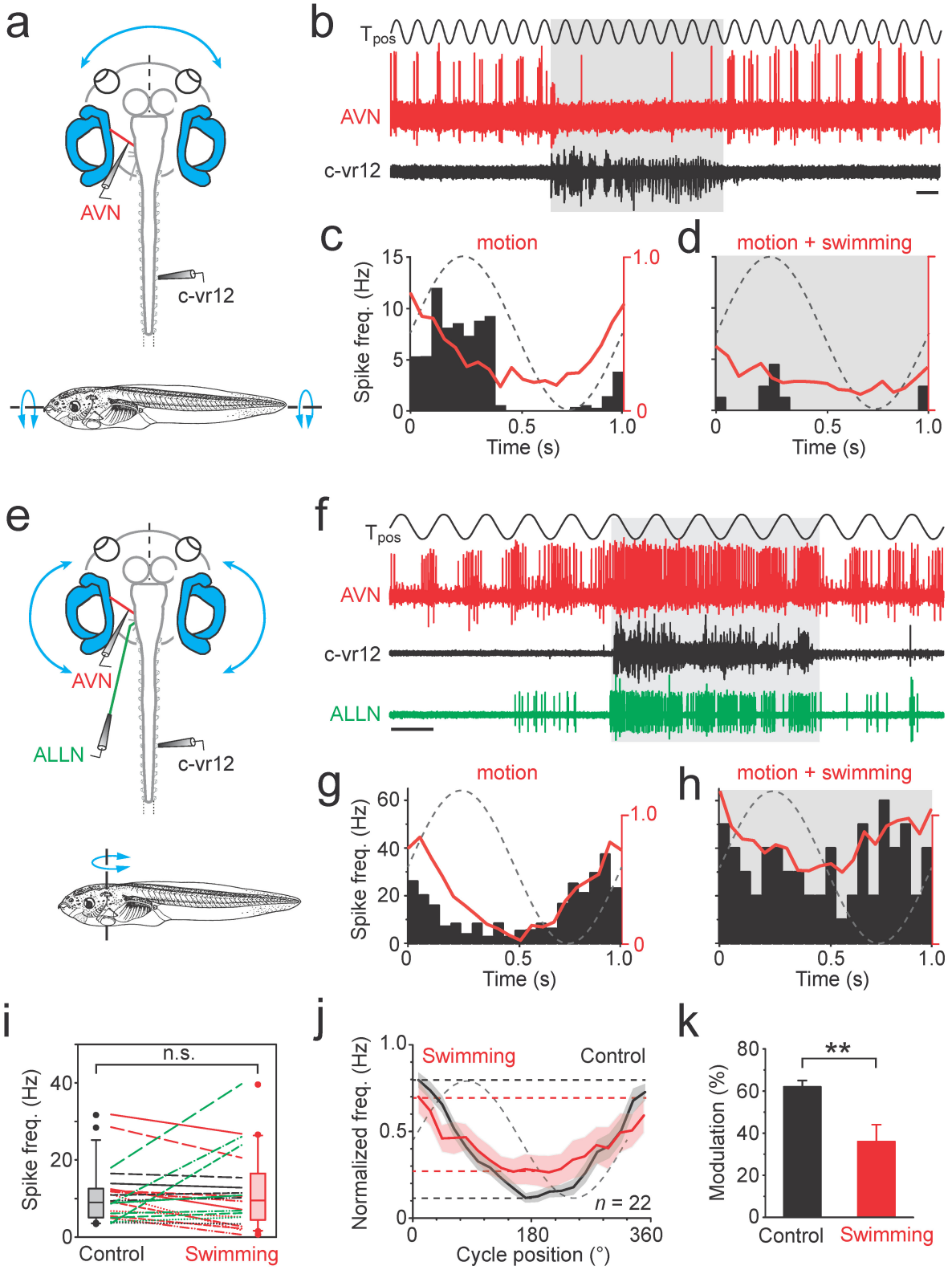

Figure 6. Locomotor corollary discharge influence on vestibular sensory encoding. a-h, Recordings of right vr12 (black traces in b,f), the left ALLN (green trace in f) and *en passant* recordings of afferent fibers in the left AVN (red traces in b,f) in semi-isolated preparations with intact inner ear hair cell-vestibular nerve connectivity (a,e) during sinusoidal (1 Hz, ±60°/s) horizontal-axis roll-motion (a) or vertical-axis head rotations (e) imposed by a two-

axis turntable (T_{pos}). During fictive swimming (shaded areas in b,f), the firing of some vestibular afferent fibers was attenuated (b-d), but facilitated in others (f-h). c,d,g,h, Histogram (black bars), depicting the mean afferent firing rate modulation (responses of fibers recorded in b,f) over a single cycle of turntable motion (dashed lines) in the absence (c,g) and presence (d,h) of locomotor CPG activity; also plotted are the respective population averages (red curves) of fibers with decreasing (c,d) and increasing firing (g,h) during swimming activity. i, Plots of individual mean firing rate alterations during motion stimulation (green - increase, red - decrease, black - no change) before (Control) and during swimming activity. Gray and red boxes with whisker plots show the distributions of the average firing rates in the two conditions. *ns*, not significant. j,k, Averaged response of all recorded afferent fibers (± SEM, shaded areas in j; $n = 22$) over a single cycle of turntable motion (dashed gray line) before (black plot) and during (red plot) locomotor CPG activity (j). k, Averaged extent of firing rate modulation before (Control) and during fictive swimming (k). ** $p \leq 0.001$ (Wilcoxon signed-rank test). Horizontal calibration bar in b,f: 1 s.

Discussion

During rhythmic locomotor activity, cranial mechanosensory efferent neurons fire in a cyclic burst pattern that derives from an efference copy drive from the spinal central pattern generator. This predictive intrinsic signal informs the hair cell sensory periphery in both the inner ear and neuromasts of the lateral line system about the temporal structure of the ongoing locomotor command. Despite a variable influence of locomotor corollary discharge on individual vestibular and lateral line afferents, in both cases the evoked population response during coincident natural stimulation is reduced, commensurate with an adaption of sensory encoding to the altered stimulus statistics that occur during locomotion.

Active movements such as locomotion generate reafferent sensory signals that interfere with the detection and interpretation of concurrent extrinsically-induced passive motion [38,39]. However, intrinsic neural copies of the actual commands that produce locomotor movement offer a convenient substrate for neural computations that account for the expected sensory outcome of active self-motion [40]. In this way, locomotor efference copy [8] or corollary discharge [7] is highly suited to influence the processing of head/body motion signals at the vestibular/lateral line sensory periphery as well as within associated central circuitry [38].

The functional impact of intrinsic corollary discharges is particularly well understood in the mormyrid fish electrosensory system, which is evolutionarily closely related to the vestibular and lateral line systems [41]. During electric organ activity of weakly electric fish, corollary discharges of the electromotor commands suppress reafferent stimulation at the first central relay station in the cerebellum-like electrosensory lobe [42,43]. Moreover, the correct interpretation of external electrosensory signals is not only impaired by self-generated electric fields but also by body motion due to locomotor or ventilatory activity [44-48]. However, in the absence of efferent innervation of electroreceptors and their associated afferent fibers at the sensory periphery [41], the influence of motor corollary discharges occurs entirely centrally, where these intrinsic signals generate cancelling negative images of the sensory consequences of the fish's own movements in neurons of the electrosensory lobe [48].

In contrast to the electrosensory system, the mechanosensory endorgans of both the vestibular and lateral line systems are richly innervated by efferent neuron populations, thereby offering the additional possibility to influence signal encoding at the first neuronal level. Indeed, efferent pathways to peripheral sensors constitute an essential component for informing these movement-detecting systems about the altered stimulus conditions during

locomotion [11]. However, despite known morphological, physiological and pharmacological properties of vestibular nerve efferent fibers (Hellmann and Fritzsch, 1996; Holt et al., 2006; Leijon and Magnusson, 2014)(Hellmann and Fritzsch, 1996; Holt et al., 2006; Leijon and Magnusson, 2014)[12,15,27], their direct electrical or sensory activation has yielded widely differing effects on vestibular afferent fiber activity in various species and under diverse experimental conditions [13,20,21,23,24,28-30,49]. Consequently, the functional role of vestibular efferent innervation has so far remained enigmatic. The results of the present study therefore place these earlier disparate observations into perspective by identifying a context-dependent role for vestibular ENs during the expression of an essential and definable natural behavior. While our discovery of rhythmic locomotor-related signals occurring in vestibular nerve efferents is novel, the activation of lateral line efferent fibers during swimming in dogfish and *Xenopus* has been previously reported [17,19]. Our data also demonstrate for the first time that cranial mechanosensory efferent pathways reliably inform both the lateral line and vestibular sensory peripheries about ongoing locomotor activity by conveying parallel neural replicas of spinal CPG output to lateral line neuromasts and inner ear endorgans.

Significantly, the distinct behavioral context in which these efferent pathways are engaged is inscribed in the information content of their corollary activation (Fig. 3). As found in a number of other systems, efference copies of motor behaviors with relatively predictable outcomes either adapt the sensory periphery to an altered stimulus condition or compensate for unwanted sensory consequences of the behavior in question [10,39,50-52]. The corollary discharge signal conveyed by vestibular and lateral line mechanosensory efferents is therefore ideally suited to notify peripheral hair cell targets about the precise dynamics of ongoing locomotor activity. The neural origin of this internal signal within the first 10 cord segments complies with the large undulatory head movements that result exclusively from the alternating left/right contractions of rostral tail and trunk muscles during swimming, as found previously for the spinal source of locomotor efference copy-driven eye movements [51](Lambert et al., 2012)(Lambert et al., 2012). However, although the corollary activity of ENs consists of discrete locomotor-timed bursts, these phasic signals are also likely to be converted into a more persistent postsynaptic hair cell/afferent fiber response, as shown in toadfish upon electrical activation of its mechanosensory efferent system [13,20,21].

The previously reported effects of experimentally elicited vestibular efferent discharge on afferent firing patterns [20,23,24,30,49,53] comply with the variable influences of locomotor corollary EN activation found in the current study. However, despite the diverse

effects of efferent firing on the spontaneous activity of vestibular and lateral line afferents, the overall mechanosensory responsiveness of both afferent populations is significantly attenuated during locomotor activity. The finding that the resting rates of vestibular afferents may either decrease, remain unaltered or even increase in response to EN firing is possibly related to the bilateral push-pull organization of the vestibular system, in contrast to the lateral line system. In the semicircular canal system, any imbalance in afferent signaling between the two sides is interpreted centrally as resulting from head rotation [5](Straka and Dieringer, 2004)(Straka and Dieringer, 2004). Thus, maintaining bilaterally symmetrical global rates of afferent fiber resting activity by averaging out the opposing effects of locomotor corollary efferent signals would in turn ensure equilibrated resting activity within the bilateral central vestibular circuitry, in accordance with an underlying principle for effectively encoding angular motion in space [4,5]. In contrast to vestibular (semicircular canal) sensory processing, which relies on bilateral organs for differential neural computations, the effective encoding of water motion in central lateral line nuclei only requires single patches of neuromasts containing hair cells with opposite polarities. The latter are innervated by separate lateral line afferent fibers, and thus comprise distinct perceptive entities that allow encoding bidirectional water motion without the necessity to extract integrative signals from bilateral comparisons (Bleckmann, 2008)(Bleckmann, 2008)[54]. The substrates for encoding head/body movement and water motion are also paralleled by differences in their respective efferent innervation patterns. While lateral line efferent neurons connect uniquely with their hair cell targets, vestibular ENs make synaptic connections with both hair cells and the afferent pathways that serve them [55] (Fig. 7). This latter dual innervation pattern coupled with an apparent greater pharmacological diversity in target influence [20,23,27,56] again points to a potentially more variable functional outcome of efferent pathway activation for vestibular signal encoding.

Unlike the evident adaptive tuning of motion encoding in vestibular afferent fibers during locomotion in larval *Xenopus*, a corresponding efference copy influence on afferent discharge modulation during active head motion in primates has not been encountered [57,58](Cullen and Minor, 2002; Sadeghi et al., 2007; Jamali et al., 2009)(Cullen and Minor, 2002; Sadeghi et al., 2007; Jamali et al., 2009). While this difference might be related to species-specific diversity in neuronal computational requirements, it is more likely to be due to the difference in neural origins of the two underlying motor programs. In *Xenopus*, rhythmic locomotor behavior originates from a spinal CPG network whose associated

corollary discharge is conveyed by ascending spino-cerebral pathways that are likely to be the same as those that drive compensatory eye movements (Lambert et al., 2012). In monkeys, however, voluntary head movements are driven by descending cortical commands [38,59,60](Cullen et al., 2011; Medrea and Cullen, 2013; Brooks and Cullen, 2014)(Cullen et al., 2011; Medrea and Cullen, 2013; Brooks and Cullen, 2014). Even though there is no difference between vestibular afferent encoding of active and passive head movements, motor efference copies together with proprioceptive inputs during voluntary neck movements, that likely originate from descending cortico-spinal pathways, cause a suppression of sensory inputs in primate central vestibular neurons [28], thereby differentiating the two motion components. Thus, depending on the origin and nature of a motor program for self-motion, an accompanying efference copy may exert its influence on reafferent sensory signaling at different, yet potentially overlapping levels of the nervous system. Since spinal CPG-derived efference copies were probably already present in aquatic vertebrate ancestors as evidenced by current protochordate lineages [61,62], a corollary influence on mechanosensory afferent encoding via an associated efferent system is likely to represent an evolutionarily conserved condition that might also be effectively implemented during primate locomotion. Interestingly, supporting evidence for this idea comes from previous clinical studies in which human subjects with and without a vestibulopathy expressed a more stable posture during running than during walking [63,64](Brandt et al., 1999; Jahn et al., 2000)(Brandt et al., 1999; Jahn et al., 2000). This observation led to the conclusion that spinal locomotor signals might exert a direct influence on the vestibular sensory periphery, very reminiscent of the effects demonstrated in our study. Therefore, and in line with a parallel anecdotal report on a vestibular-impaired dog [63], an adaptation of neural encoding at the sensory periphery during locomotion may serve as a general mechanism amongst vertebrates.

Methods

Experiments were performed on semi-isolated *in vitro* preparations of larval *Xenopus laevis* at stages 48-55 [65] in compliance with the "Principles of Animal Care", publication by the National Institute of Health and the German law for animal protection (Tierschutzgesetz). Permission for the *in vitro* experiments was granted by the Regierung von Oberbayern (55.2-1-54-2531.3-18-10). All animals were obtained from the in-house breeding facility at the Biocenter-Martinsried of the LMU Munich.

Preparations

In all experiments, animals were first anesthetized in 0.02% 3-aminobenzoic acid ethyl ester (MS-222; Sigma-Aldrich, Germany) in ice-cold frog Ringer (composition in mM: NaCl, 75; KCl, 25; $CaCl_2$, 2; $MgCl_2$, 0,5; $NaHCO_3$, 25; Glucose, 11; pH 7.4) [66]. The ventral part of the skull, including the jaw, was carefully removed with the tail remaining attached to the head. Preparations were transferred to a Sylgard-lined Petri dish and the skin covering the dorsal head surface was removed, the soft skull tissue opened and the forebrain disconnected. The rostral spinal cord and ventral roots until segment 20 were exposed, then the latter were disconnected from tail/trunk musculature and the cord region was isolated from the surrounding tissue. In some preparations, the remaining caudal part of the tail was firmly secured with insect pins to the Sylgard floor at the level of segments 21 - 25 with the caudal part left free to perform undulatory swimming-related movements. Preparations were rinsed in fresh Ringer solution, transferred to a Sylgard-lined Petri dish (volume 5 ml) and continuously superfused with oxygenated Ringer solution at a rate of 1.3 - 2.1 ml/min. The temperature of the bathing solution was maintained at 17 ± 0.2°C.

Electrophysiology

Fictive swimming

Motor output of the spinal locomotor CPG in such semi-isolated preparations was monitored in spinal ventral roots (vrs) recorded uni- or bilaterally from cord segments 3 to 18 during episodes of so-called ‘fictive swimming’, the neural correlate of actual behavior that has been previously established in a number of animal model systems including locomotion in lamprey [67] and *Xenopus* [33,68,69] and vocalization in toadfish [70]. In addition to the mostly spontaneous expression of fictive swimming under such *in vitro* conditions, and to more

predictably obtain swimming episodes, electrical stimulation of the head and caudal part of the tail was occasionally used to instigate locomotor sequences. Electrical stimuli were generated with an integrated stimulus isolation unit (STG 4004, Multichannel Systems, Germany) and consisted of trains of 2-10 pulses (0.2 ms, ~100 µA at 100 Hz) that were delivered through a pair of Teflon-coated silver wires (diameter: 0.76 mm; AG 25-T, Science Products, Germany).

Mechanosensory efferent activity

To record vestibular (VIIIth cranial) nerve efferent activity, the otic capsule on one or both sides was opened and the anterior and/or posterior branches of the vestibular nerve (AVN, PVN) were carefully isolated from their respective endorgans and cleaned from surrounding tissue. To record lateral line efferent fiber activity, the anterior and posterior lateral line nerves (ALLN, PLLN) were exposed bilaterally outside the brain case and disconnected from the sensory periphery.

Mechanosensory afferent activity

The potential influence of locomotor-related efferent fiber activity on afferent mechanosensory encoding was assessed in semi-isolated preparations with still intact sensory organs (inner ear, lateral line) and hair-cell afferent connectivity. *En passant* recordings from mechanosensory afferents and, in a few fortuitous cases, efferent nerve fibers were made during natural sensory stimulation and fictive locomotion recorded conjointly from spinal ventral roots.

Vestibular afferent activity. Recordings from semicircular canal afferent fibers were made in preparations with intact otic capsules and functional inner ear endorgans in the absence and presence of fictive swimming. Semi-isolated preparations were secured to the Sylgard floor of a recording chamber with the ventral side up. A ventral opening of the cranium gave access to the VIIIth nerve between the intact otic capsule and the hindbrain. This allowed *en passant* recordings of sensory stimulus-evoked activity of vestibular nerve afferent fibers to be made in a condition where the connectivity of efferent fibers and the sensory periphery were preserved. For application of natural vestibular stimuli, the recording chamber was mounted on a computer-controlled, motorized two-axis turntable (Acutronic

Deutschland GmbH). Natural motion stimuli consisted of sinusoidal rotations around the yaw and roll axis at frequencies of 0.5-1 Hz with corresponding peak velocities of ±30-60°/s.

Lateral line afferent activity. Recordings from the PLLN were made in preparations with intact tail musculature and cutaneous neuromasts at the dorso-lateral region of the head/tail. Transecting the spinal cord caudal to segment 15 prevented any potential residual motion artifacts during fictive swimming. For *en passant* recordings of afferent neuron activity, a short (~0.5-1 mm) section of the PLLN branch was detached from the skin and cleaned from surrounding tissue. Nerve afferent activity was recorded in the absence and presence of hydrodynamic stimuli. For the latter, neuromast hair cells on the skin surface were stimulated by a constant Ringer flow (~10 mm/s) that was directed rostro-caudally along the surface of the preparation.

Electrophysiological recordings

All extracellular recordings, including *en passant* recordings of vestibular and lateral line afferent and efferent fibers were made with glass suction electrodes fabricated with a horizontal puller (P-97 Brown/Flaming). To optimize recordings of spike discharges (both single- and multi-unit) in spinal vrs (from segments 3 to 18) and the central stumps of mechanosensory nerve branches, the tip diameter of electrodes was individually adjusted to match the respective nerve size. For *en passant* recordings, electrodes were broken back to a tip size of ~2 μm. Recorded activity was amplified (EXT 10-2F; npi electronics, Tamm, Germany), digitized at 10 kHz (CED 1401, Cambridge Electronic Design, Cambridge, UK), processed with commercial software (Spike 2, Cambridge Electronic Design, Cambridge, UK), stored on a PC and analyzed off-line.

Recording analysis

Recordings were analyzed using Igor pro software (Wavemetrics, USA) and custom-written macros. Spike time measurements were used to calculate the instantaneous frequency for spinal vr, vestibular (VIIIth cranial) and lateral line nerve activity. Rate measurements included all spikes in a given multi-unit recording. The discharge of mechanosensory efferent neurons was compared with the corresponding phase of the swimming cycle by triggering instantaneous frequency measurements from the onset of each associated vr burst. The timing of efferent neuron firing relative to vr activity was transformed into a phase angle and

displayed as a polar plot in which the direction and length of an individual vector indicated the phase (0°, synchrony; 180°, alternation) and strength of coupling, respectively. Multiple episodes of locomotor activity were analyzed for each nerve recording with at least 10 cycles of stable fictive swimming per episode. The total duration of efferent neuronal and vr activity was defined as the time between the first and last bursts of a given fictive swimming episode. The frequency of rhythmic vr and efferent neuron bursting was calculated from the inverse of the interval between consecutive bursts in each case. The relationship between the magnitudes of vr and efferent neuron discharge was determined by calculating the respective integral from the raw vr and mechanosensory nerve recordings using a bin width of 10 ms. Due to the variable number of monitored axons in the different vr recordings, integrals were normalized within each animal. The timing of burst integral peaks was also used to separate single-phase (1:1 matching between efferent and vr burst rhythms) from bi-phasic (two efferent bursts per vr burst cycle) coupling patterns.

Lesion experiments

To identify the neural trajectories that convey corollary discharge signals from locomotor centers to the hindbrain mechanosensory efferent nuclei, various combinations of surgical lesions were made in semi-isolated CNS preparations. In a first set of experiments, the midbrain was removed by a transection of the brainstem rostral to the cerebellum, followed by a spinal hemisection immediately caudal to the obex. In a second series, successive complete transections of the spinal cord were made from vr20 in various step sizes until vr5. Following each surgical intervention, the preparation was allowed to recover for a period of 30 min before recording of neuronal activity commenced. After completion of physiological recordings, preparations were fixed in 4% paraformaldehyde (PFA) in 0.1 M phosphate buffer (PB; pH 7.4) for 5-6 hours and preserved for *post hoc* verification of lesion specificity by whole-mount light-microscopy.

Central anatomy of mechanosensory efferent neurons

The hindbrain segmental location and topographical organization of efferent neurons with axonal projections in the different lateral line and vestibular nerve branches were determined by retrograde transport following application of fluorescent tracers (Alexa Fluor 488, 546 dextran, Life technologies, USA) in various combinations to the cut ends of the

mechanosensory nerves in semi-isolated *in vitro* preparations (Straka et al., 2001)(Straka et al., 2001)[71]. Crystals of the tracers, melted onto the tip of an injection needle were inserted into the lateral line nerves close to the cranial exit of the ALLN and PLLN roots or into one of the two vestibular nerve branches (AVN, PVN) after opening of the otic capsule. Following incubation for 24 - 48 hours in oxygenated Ringer solution at 14°C, preparations were fixed in 4% PFA in 0.1 M phosphate buffer (pH 7.4) at 10°C for 5 - 6 hours and rinsed (3 x 10 min) in cold 0.1 M PBS (phosphate buffer saline, pH 7.4). The brainstems were removed, cleaned of surrounding tissue, mounted on slides and coverslipped using Vectashield (Vector Laboratories, Burlingame, USA). The labeled somata and central projections of mechanosensory efferent neurons and afferent axon terminals were reconstructed from stacks of optical sections obtained from scanning on a confocal microscope (Leica SP5). Z-axis projections were generated using the ImageJ software package (http://fiji.sc/wiki/index.php/Fiji). In order to map the position of retrogradely labeled efferent neurons onto the hindbrain segmental scaffold, preparations were scanned with an illumination wavelength of 612 nm to demark rhombomere outlines.

Ca^{2+}-imaging of mechanosensory efferent neurons

Efferent neuron cell bodies were retrogradely loaded with Calcium Green™-1 dextran (Invitrogen, Eugene, OR, USA) applied as crystals to the peripheral ending of the AVN 24 hours prior to an experiment. Imaging of Ca^{2+}-transients was performed with an epifluorescence microscope (Axio Examiner Z1, Carl Zeiss, Germany) and a CCD camera (Axiocam Hsm, Carl Zeiss, Germany) in both the absence and presence of locomotor activity. In order to prevent potential movement artifacts during imaging, all residual muscular elements of preparations were removed. Images were captured at a rate of 10-20 frames/s (Axiovision, Zeiss), stored and analyzed *post hoc* using the MBF-ImageJ Java software package (http://rsb.info.nih.gov/ij/) and custom written scripts. The background fluorescence was subtracted and bleaching effects were corrected using a linear regression algorithm. All data were presented as relative changes in fluorescence ($\Delta F/F$). The duration of an individual Ca^{2+}-transient was taken as the time at half maximal amplitude of the fluorescence change during a given swimming episode.

Supplemental figures

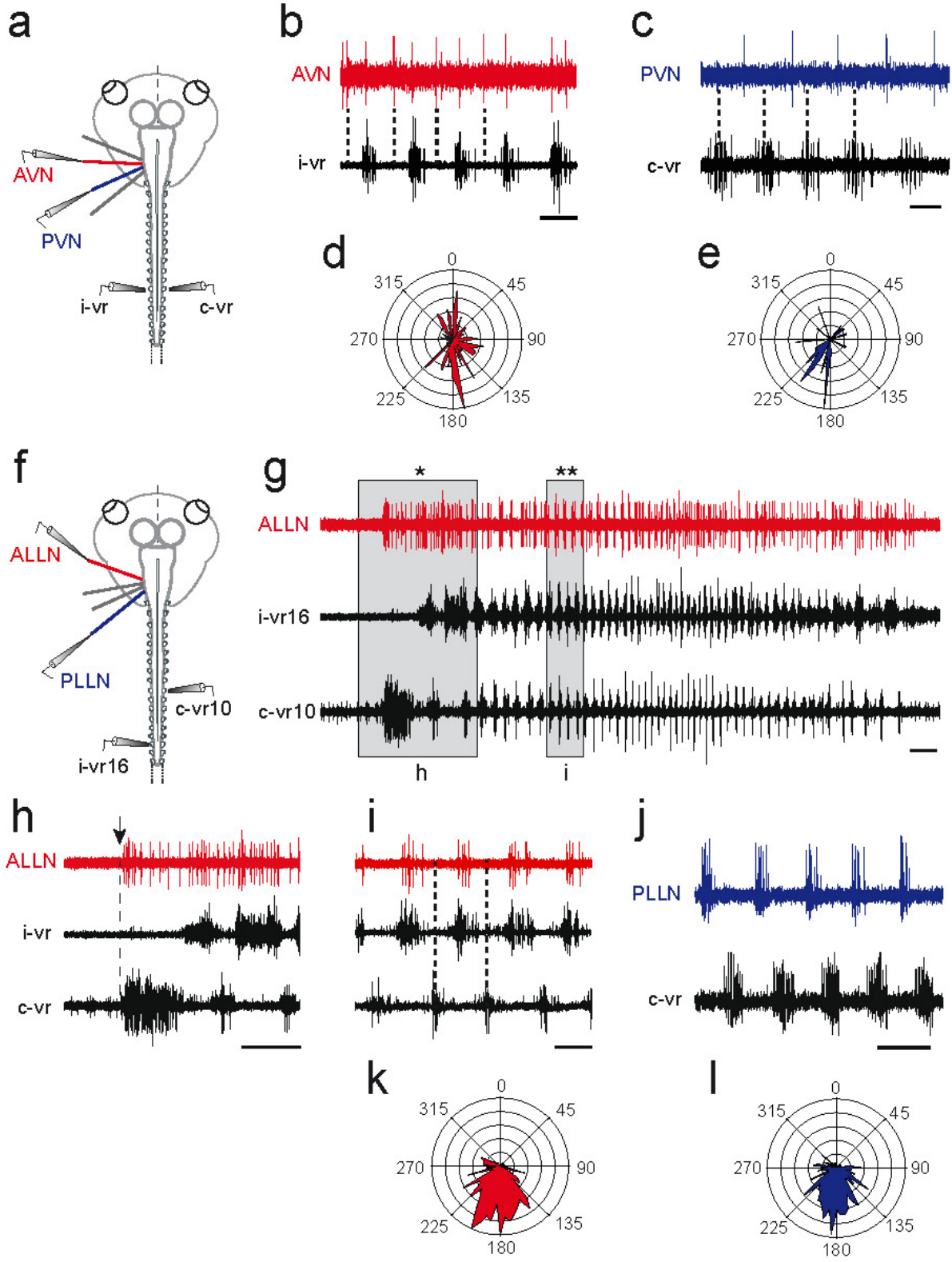

Supplemental figure 1 Coupling of spinal vr and mechanosensory nerve discharge during fictive locomotion in semi-isolated *Xenopus* tadpole preparations (a,f). b,c,g-j, Simultaneous

recordings of various combinations of a left/right spinal vr and the left AVN (b), PVN (c), ALLN (g-i) or PLLN (j) showing activity coordinated mainly in phase opposition (see corresponding polar plots in d,e,k,l). Note that a bi-phasic (coincident as well as alternating) coupling pattern was occasionally observed (dashed line in b; polar plot in d). The initial discharge at episode onset (*) and subsequent expression of regular rhythmic bursting (**; grey areas in g) are shown for simultaneously recorded ALLN and bilateral vrs on an extended time scale in h and i, respectively. After initial tonic firing at swim episode onset (h), the ALLN (i) and PLLN (j) express bursting that remains in strict phase opposition with bursts in the c-vr (see black dashed lines in I and corresponding plots in k and l).

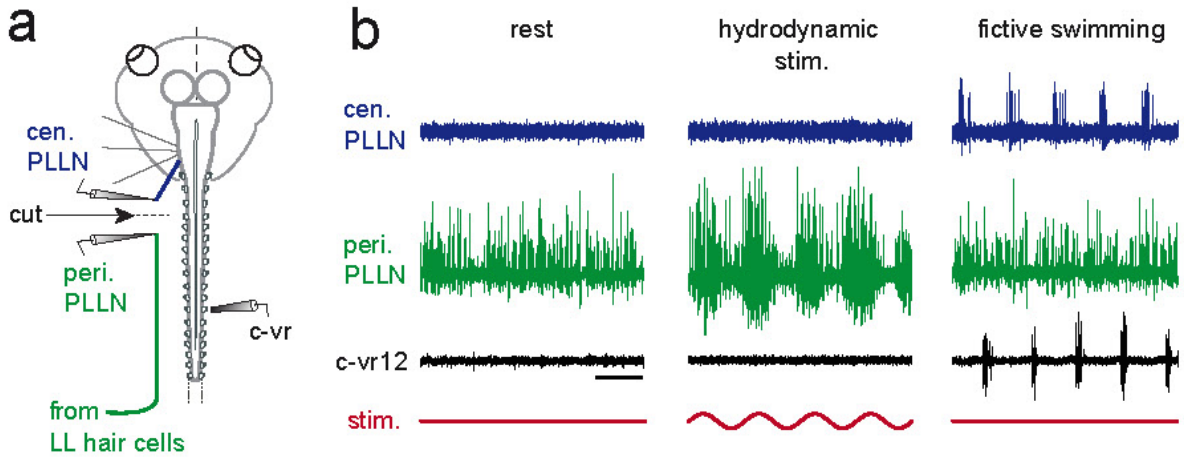

Supplemental figure 2 Identification of efferent and afferent mechanosensory activity in a semi-isolated *in vitro* preparation (a). b, Simultaneous recordings of a spinal vr (c-vr12; black trace in b) and the central (blue in a,b) and peripheral PLLN stumps (green in a,b) after transection of the nerve outside the cranium in a semi-isolated preparation with still intact neuromasts. Recordings in b were made at rest (left panel), during sinusoidal hydrodynamic stimulation (lower red trace) of the neuromasts (middle panel), and during fictive locomotion (right panel). Calibration bar in b: 0.2 s.

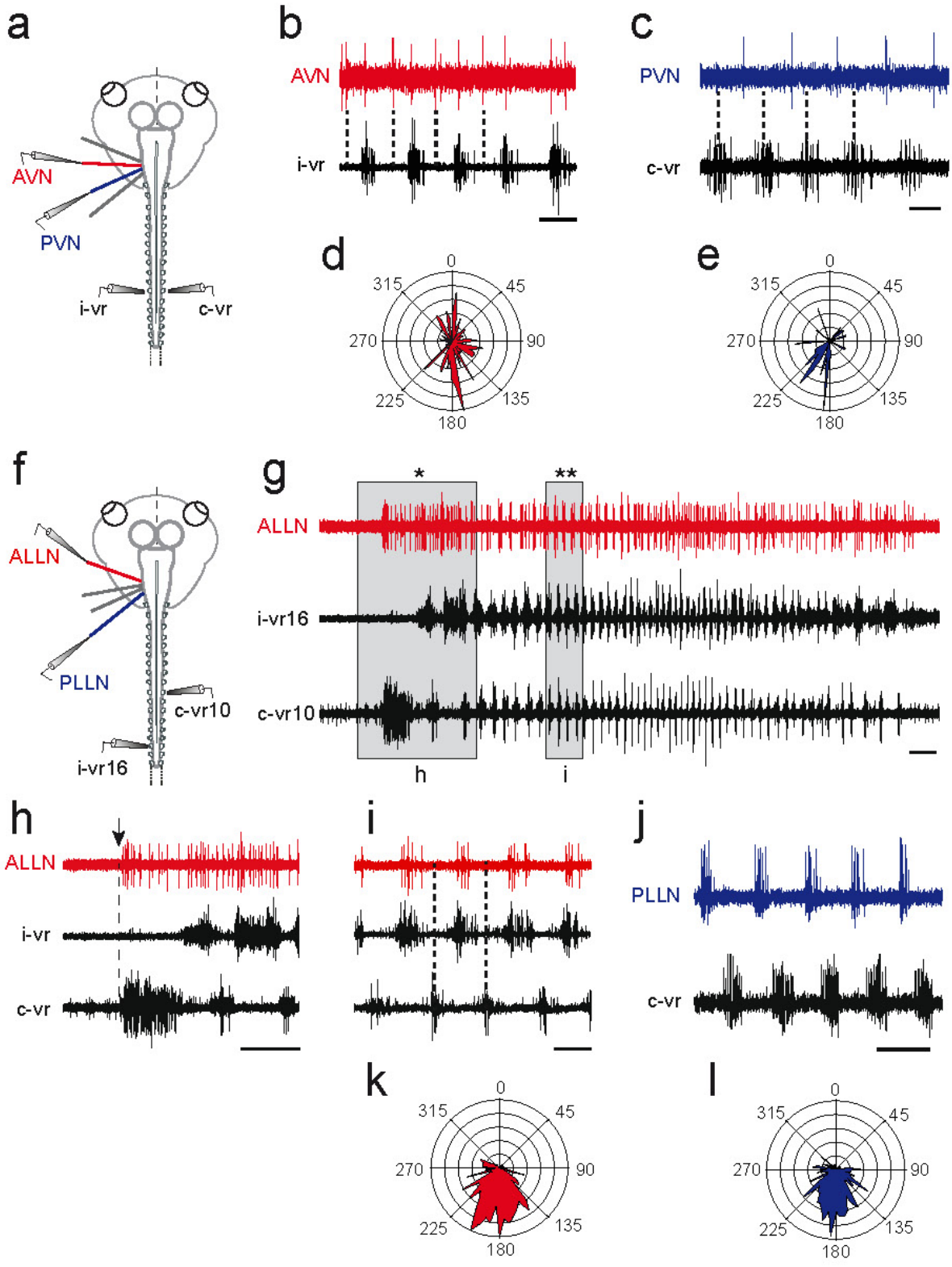

Supplemental figure 3 Vestibular afferent neuron firing at rest and during fictive swimming. a-d, Spontaneous afferent discharge (red traces; upper, raw; lower, instantaneous frequency) in the AVN of controls (a,c) either increases (b) or decreases (d) during locomotor-related rhythmic bursting in a contralateral spinal vr (blue traces). e,f, Box and whisker plots comparing resting rates (e) and discharge regularity (cv^2; f) of all recorded afferent fibers (C; n = 22) in the absence of fictive swimming, and of a subpopulation (n = 6) that was

successfully recorded both before (C') and during fictive swimming (S'). Horizontal calibration bar: 0.2 s for all traces.

References

1 Lewicki, M. S. Efficient coding of natural sounds. *Nat Neurosci* **5**, 356-363 (2002).

2 Smith, E. C. & Lewicki, M. S. Efficient auditory coding. *Nature* **439**, 978-982 (2006).

3 Wark, B., Lundstrom, B. N. & Fairhall, A. Sensory adaptation. *Curr Opin Neurobiol* **17**, 423-429 (2007).

4 Angelaki, D. E. & Cullen, K. E. Vestibular system: the many facets of a multimodal sense. *Annu Rev Neurosci* **31**, 125-150 (2008).

5 Straka, H. & Dieringer, N. Basic organization principles of the VOR: lessons from frogs. *Prog. Neurobiol.* **73**, 259–309 (2004).

6 Carriot, J., Jamali, M., Chacron, M. J. & Cullen, K. E. Statistics of the vestibular input experienced during natural self-motion: implications for neural processing. *J Neurosci* **34**, 8347-8357 (2014).

7 Sperry, R. Neural basis of the spontaneous optokinetic response produced by visual inversion. *J Comp Physiol Psychol* **43**, 482-489 (1950).

8 Holst, E. & Mittelstaedt, H. Das Reafferenzprinzip. *Naturwissenschaften* **37**, 464-476 (1950).

9 Sommer, M. A. & Wurtz, R. H. Brain circuits for the internal monitoring of movements. *Annu Rev Neurosci* **31**, 317-338 (2008).

10 Crapse, T. B. & Sommer, M. A. Corollary discharge across the animal kingdom. *Nat Rev Neurosci* **9**, 587-600 (2008).

11 Sienknecht, U. J., Köppl, C. & Fritzsch, B. Evolution and development of hair cell polarity and efferent function in the inner ear. *Brain Behav Evol* **83**, 150-161 (2014).

12 Leijon, S. & Magnusson, A. K. Physiological characterization of vestibular efferent brainstem neurons using a transgenic mouse model. *PLoS ONE* **9**, e98277 (2014).

13 Highstein, S. M. & Baker, R. Organization of the efferent, vestibular nuclei and nerves of the toadfish, *Opsanus tau*. *J Comp Neurol* **243**, 309-325 (1986).

14 Fritzsch, B. Development of the labyrinthine efferent systema. *Ann N Y Acad Sci* **781**, 21-33 (1996).

15 Hellmann, B. & Fritzsch, B. Neuroanatomical and histochemical evidence for the presence of common lateral line and inner ear efferents and of efferents to the basilar papilla in a frog, *Xenopus laevis*. *Brain Behav Evol* **47**, 185-194 (1996).

16 Roberts, B. L. & Russell, I. J. The activity of lateral-line efferent neurones in stationary and swimming dogfish. *J Exp Biol* **57**, 435-448 (1972).

17 Russell, I. J. The role of the lateral-line efferent system in *Xenopus laevis*. *J Exp Biol* **54**, 621-641 (1971).

18 Tricas, T. C. & Highstein, S. M. Action of the octavolateralis efferent system upon the lateral line of free-swimming toadfish, *Opsanus tau*. *J Comp Physiol A* **169**, 25-37 (1991).

19 Russell, I. J. & Roberts, B. L. Inhibition of spontaneous lateral-line activity by efferent nerve stimulation. *J Exp Biol* **57**, 77-82 (1972).

20 Boyle, R., Rabbitt, R. D. & Highstein, S. M. Efferent control of hair cell and afferent responses in the semicircular canals. *J Neurophysiol* **102**, 1513-1525 (2009).

21 Highstein, S. M. & Baker, R. Action of the efferent vestibular system on primary afferents in the toadfish, *Opsanus tau*. *J Neurophysiol* **54**, 370-384 (1985).

22 Boyle, R. & Highstein, S. Efferent vestibular system in the toadfish: action upon horizontal semicircular canal afferents. *J Neurosci* **10**, 1570-1582 (1990).

23 Rabbitt, R. D., Boyle, R., Holstein, G. R. & Highstein, S. M. Hair-cell versus afferent adaptation in the semicircular canals. *J Neurophysiol* **93**, 424-436 (2004).

24 Myers, S. F., Salem, H. H. & Kaltenbach, J. A. Efferent neurons and vestibular cross talk in the frog. *J Neurophysiol* **77**, 2061-2070 (1997).

25 Goldberg, J. M. & Fernandez, C. Efferent vestibular system in the squirrel monkey: anatomical location and influence on afferent activity. *J Neurophysiol* **43**, 986-1025 (1980).

26 Brichta, A. M. & Goldberg, J. M. Responses to efferent activation and excitatory response-intensity relations of turtle posterior-crista afferents. *J Neurophysiol* **83**, 1224-1242 (2000).

27 Holt, J. C., Lysakowski, A. & Goldberg, J. M. Mechanisms of efferent-mediated responses in the turtle posterior crista. *J Neurosci* **26**, 13180-13193 (2006).

28 Sadeghi, S. G., Goldberg, J. M., Minor, L. B. & Cullen, K. E. Efferent-mediated responses in vestibular nerve afferents of the alert macaque. *J Neurophysiol* **101**, 988-1001 (2009).

29 Jordan, P. M., Parks, X. X., Contini, D. & Holt, J. C. A review of synaptic mechanisms of vestibular efferent signaling in turtles: extrapolation to efferent actions in mammals. *J Vestib Res* **23**, 161-175 (2013).

30 Rossi, M. L., Prigioni, I., Valli, P. & Casella, C. Activation of the efferent system in the isolated frog labyrinth: effects on the afferent EPSPs and spike discharge recorded from single fibers of the posterior nerve. *Brain Res* **185**, 125-137 (1980).

31 Highstein, S. M. The central nervous system efferent control of the organs of balance and equilibrium. *Neuroscience Research* **12**, 13-30 (1991).

32 Tomchik, S. & Lu, Z. Auditory physiology and anatomy of octavolateral efferent neurons in a teleost fish. *J Comp Physiol A* **192**, 51-67 (2006).

33 Combes, D., Merrywest, S. D., Simmers, J. & Sillar, K. T. Developmental segregation of spinal networks driving axial- and hindlimb-based locomotion in metamorphosing *Xenopus laevis*. *J Physiol* **559**, 17-24 (2004).

34 Birinyi, A., Straka, H., Matesz, C. & Dieringer, N. Location of dye-coupled second order and of efferent vestibular neurons labeled from individual semicircular canal or otolith organs in the frog. *Brain Res* **921**, 44-59 (2001).

35 Saitoh, K., Ménard, A. & Grillner, S. Tectal control of locomotion, steering, and eye movements in lamprey. *J Neurophysiol* **97**, 3093-3108 (2007).

36 Cabelguen, J.-M., Bourcier-Lucas, C. & Dubuc, R. Bimodal locomotion elicited by electrical stimulation of the midbrain in the salamander *Notophthalmus viridescens*. *J Neurosci* **23**, 2434-2439 (2003).

37 Lambert, F. M., Beck, J. C., Baker, R. & Straka, H. Semicircular canal size matters for detection of angular self motion. *J Neurosci* **28**, 8086-8096 (2008).

38 Cullen, K., Brooks, J., Jamali, M., Carriot, J. & Massot, C. Internal models of self-motion: computations that suppress vestibular reafference in early vestibular processing. *Exp Brain Res* **210**, 377-388 (2011).

39 Cullen, K. E. Sensory signals during active versus passive movement. *Curr Opin Neurobiol* **14**, 698-706 (2004).

40 Chagnaud, B. P., Simmers, J. & Straka, H. Predictability of visual perturbation during locomotion: implications for corrective efference copy signaling. *Biol Cybern* **106**, 669-679 (2012).

41 Wullimann, M. & Grothe, B. in *The Lateral Line System* Vol. 48 *Springer Handbook of Auditory Research* (eds Sheryl Coombs, Horst Bleckmann, Richard R. Fay, & Arthur N. Popper) Ch. 18, 195-251 (Springer New York, 2014).

42 Bell, C. An efference copy which is modified by reafferent input. *Science* **214**, 450-453 (1981).

43 Kennedy, A. *et al.* A temporal basis for predicting the sensory consequences of motor commands in an electric fish. *Nat Neurosci* **17**, 416-422 (2014).

44 Montgomery, J., Bodznick, D. & Halstead, M. Hindbrain signal processing in the lateral line system of the dwarf scorpionfish *Scopeana papillosus*. *J Exp Biol* **199**, 893-899 (1996).

45 Montgomery, J. C. & Bodznick, D. An adaptive filter that cancels self-induced noise in the electrosensory and lateral line mechanosensory systems of fish. *Neurosci Lett* **174**, 145-148 (1994).

46 Montgomery, J. C. & Bodznick, D. Signals and noise in the elasmobranch electrosensory system. *J Exp Biol* **202**, 1349-1355 (1999).

47 Requarth, T., Kaifosh, P. & Sawtell, N. B. A role for mixed corollary discharge and proprioceptive signals in predicting the sensory consequences of movements. *J Neurosci* **34**, 16103-16116 (2014).

48 Requarth, T. & Sawtell, Nathaniel B. Plastic corollary discharge predicts sensory consequences of movements in a cerebellum-like circuit. *Neuron* **82**, 896-907 (2014).

49 Boyle, R., Carey, J. P. & Highstein, S. M. Morphological correlates of response dynamics and efferent stimulation in horizontal semicircular canal afferents of the toadfish, *Opsanus tau*. *J Neurophysiol* **66**, 1504-1521 (1991).

50 Weeg, M. S., Land, B. R. & Bass, A. H. Vocal pathways modulate efferent neurons to the inner ear and lateral line. *J Neurosci* **25**, 5967-5974 (2005).

51 Lambert, F. M., Combes, D., Simmers, J. & Straka, H. Gaze stabilization by efference copy signaling without sensory feedback during vertebrate locomotion. *Curr Biol* **22**, 1649-1658 (2012).

52 Chagnaud, B. P. & Bass, A. H. Vocal corollary discharge communicates call duration to vertebrate auditory system. *J Neurosci* **33**, 18775–11878 (2013).

53 Goldberg, J. M. & Fernandez, C. Physiology of peripheral neurons innervating semicircular canals of the squirrel monkey. 3. Variations among units in their discharge properties. *J Neurophysiol* **34**, 676-684 (1971).

54 Bleckmann, H. Peripheral and central processing of lateral line information. *J Comp Physiol A* **194**, 145-158 (2008).

55 Goldberg, J. M. Afferent diversity and the organization of central vestibular pathways. *Exp Brain Res* **130**, 277-297 (2000).

56 Cochran, S. L. Evidence against a hypothesis of vestibular efferent function. *Brain Res* **642**, 344-347 (1994).

57 Sadeghi, S. G., Chacron, M. J., Taylor, M. C. & Cullen, K. E. Neural variability, detection thresholds, and information transmission in the vestibular system. *J Neurosci* **27**, 771-781 (2007).

58 Jamali, M., Sadeghi, S. G. & Cullen, K. E. Response of vestibular nerve afferents innervating utricle and saccule during passive and active translations. *J Neurophysiol* **101**, 141-149 (2009).

59 Brooks, J. X. & Cullen, K. E. Early vestibular processing does not discriminate active from passive self-motion if there is a discrepancy between predicted and actual proprioceptive feedback. *J Neurophysiol* **111**, 2465-2478 (2014).

60 Medrea, I. & Cullen, K. E. Multisensory integration in early vestibular processing in mice: the encoding of passive vs. active motion. *J Neurophysiol* **110**, 2704-2717 (2013).

61 Wada, H. Evolutionary history of free-swimming and sessile lifestyles in urochordates as deduced from 18S rDNA molecular phylogeny. *Mol Biol Evol* **15**, 1189-1194 (1998).

62 Lacalli, T. C. New perspectives on the evolution of protochordate sensory and locomotory systems, and the origin of brains and heads. *Phil. Trans R. Soc. London Ser B* **356**, 1565-1572 (2001).

63 Brandt, T., Strupp, M. & Benson, J. You are better off running than walking with acute vestibulopathy. *Lancet* **354**, 746 (1999).

64 Jahn, K., Strupp, M., Schneider, E., Dieterich, M. & Brandt, T. Differential effects of vestibular stimulation on walking and running. *NeuroReport* **11**, 1745-1748 (2000).

65 Nieuwkoop, P. D. & Faber, J. *Normal table of Xenopus laevis (Daudin). A systematical and chronological survey of the development from the fertilized egg till the end of metamorphosis*. (Garland Science, 1994).

66 Ramlochansingh, C., Branoner, F., Chagnaud, B. P. & Straka, H. Efficacy of tricaine methanesulfonate (MS-222) as an anesthetic agent for blocking sensory-motor responses in *Xenopus laevis* tadpoles. *PLoS ONE* **9**, e101606 (2014).

67 Wallén, P. & Williams, T. Fictive locomotion in the lamprey spinal cord *in vitro* compared with swimming in the intact animal. *J. Physiol.* **347**, 225-239 (1983).

68 Kahn, J. & Roberts, A. Experiments on the central pattern generator for swimming in embryos oft he amphibian *Xenopus laevis*. *Phil. Trans R. Soc. London Ser B* **296**, 229-243 (1982).

69 Sillar, K. T., Wedderburn, J. F. S. & Simmers, A. J. The development of swimming rhythmicity in post-embryonic *Xenopus laevis*. *Phil. Trans R. Soc. London Ser B* **246**, 147-153 (1991).

70 Chagnaud, B. P., Baker, R. & Bass, A. H. Vocalization frequency and duration are coded in separate hindbrain nuclei. *Nat Commun* **2:346**, 1-11 (2011).

71 Straka, H., Baker, R. & Gilland, E. Rhombomeric organization of vestibular pathways in larval frogs. *J Comp Neurol* **437**, 42-55 (2001).

3. Discussion

3.1 Experimental advantages of isolated preparations

Reduced amphibian preparations are well suited to study the morpho-functional organization of neuronal circuits, which can be considered to be homologues of those found in amniote vertebrates. The possibility of investigating properties of single neurons or of populations of neurons, which still receive peripheral and central inputs as in a behaving animal, represents a link between slice preparations, cell cultures and *in-vivo* approaches. Other advantages are given by the presence of relatively simple central and peripheral nervous system (CNS, PNS). The accessibility of all neuronal structures (see Fig. 1, 4) allows, by means of tract-tracing techniques, the identification of neuronal subtypes also in the absence of specific genetic tools. The axolotl *in-vitro* preparation, due to the remarkably unfolded and flat morphology of hindbrain regions (Fig. 1), the excellent optical properties of the neuronal tissue, the presence of large neurons (Roth et al., 1993) and to the long survival time in isolation, is perfectly suited for studies necessitating imaging techniques. Using the combination of known and newly established experimental approaches, the central and peripheral connectivity of single neurons can be compared with their responses to a variety of natural stimuli together with their specific genetic (rhombomeric) identity. All these aspects can also be investigated in the presence of fictive motor behaviors. During these motor programs, the possibility to completely remove all sensory feedback allows to unequivocally reveal the presence of CD signals in the different identified cellular subtypes. The origin of these CDs can also be addressed by selective ablations of brain regions. Alternatively, feedback (sensory periphery) and the feedforward mechanisms (CDs) can be kept functional and their interaction can be studied at different levels of sensory-motor processing.

The study of sensory processing and CDs effect in mammalian animal models is often constrained by the CNS complexity together with the large repertoire of locomotor strategies. In contrast, tail/limb-based swimming/walking in amphibians and fishes represent simpler and stereotyped locomotor patterns (Wassersug and Hoff, 1985) with corresponding simpler structures of the related CDs.

3.2 Motor function of CDs

The classical action of CDs on sensory systems has been proposed to be the suppression of reafferent stimulation. In this thesis, I demonstrated one example of locomotor CD, which affects the sensory transduction of passive head movement related signals in vestibular afferent fibers and of water motion related signals in lateral line afferent fibers, thus possibly preventing reafferent stimulation. In addition, I found evidence for another CD also present during locomotion that is directed to a subdivision of the trigeminal motor system. In this case the CD is responsible for the coupling of two otherwise discrete motor behaviors, swimming and tentacle movements. In the latter case, the CD influences a motor system and indirectly also affects a sensory system.

Xenopus larvae display an undulatory tail-based swimming behavior. The propulsive effect of this locomotor activity can be changed by modulating the frequency (up to 5 Hz) and excursion (amplitude) of the single tail beating cycles. The absence of a neck in amphibians leads to a direct mechanical coupling of the tail dynamics with the head structures. The touch sensitive tentacles (up to 1 cm in length) are examples of head structures subjected to rhythmic displacement during swimming. In the absence of a stabilizing mechanism, the constant left-right displacement of the tentacles would potentially produce undesired touch sensation due to contacts with the head or to water friction. However, activation of the tentacle muscles during swimming produces a retraction of these appendages to a stable position at the side of the head, thus potentially preventing reafferent stimulation of the touch sensors. These tentacle retractions are adjusted to the swimming dynamics. Particularly, the tentacles were found to be in the retracted position during high amplitude/frequency swimming (large and fast head oscillations) and extended, due to the lack of corollary activation of tentacle motor neurons, during low amplitude/frequency swimming. These results might be due to the fact that in freely behaving animals during low intensity swimming the tentacles are not subjected to reafferent stimulation and are kept in an extended position to explore the environment. An indirect effect of a CD on a sensory system via the direct activation of a motor system is also represented by the recruitment of the extraocular motor system via locomotor intrinsic signals (Lambert et al., 2012). In this case the compensatory eye movements produced by the locomotor CD stabilize the image on the retina, to maintain a stable perception of visual environment.

Despite the possible function of attenuating overstimulation of the tentacle touch receptors, appendage retraction has been shown to streamline the body shape and increase the efficiency of swimming (Liu et al., 1997). The extended tentacles would produce a significant hydrodynamic drag and thus could impair the rhythmic motion of the head, especially during high intensity (amplitude/frequency) swimming. A comparable alignment of appendages (fore- and hind limbs) to the body in order to achieve streamlining has been found in salamanders (Devolve et al., 1997). In axolotl it has been reported that the external gills are retracted during swimming (D'Aout and Aerts, 1997). From these studies and from the results shown in this thesis, it appears that head appendages (tentacles, gills) and limb retraction represent a common strategy across different amphibian taxa to improve locomotor performances. Limb adduction, as described for salamanders, also occurs in alligators (Manter, 1940; Fish, 1984) and in 'terrestrial swimming' sandfish lizards (Maladen et al., 2009) during the performance of tail-based swimming. Although in all of these studies appendage retraction has been found to be coupled to tail-based undulatory swimming, the neuronal mechanisms involved still remain unknown. However it can be hypothesized that locomotor related CDs, as I showed to be responsible for tentacle retraction in *Xenopus*, might also be the neuronal basis for appendage retraction present in all other vertebrates during locomotion.

3.3 Evolutionary origin of CDs

During evolution, animals developed a way to resolve ambiguity regarding the nature of sensory inputs (Crapse and Sommer, 2008), in order to be able to perceive the world while moving. A conceptually similar strategy for reducing the effect of reafferent stimulation appears to be shared among the different species. The motor command responsible for producing muscle contraction is also used to inform sensory systems or other motor systems about impeding movements. The convergence of these motor copies together with the sensory inputs resulting from the actual motor activity (vestibular, lateral line, proprioceptive, auditory, visual inputs) was probably an evolutionary advantage for acquiring new complex motor behaviors. The comparison between motor commands and the resulting actual motor performance still plays a crucial role in learning of motor skills during animal development (e.g. vocalization, locomotion; Crapse and Sommer, 2008). Moreover corollary discharges were likely used to assist a variety of sensory systems even before the evolutionary appearance of a complex system for the detection of body motion in space (e.g. 'present day' vestibular system). In chordate ancestors, already able to perform undulatory swimming (Fetcho, 1992; Wada, 1998), a vestibular system driving compensatory eye movements and thus stabilizing the gaze during swimming, was unlikely present. A vestibular system able to sense horizontal angular displacement of the head appeared relatively late during evolution in jaw-bearing vertebrates (Fritzsch and Beisel, 2001; Beisel et al., 2005). In the absence of such a 'modern' vestibular system, gaze stabilization in the horizontal plane could be achieved via an appropriate coupling of locomotor regions responsible for the undulatory swimming with the brainstem extraocular motor system (driving eye movements). This possibility can be observed in *Xenopus* tadpoles where a CD originating in spinal premotor areas, is able to generate compensatory eye movements during swimming (also) in the absence of vestibular inputs (Lambert et al., 2012). In this thesis I showed the existence of two additional spinal CDs directed to hindbrain nuclei. The CD to the trigeminal nucleus is able to ensure tentacle retraction during intense locomotor activity, potentially adapting the tadpole hydrodynamics and touch sensation processing during swimming. The other CD is directed to the vestibulo-lateral line efferent nucleus and is involved in tuning the respective peripheral sensory processing, predominantly during intense swimming. These intrinsic signals, originating in the spinal cord and projecting to a variety of hindbrain nuclei in larval *Xenopus*, could represent an evolutionary retained condition, which was already present in

common ancestors of all vertebrates. It is possible that in common ancestors, spinal corollary discharges were present in all sensory modalities and later on were differentially lost/conserved within the different vertebrate subgroups, according to the specific evolutionary selection pressures. Another possibility is that these hindbrain nuclei receiving locomotor CDs were already part of the motor system. In agreement with this hypothesis is the organization of the most rostral neuroaxis (sharing homologies with the vertebrates hindbrain) of the cephalochordate amphioxus, which is closely related to vertebrates (Fritzsch, 1996; Wicht and Lacalli, 2005). In these animals this part of the nervous system is assembled as a partial extension of the spinal cord and contains myotomal motor circuits. Vertebrate hindbrain nuclei receiving locomotor inputs from spinal central pattern generators (sCPGs) could thus reassemble parts of the cephalochordate motor circuitries, which were already extending from the spinal cord to the rostral CNS region homologous of the hindbrain.

Interestingly, all neurons in the hindbrain which were found to receive spinal locomotor CDs are motor neurons (i.e., extraocular motoneurons, Combes et al., 2008; Lambert et al., 2012; trigeminal tentacle motoneurons, this thesis), or originate from motoneurons (i.e., vestibular and lateral line efferent neurons, this thesis). Developmental studies of the efferent peripheral sensory innervation have shown that these latter cells derive from facial brachial motor neurons, which where rerouted from the primitive innervation of facial motor neurons to the newly evolved hair cells of the lateral line and inner ear (Simmons, 2002; Sienknecht et al., 2014).

3.4 Effect of CDs during voluntary and stereotyped movement: context dependent adaptation of sensory-motor systems

Across vertebrates the vestibulo-ocular reflex (VOR) stabilizes gaze during animals daily activities by producing eye movements with the appropriate amplitude and opposite direction with respect to the head motion. At the same time this system ensures posture control during head/body movements (Angelaki and Cullen, 2008; Cullen, 2012; Carriot et al., 2014).

The classical view of these sensory-motor transformations as hardwired reflexes appears to be in contrast with the experimental findings of the last decade, where a variety of possible context dependent adaptations in the sensory-motor transformation have emerged. In humans (Zangemeister and Stark, 1982; André-Deshays et al., 1988) and non-human primates (Bizzi et al., 1971; Tomlinson and Bahra, 1986) gaze can be voluntarily redirected to a new spatial point by coordinated movements of the head and eyes. During this gaze shift, the VOR would produce eye movements in the opposite direction compared to the head rotation, not allowing the intended fixation of the new point. A variety of behavioral experiments in humans (Laurutis and Robinson, 1986; Guitton and Volle, 1987; Pelisson et al., 1988) and monkeys (Tomlinson and Bahra, 1986) have proved that the VOR is attenuated during the gaze shift, with a degree that is proportional to the amplitude of the head motion. Electrophysiological experiments conducted in monkeys revealed the neuronal correlate for the behavioral observations (Roy and Cullen, 1998, 2004). Vestibular neurons receiving afferent fibers and projecting to the extraocular motoneurons were found to encode head velocity during passive rotation of the entire body to a larger degree compared to voluntary head-gaze shifts. Furthermore, as it was the case in the behavioral experiments, the attenuation of encoded velocity, found at the level of the single vestibular neuron, was proportional to the magnitude of the gaze shift. For the first time, it clearly emerged that the VOR is not a hardwired reflex; it can be differentially modulated to efficiently enable specific behavioral tasks. Vestibular neurons in monkeys receive direct projections from afferent fibers encoding passive and voluntary head motions (Cullen and Minor, 2002), compatible with the absence of a peripheral sensory filtration. A subpopulation of these neurons, called vestibular only (VO) neurons carry information about motion only during passive and not during voluntary head rotation (Boyle et al., 1996; McCrea et al., 1999; Roy and Cullen, 2001). These cancellation signals at the level of VO neurons were found only when the head of the monkey was left free to perform actual rotational movements. In a head-restrained condition, the simple

attempt to perform head rotations did not cause any change in the resting firing rate of the VO neurons (Roy and Cullen, 2004). It was concluded that an integration between efference copies of the signals going to the neck muscles and proprioceptive inputs from these muscles, only present during actual head rotations, has to take place in order to generate the inhibition. From this study we can conclude that the adaptation of the VOR during voluntary head movements takes place, at least in monkeys, at the level of the central processing regions, since vestibular afferent fibers equally encode passive and active head movements. It still remains unknown if the efferent nucleus, projecting to hair cells and afferent fibers, is activated during this motor behavior, even though it is not responsible for this task-dependent tuning of the vestibular system in these animals. In contrast to this evidence from monkeys, in this thesis it has been shown that the vestibulo-lateral line efferent nucleus is active during another motor behavior, namely locomotion. This CD activation, mediated by the sCPG (spinal central pattern generator), in the absence of any sensory feedback, is able to produce attenuation in the sensory processing of natural head movements already at the level of the sensory periphery (afferent fibers). At the same time, in these animals, another previously identified spinal locomotor CD (Lambert et al., 2012) acts as a feedforward mechanism to stabilize gaze during swimming-induced head rotation. Interestingly, behavioral studies in mammals, including humans, have found a differential processing of vestibular inputs during walking or running (Brandt et al., 1999; Jahn et al., 2000). In studies, conducted on healthy humans with a reversible impairment of the vestibular system or in patients with vestibular deficits, the ability to maintain balance or to walk parallel to a straight line was greater during running than during walking. From these observations, the authors hypothesized that the independent spinal networks, predominantly active during running, could be responsible for the attenuated vestibular control of locomotion seen during running compared to walking (Jahn et al., 2000). It appears that once a stereotyped, automatic motor program has been initiated, the processing of vestibular inputs can be suppressed. In my thesis I showed that also in amphibian larvae, such a differential gating of vestibular inputs is present during stereotyped locomotor behavior. The spinal nature of the CD was also proved, as it was hypothesized for humans. Furthermore, one of the possible neuronal substrates for this adaptation was revealed, namely the activation of the vestibular efferent nucleus during locomotion. The behavioral differences found in humans during walking and running could be explained by means of a differential activation of the efferent system, similarly to what we could show in amphibians. Particularly, we found that all locomotor parameters (intensity/frequency, amplitude and duration) are reliably represented in the firing

pattern of the efferent nucleus and that, depending on these variables, the encoding of head motion is dynamically adjusted. From comparing these results with the vestibular adaptation present during active head movements and walking in monkeys and humans, some interesting and important considerations arise.

1) Voluntary neck-driven movements of the head represent a non-stereotyped and non-automatic motor behavior leading to an active, direct stimulation of the vestibular system.

2) Running/swimming behaviors, on the other hand, are stereotyped, automatic and 'unconscious' motor behaviors, causing movement of the entire body and thus indirect stimulation of the vestibular system.

3) It might be possible that, depending on the nature of motor programs (stereotyped and non-stereotyped), two different CDs originating at two different levels of the nervous system (cortical premotor areas and spinal CPGs) are implemented to filter vestibular sensations.

4) The two CDs act at different levels of the sensory-motor transformation: peripheral level via efferent neurons (spinal CD) and central level via second order vestibular neurons and cerebellum (cortical CD).

3.5 Tuning of sensory systems to stimulus statistics

Animals experience a large variety of stimuli that are detected by the specific sensory systems. Stimuli that are encoded within the same sensory modality can assume a widely extended range of values in different dimensions (e.g. amplitude, frequency, time, space).

To understand this dimensional complexity, the natural visual environment can be considered. During daylight, luminance and contrast differ over orders of magnitudes in time and space; all these possible values can be referred to as the global (e.g. over the entire day and space) distribution of the stimuli. This distribution contains all the possible local distributions of the stimuli (e.g. over a smaller time or space scale), which can differ a lot from each other. Barlow (1961) hypothesized that, given a finite capacity to transmit information (given by a finite detection range for a sensory system), neuronal systems have to employ efficient coding strategies to maximally represent inputs that they mostly have to process. It clearly appears that, to achieve an efficient coding over the global distribution of stimuli (e.g. visual representation of the entire day), a sensory system has to be constantly tuned to the very different local distributions (Wark et al., 2007). Across animals, a variety of studies have shown that sensory systems can dynamically adapt over multiple time scales in

order to most efficiently detect and process stimuli which are more likely over that specific period of time (Wark et al., 2007).

In experiments underlying this thesis, sensory adaptation was investigated for the vestibular and lateral line systems as well as its potential role in touch reception. The vestibular system has to deal with a global distribution of movement related stimuli, which comprises a variety of different local distributions encountered during the disparate animals daily motor activities (e.g. standing, voluntary head movements, head movements related to different locomotor strategies). During the different motor tasks, body/head acceleration can vary strongly along the different dimensions (magnitude, space and time); to ensure an efficient posture and gaze stabilization across these local distributions, an adaptation of the sensory-motor transformation, weighted on the stimulus statistics, has to take place. Maintaining body posture and stable gaze during a relatively stationary condition (standing, floating) requires compensation of small and slow movements. During these conditions, the sensory encoding has to be highly sensitive to small changes in head/body position. This high sensitivity would generate an overstimulation of the system during much higher amplitude and faster dynamics of head/body motion (e.g. walking/running, swimming), impairing the encoding of stimuli in this range. In my thesis, I showed that a dynamic tuning of the vestibular system is indeed present at the level of the sensory periphery. During swimming behavior in *Xenopus* tadpoles, large oscillations of the head are present compared to the relatively small motion in the absence of sustained tail-based propulsion. In these animals, the degree of adaptation is particularly related to the level of locomotor intensity, in accordance with the different stimulus statistics. The sensory periphery is informed about intense ongoing swimming activity driven by the entire trunk-tail musculature, which produces large oscillations of the head. During non-undulatory swimming (related to a drifting of the larvae with no oscillations of the head), produced by the most caudal part of the tail, no peripheral sensory gating is produced. This complies with the fact that the vestibular system has to maintain a high sensitivity for small amplitudes of slow motion related stimuli.

The dynamic adaptation of head/body movement sensitivities might be responsible for ensuring efficient encoding across the global natural stimuli range encountered by the tadpoles.

Conceptually similar functional consequences can be discussed for the adaptation of the lateral line sensory periphery also found in *Xenopus* during swimming. As previously discussed, the fact that the vestibular system has to deal with different stimulus statics is directly linked to its intrinsic sensitivity to movement related stimuli. For the lateral line

system, even if an intrinsic sensitivity to self-produced movements is not present, the change in stimulus statistics is related to the water motion produced during active body movements. The turbulences and the reflected water waves, consequences of intense undulatory swimming, can be detected by the lateral line neuromasts along the animal´s body axis as already shown in different fish species (Montgomery et al., 2009). Also in this case, we can argue that there are multitudes of local stimulus distributions related to the modulation of the different locomotor parameters. To ensure an efficient coding along the wide distribution of values it was found that the attenuation in water motion sensitivity is related to the swimming intensity. Also for this system, during non-undulatory swimming behavior (related to exclusive motor activity in the caudal spinal cord), no peripheral sensory adaptation was encountered.

Across different sensory modalities and animals (reviewed in Wark et al., 2007), adequate time-scales have been shown to be necessary for the systems to acquire information about the local stimulus statistics in order to efficiently adapt the encoding process. In sensory systems involved in the processing of external stimuli (e.g. visual, auditory), the environment has a large impact in changing the stimulus statistics and thus a feedback mechanism has to be used to tune the system at the peripheral or central level (Fairhall et al., 2001; Zaghloul et al., 2005; Nagel and Doupe, 2006). Due to the unpredictability of the environmental inputs, an *a posteriori* estimate of the stimulus probability distribution has to be computed in order to tune the encoding process. As discussed above, in the vestibular and lateral line system an *a priori* estimation can be implemented to ensure an efficient encoding across different stimulus statistics. In these sensory modalities, active body motion predicts different local stimulus distributions. A feed-forward mechanism, informing the sensory periphery about detailed locomotor parameters, is thus predictive of the impeding local stimulus statistics and can reliably be used to dynamically adapt sensory processing. Furthermore, it can be hypothesized that in the latter systems, depending on the specific motor tasks and the presence or absence of external stimuli, feedforward and feedback signals are integrated at different central levels of the nervous system to ensure optimal sensory encoding.

3.6 Open Questions

In this thesis I showed that feedforward mechanisms are used in amphibian larvae to compensate for the reafferent stimulation of the sensory periphery resulting from locomotor activity. Thus, these locomotor CDs have been found to influence sensory processing directly at the peripheral level (otic capsule, lateral line neuromasts and tentacles). Future studies should reveal if spinal CPG-CDs are also involved in regulating the central gating of sensory information and thus if there is an interaction between intrinsic motion driving signals and the resulting motion sensory feedback signals (vestibular, lateral line, visual, muscle proprioception). The comparison between intrinsic and sensory signals has been shown to be essential in producing tuning at the level of the central vestibular system during voluntary head movements in monkeys (Cullen, 2004; Roy and Cullen, 2004). During this motor task the activation of extraocular motoneurons (i.e. the output of the vestibular sensory-motor transformation) is suppressed by inhibiting their central inputs (i.e. central vestibular neurons). In contrast, the peripheral inputs to central vestibular neurons (vestibular afferent fibers) are not affected during the motor behavior. From previous studies in *Xenopu*s larvae it emerges that during locomotion there is a complete suppression of vestibular inputs to a specific sup-population of extraocular motoneurons; for these neurons the vestibular inputs are cancelled, with compensatory eye movements exclusively driven by the locomotor CD (Combes et al., 2008; Lambert et al., 2012). The complete cancelation of the VOR seen in these studies, due to the evidence found in my study, appears to be in disagreement with a pure peripheral suppression. The vestibular peripheral inputs (i.e. from hair cells/afferent fibers, to central vestibular neurons) are not completely cancelled during locomotion but only partially suppressed (40% reduction). From these considerations we can infer the presence of a central suppression of vestibular processing, which requires investigation in future studies.
During preliminary experiments in axolotl at larval and juvenile stages (see Fig. 6) I could show that also in these animals the efferent nucleus of the vestibular system receives a locomotion (walking) related CD. Salamander species, due to their bimodal locomotor pattern (walking/swimming), offer great advantages for understanding the neuronal networks responsible for these two motor behaviors (Cabelguen et al., 2003; Chevallier et al., 2007). The spinal premotor network (i.e. sCPGs) has been investigated in great details over the last decades; clusters of specifically identified and localized CPGs have been shown to selectively drive the rhythmic/alternated flexion and extension of the limbs during walking

(Cheng et al., 1998; Delvolvé et al., 1999).

Further experiments in axolotl could thus elucidate which of the locomotor related features are transmitted to the vestibular and lateral line efferent nucleus and in which subpopulations of sCPGs (extensor/flexor) the CD originates.

3.7 Conclusion

In this thesis, novel and already established experimental approaches were combined to understand basic organizational and functional properties of brainstem sensory-motor circuits. This work represents one of the first steps in revealing neuronal substrates responsible for the diverse motor and sensory system adaptations, which have to take place during animal locomotion. Feedforward mechanisms, in absence of feedback inputs, were found to play a crucial role in creating a sensory-motor balance during rhythmic locomotor behaviors, potentially ensuring optimal efficiency of sensory encoding and motor performances.

References

André-Deshays C, Berthoz A, Revel M (1988) Eye-head coupling in humans. I. Simultaneous recording of isolated motor units in dorsal neck muscles and horizontal eye movements. Exp brain Res 69:399–406.

Angelaki DE, Cullen KE (2008) Vestibular system: the many facets of a multimodal sense. Annu Rev Neurosci 31:125–150.

Barlow H (1961) Possible principles underlying the transformation of sensory messages. In: Sensory Communication (W.Rosenblith, ed), pp 217–234. Cambridge,Mass: M.I.T. Press.

Beisel KW, Wang-Lundberg Y, Maklad A, Fritzsch B (2005) Development and evolution of the vestibular sensory apparatus of the mammalian ear. J Vestib Res 15:225–241.

Berg RW, Kleinfeld D (2003) Rhythmic whisking by rat: retraction as well as protraction of the vibrissae is under active muscular control. J Neurophysiol 89:104–117.

Bernard C, Cochran SL, Precht W (1985) Presynaptic actions of cholinergic agents upon the hair cell-afferent fiber synapse in the vestibular labyrinth of the frog. Brain Res 338:225–236.

Bizzi E, Kalil RE, Tagliasco V (1971) Eye-head coordination in monkeys: evidence for centrally patterned organization. Science 173:452–454.

Blakemore SJ, Wolpert DM, Frith CD (1998) Central cancellation of self-produced tickle sensation. Nat Neurosci 1:635–640.

Bleckmann H (2008) Peripheral and central processing of lateral line information. J Comp Physiol A Neuroethol Sens Neural Behav Physiol 194:145–158.

Boyle R, Belton T, McCrea RA (1996) Responses of identified vestibulospinal neurons to voluntary eye and head movements in the squirrel monkey. Ann N Y Acad Sci 781:244–263.

Boyle R, Carey JP, Highstein SM (1991) Morphological correlates of response dynamics and efferent stimulation in horizontal semicircular canal afferents of the toadfish, Opsanus tau. J Neurophysiol 66:1504–1521.

Brainard MS, Doupe AJ (2000) Auditory feedback in learning and maintenance of vocal behaviour. Nat Rev Neurosci 1:31–40.

Brandt T, Strupp M, Benson J (1999) You are better off running than walking with acute vestibulopathy. Lancet 354:746.

Branoner F, Straka H (2014) Semicircular canal-dependent developmental tuning of translational vestibulo-ocular reflexes in Xenopus laevis. Dev Neurobiol.

Brichta AM, Goldberg JM (2000) Responses to Efferent Activation and Excitatory Response-Intensity Relations of Turtle Posterior-Crista Afferents. J Neurophysiol 83:1224–1242.

Brooks JX, Cullen KE (2014) Early vestibular processing does not discriminate active from passive self-motion if there is a discrepancy between predicted and actual proprioceptive feedback. J Neurophysiol 111:2465–2478.

Cabelguen J-M, Bourcier-Lucas C, Dubuc R (2003) Bimodal Locomotion Elicited by Electrical Stimulation of the Midbrain in the Salamander Notophthalmus viridescens. J Neurosci 23:2434–2439.

Cannone A, Kelly P (1977) The tentacles of Xenopus laevis tadpoles - Evidence for a mechano-receptive role. South African Med J 52:406–418.

Carriot J, Jamali M, Chacron MJ, Cullen KE (2014) Statistics of the vestibular input experienced during natural self-motion: implications for neural processing. J Neurosci 34:8347–8357.

Chagnaud BP, Bass AH (2013) Vocal corollary discharge communicates call duration to vertebrate auditory system. J Neurosci 33:18775–18780.

Chapman CE (1994) Active versus passive touch: factors influencing the transmission of somatosensory signals to primary somatosensory cortex. Can J Physiol Pharmacol 72:558–570.

Cheng J, Stein RB, Jovanović K, Yoshida K, Bennett DJ, Han Y (1998) Identification, localization, and modulation of neural networks for walking in the mudpuppy (Necturus maculatus) spinal cord. J Neurosci 18:4295–4304.

Chevallier S, Jan A, Ryczko D, Nagy F, Cabelguen J (2007) Organisation of the spinal central pattern generators for locomotion in the salamander : Biology and modelling. 57.

Combes D, Le Ray D, Lambert FM, Simmers J, Straka H (2008) An intrinsic feed-forward mechanism for vertebrate gaze stabilization. Curr Biol 18:R241–R243.

Combes D, Merrywest SD, Simmers J, Sillar KT (2004) Developmental segregation of spinal networks driving axial- and hindlimb-based locomotion in metamorphosing Xenopus laevis. J Physiol 559:17–24.

Crapse TB, Sommer MA (2008) Corollary discharge across the animal kingdom. Nat Rev Neurosci 9:587–600.

Cullen KE (2004) Sensory signals during active versus passive movement. Curr Opin Neurobiol 14:698–706.

Cullen KE (2012) The vestibular system: multimodal integration and encoding of self-motion for motor control. Trends Neurosci 35:185–196.

Cullen KE, Brooks JX, Jamali M, Carriot J, Massot C (2011) Internal models of self-motion: computations that suppress vestibular reafference in early vestibular processing. Exp Brain Res 210:377–388.

Cullen KE, Minor LB (2002) Semicircular canal afferents similarly encode active and passive head-on-body rotations: implications for the role of vestibular efference. J Neurosci 22:1–7.

D'Aout K, Aerts P (1997) Kinematics and efficiency of steady swimming in adult axolotls (Ambystoma mexicanum). J Exp Biol 200:1863–1871.

Davis WJ, Siegler M V, Mpitoses (1973) Distributed neuronal oscillators and efference copy in the feeding system of Pleurobranchaea. J Neurophysiol 36:258–274.

Delvolvé I, Branchereau P, Dubuc R, Cabelguen J, Chau C, Giroux N, Barbeau H, Jordan L, Rossignol S (1999) Fictive Rhythmic Motor Patterns Induced by NMDA in an In Vitro Brain Stem − Spinal Cord Preparation From an Adult Urodele. :1074–1077.

Dieringer N, Precht W (1979) Mechanisms of compensation for vestibular deficits in the frog. Exp Brain Res 36:311–328.

Fairhall AL, Lewen GD, Bialek W, de Ruyter van Steveninck RR (2001) Efficiency and ambiguity in an adaptive neural code. Nature 412:787–792.

Fee MS, Mitra PP, Kleinfeld D (1997) Central versus Peripheral Determinants of Patterned Spike Activity in Rat Vibrissa Cortex During Whisking. J Neurophysiol 78:1144–1149.

Fetcho JR (1992) The spinal motor system in early vertebrates and some of its evolutionary changes. Brain Behav Evol 40:82–97.

Fish FE (1984) Kinematics of Undulatory Swimming in the American Alligator. Copeia 1984:839–843.

Fox H (1999) Barbels and barbel-like tentacular structures in sub-mammalian vertebrates : a review. :153–193.

Fritzsch B (1996) Development of the labyrinthine efferent system. Ann N Y Acad Sci 781:21–33.

Fritzsch B, Beisel K. (2001) Evolution and development of the vertebrate ear. Brain Res Bull 55:711–721.

Gibson JJ (1962) Observations on active touch. Psychol Rev 69:477–491.

Gilland E, Baker R (2005) Evolutionary patterns of cranial nerve efferent nuclei in vertebrates. Brain Behav Evol 66:234–254.

Gilland E, Straka H, Wong TW, Baker R, Zottoli SJ (2014) A hindbrain segmental scaffold specifying neuronal location in the adult goldfish, Carassius auratus. J Comp Neurol 522:2446–2464.

Goldberg JM, Fernández C (1980) Efferent vestibular system in the squirrel monkey: anatomical location and influence on afferent activity. J Neurophysiol 43:986–1025.

Grewe BF, Langer D, Kasper H, Kampa BM, Helmchen F (2010) High-speed in vivo calcium imaging reveals neuronal network activity with near-millisecond precision. Nat Methods 7:399–405.

Guitton D, Volle M (1987) Gaze control in humans: eye-head coordination during orienting movements to targets within and beyond the oculomotor range. J Neurophysiol 58:427–459.

Hage SR, Jürgens U (2006) On the role of the pontine brainstem in vocal pattern generation: a telemetric single-unit recording study in the squirrel monkey. J Neurosci 26:7105–7115.

Hanneman E, Trevarrow B, Metcalfe WK, Kimmel CB, Westerfield M (1988) Segmental pattern of development of the hindbrain and spinal cord of the zebrafish embryo. 58.

Häusser M (2014) Optogenetics: the age of light. Nat Methods 11:1012–1014.

Hellmann B, Fritzsch B (1996) Neuroanatomical and histochemical evidence for the presence of common lateral line and inner ear efferents and of efferents to the basilar papilla in a frog, Xenopus laevis. Brain Behav Evol 47.

Highstein SM, Baker R (1985) Action of the efferent vestibular system on primary afferents in the toadfish, Opsanus tau. J Neurophysiol 54:370–384.

Holt JC, Lysakowski A, Goldberg JM (2006) Mechanisms of efferent-mediated responses in the turtle posterior crista. J Neurosci 26:13180–13193.

Jahn K, Strupp M, Schneider E, Dieterich M, Brandt T (2000) Differential effects of vestibular stimulation on walking and running. Neuroreport 11:1745–1748.

Jamali M, Sadeghi SG, Cullen KE (2009) Response of vestibular nerve afferents innervating utricle and saccule during passive and active translations. J Neurophysiol 101:141–149.

Kleinfeld D, Ahissar E, Diamond ME (2006) Active sensation: insights from the rodent vibrissa sensorimotor system. Curr Opin Neurobiol 16:435–444.

Lambert F, Malinvaud D, Gratacap M, Straka H, Vidal P-P (2013) Restricted neural plasticity in vestibulospinal pathways after unilateral labyrinthectomy as the origin for scoliotic deformations. J Neurosci 33:6845–6856.

Lambert FM, Beck JC, Baker R, Straka H (2008) Semicircular canal size determines the developmental onset of angular vestibuloocular reflexes in larval Xenopus. J Neurosci 28:8086–8095.

Lambert FM, Combes D, Simmers J, Straka H (2012) Gaze stabilization by efference copy signaling without sensory feedback during vertebrate locomotion. Curr Biol 22:1649–1658.

Laurutis VP, Robinson DA (1986) The vestibulo-ocular reflex during human saccadic eye movements. J Physiol 373:209–233.

Lee RK, Eaton RC (1991) IIdentifiable reticulospinal neurons of the adult zebrafish, Brachydanio rerio. 3432.

Lee RK, Eaton RC, Zottoli SJ (1993) Segmental arrangement of reticulospinal neurons in the goldfish hindbrain. J Comp Neurol 329:539–556.

Leijon S, Magnusson AK (2014) Physiological characterization of vestibular efferent brainstem neurons using a transgenic mouse model. PLoS One 9:e98277.

Liu H, Wassersug R, Kawachi K (1997) The three-dimensional hydrodynamics of tadpole locomotion. J Exp Biol 200:2807–2819.

Magherini PC, Giretti ML, Precht W (1975) Cerebellar control of vestibular neurons of the frog. Pflugers Arch Eur J Physiol 356:99–109.

Maladen RD, Ding Y, Li C, Goldman DI (2009) Undulatory swimming in sand: subsurface locomotion of the sandfish lizard. Science 325:314–318.

Malinvaud D, Vassias I, Reichenberger I, Rössert C, Straka H (2010) Functional organization of vestibular commissural connections in frog. J Neurosci 30:3310–3325.

Manter JT (1940) The mechanics of swimming in the alligator. J Exp Zool 83:345–358.

Margoliash D (1997) Functional organization of forebrain pathways for song production and perception. J Neurobiol 33:671–693.

Margoliash D (2002) Evaluating theories of bird song learning: implications for future directions. J Comp Physiol A Neuroethol Sens Neural Behav Physiol 188:851–866.

Maricich SM, Wellnitz SA, Nelson AM, Lesniak DR, Gerling GJ, Lumpkin EA, Zoghbi HY (2009) Merkel cells are essential for light-touch responses. Science 324:1580–1582.

McCrea RA, Gdowski GT, Boyle R, Belton T (1999) Firing behavior of vestibular neurons during active and passive head movements: vestibulo-spinal and other non-eye-movement related neurons. J Neurophysiol 82:416–428.

Medrea I, Cullen KE (2013) Multisensory integration in early vestibular processing in mice: the encoding of passive versus active motion. J Neurophysiol:2704–2717.

Metcalfe WK, Mendelson B, Kimmel CB (1986) Segmental homologies among reticulospinal neurons in the hindbrain of the zebrafish larva. J Comp Neurol 251:147–159.

Minor L, Goldberg J (1991) Vestibular-nerve inputs to the vestibulo-ocular reflex: a functional- ablation study in the squirrel monkey. J Neurosci 11:1636–1648.

Montgomery JC, Windsor S, Bassett D (2009) Behavior and physiology of mechanoreception: separating signal and noise. Integr Zool 4:3–12.

Nagel KI, Doupe AJ (2006) Temporal processing and adaptation in the songbird auditory forebrain. Neuron 51:845–859.

Nieuwkoop and Faber J (1956) Normal Table of Xenopus Laevis (Daudin): A Systematical & Chronological Survey of the Development from the Fertilized Egg till the End of Metamorp. Garland Science.

Ovalle W (1979) Neurite complexes with Merkel cells in larval tentacles of Xenopus laevis. Cell Tissue Res 204:233–241.

Ovalle W, Shinn S, Nahirney P (1998) Ultrastructure of the larval tentacle and its skeletal muscle in Xenopus laevis. Tissue Cell 30:216–225.

Pelisson D, Prablanc C, Urquizar C (1988) Vestibuloocular reflex inhibition and gaze saccade control characteristics during eye-head orientation in humans. J Neurophysiol 59:997–1013.

Piston D (1999) Imaging living cells and tissues by two-photon excitation microscopy. Trends Cell Biol 9:66–69.

Plotnik M, Marlinski V, Goldberg JM (2002) Reflections of Efferent Activity in Rotational Responses of Chinchilla Vestibular Afferents. J Neurophysiol 88:1234–1244.

Poulet JFA, Hedwig B (2006) The cellular basis of a corollary discharge. Science 311:518–522.

Reiner A, Yamamoto K, Karten HJ (2005) Organization and evolution of the avian forebrain. Anat Rec A Discov Mol Cell Evol Biol 287:1080–1102.

Roberts BL, Russell IJ (1972) The activity of lateral-line efferent neurones in stationary and swimming dogfish. J Exp Biol 57:435–448.

Rossi ML, Martini M (1991) Efferent control of posterior canal afferent receptor discharge in the frog labyrinth. Brain Res 555:123–134.

Rossi ML, Prigioni I, Valli P, Casella C (1980) Activation of the efferent system in the isolated frog labyrinth: effects on the afferent EPSPs and spike discharge recorded from single fibres of the posterior nerve. Brain Res 185:125–137.

Roth G, Nishikawa KC, Naujoks-Manteuffel C, Schmidt A, Wake DB (1993) Paedomorphosis and simplification in the nervous system of salamanders. Brain Behav Evol 42:137–170.

Roy JE, Cullen KE (1998) A neural correlate for vestibulo-ocular reflex suppression during voluntary eye – head gaze shifts. 1.

Roy JE, Cullen KE (2001) Selective Processing of Vestibular Reafference during Self-Generated Head Motion. J Neurosci 21:2131–2142.

Roy JE, Cullen KE (2004) Dissociating self-generated from passively applied head motion: neural mechanisms in the vestibular nuclei. J Neurosci 24:2102–2111.

Russell IJ (1968) Influence of efferent fibres on a receptor. Nature 219:177–178.

Russell IJ (1971) The role of the lateral-line efferent system in Xenopus laevis. J Exp Biol 54:621–641.

Russell IJ, Roberts BL (1972) Inhibition of spontaneous lateral-line activity by efferent nerve stimulation. J Exp Biol 57:77–82.

Sadeghi SG, Chacron MJ, Taylor MC, Cullen KE (2007) Neural variability, detection thresholds, and information transmission in the vestibular system. J Neurosci 27:771–781.

Sadeghi SG, Goldberg JM, Minor LB, Cullen KE (2009) Efferent-mediated responses in vestibular nerve afferents of the alert macaque. J Neurophysiol 101:988–1001.

Saitoh K, Ménard A, Grillner S (2007) Tectal control of locomotion, steering, and eye movements in lamprey. J Neurophysiol 97:3093–3108.

Schall JD (2004) On the role of frontal eye field in guiding attention and saccades. Vision Res 44:1453–1467.

Shimazu H, Precht W (1966) Inhibition of central vestibular neurons from the contralateral labyrinth and its mediating pathway. J Neurophysiol 29:467–492.

Sienknecht UJ, Köppl C, Fritzsch B (2014) Evolution and development of hair cell polarity and efferent function in the inner ear. Brain Behav Evol 83:150–161.

Sillar KT, Roberts A (1988) A neuronal mechanism for sensory gating during locomotion in a vertebrate. Nature 331:262–265.

Simmons DD (2002) Development of the inner ear efferent system across vertebrate species. J Neurobiol 53:228–250.

Sommer MA, Wurtz RH (2002) A pathway in primate brain for internal monitoring of movements. Science 296:1480–1482.

Sperry RW (1950) Neural basis of the spontaneous optokinetic response produced by visual inversion. J Comp Physiol Psychol 43:482–489.

Straka H, Baker R, Gilland E (2001) Rhombomeric organization of vestibular pathways in larval frogs. J Comp Neurol 437:42–55.

Straka H, Baker R, Gilland E (2006) Preservation of segmental hindbrain organization in adult frogs. J Comp Neurol 494:228–245.

Straka H, Dieringer N (2000) Convergence pattern of uncrossed excitatory and inhibitory semicircular canal-specific inputs onto second-order vestibular neurons of frogs. Exp Brain Res 135:462–473.

Straka H, Dieringer N (2004) Basic organization principles of the VOR: lessons from frogs. Prog Neurobiol 73:259–309.

Straka H, Vibert N, Vidal PP, Moore LE, Dutia MB (2005) Intrinsic membrane properties of vertebrate vestibular neurons: function, development and plasticity. Prog Neurobiol 76:349–392.

Szwed M, Bagdasarian K, Ahissar E (2003) Encoding of Vibrissal Active Touch. Neuron 40:621–630.

Tomlinson RD, Bahra PS (1986) Combined eye-head gaze shifts in the primate. II. Interactions between saccades and the vestibuloocular reflex. J Neurophysiol 56:1558–1570.

Von Holst E, Mittelstaedt H (1950) Das Reafferenzprinzip. Naturwissenschaften 37:464–476.

Von Uckermann G, Le Ray D, Combes D, Straka H, Simmers J (2013) Spinal efference copy signaling and gaze stabilization during locomotion in juvenile Xenopus frogs. J Neurosci 33:4253–4264.

Wada H (1998) Evolutionary history of free-swimming and sessile lifestyles in urochordates as deduced from 18S rDNA molecular phylogeny. Mol Biol Evol 15:1189–1194.

Wark B, Lundstrom BN, Fairhall A (2007) Sensory adaptation. Curr Opin Neurobiol 17:423–429.

Wassersug RJ, Hoff K (1985) The Kinematics of Swimming in Anuran Larvae. J Exp Biol 119:1–30.

Wicht H, Lacalli TC (2005) The nervous system of amphioxus: structure, development, and evolutionary significance. Can J Zool 83:122–150.

Zaghloul KA, Boahen K, Demb JB (2005) Contrast adaptation in subthreshold and spiking responses of mammalian Y-type retinal ganglion cells. J Neurosci 25:860–868.

Zangemeister WH, Stark L (1982) Gaze latency: variable interactions of head and eye latency. Exp Neurol 75:389–406.

Affidavit/Eidesstattliche Versicherung

Hiermit versichere ich an Eides statt, dass ich die vorliegende Dissertation '**Role of locomotor corollary discharges in sensory-motor integration in *Xenopus laevis* and *Ambystoma mexicanum*'** selbstständig angefertigt habe, mich außer der angegebenen keiner weiteren Hilfsmittel bedient und alle Erkenntnisse, die aus dem Schrifttum ganz oder annähernd übernommen sind, als solche kenntlich gemacht und nach ihrer Herkunft unter Bezeichnung der Fundstelle einzeln nachgewiesen habe.

I hereby confirm that the dissertation '**Role of locomotor corollary discharges in sensory-motor integration in *Xenopus laevis* and *Ambystoma mexicanum*'** is the result of my own work and that I have only used sources or materials listed and specified in the dissertation.

München, den / Munich, date: 11.06.2015

Roberto Banchi

List of Publications

- Direnberger S, **Banchi R**, Brosel S, Seebacher C, Laimgruber S, Uhl R, Felmy F, Straka H, Kunz L (2015) Analysis of signal processing in vestibular circuits with a novel light-emitting diodes-based fluorescence microscope. Eur J Neurosci 41:1332–1344: co-first author
- Hänzi S, **Banchi R**, Straka H, Chagnaud BP (2015) Locomotor corollary activation of trigeminal motoneurons: coupling of discrete motor behaviors. J Exp Biol 218:1748–1758: co-first author
- Chagnaud BP, **Banchi R**, Simmers J and Straka H, (2015) Spinal corollary discharge modulates motion detection during vertebrate locomotion. Nat Commun: co-first author; under revision

List of Contributions

Analysis of signal processing in vestibular circuits with a novel light-emitting diodes-based fluorescence microscope

Stephan Direnberger, **Roberto Banchi**, Sonja Brosel Christian Seebacher, Stefan Laimgruber, Rainer Uhl, Felix Felmy, Hans Straka, Lars Kunz

S.D. and **R.B.** contributed equally to this work

Contributions of RB

- Establishment of the novel Axolotl semi-intact *in-vitro* preparation.
- Morphological characterization and allocation of brainstem vestibular circuitries.
- Multicolor back-filling of brainstem sub-neuronal populations to demonstrate the advantages of the novel fluorescent microscope (i.e. multicolor imaging of spatially independently adjustable field of views, Fig. 2).
- Back filling techniques and preparations for calcium imaging experiments.
- Differential calcium responses in identified central vestibular neurons located at different distances from the glutamate uncaging site (Fig. 4).
- Application of Galvanic Vestibular Stimulation (GVS) and related characterization of the physiological responses specificity in identified central vestibular neurons by means of calcium imaging techniques (Fig. 5).
- Writing and revising, together with all other authors.

Date, place: 11.06.2015, Planegg

Signature Roberto Banchi:

Signature Dr. Stephan Direnberger:

Signature Prof. Dr. Hans Straka (Supervisor):

Locomotor corollary activation of trigeminal motor neurons: coupling of discrete motor behaviors

Sara Hänzi, **Roberto Banchi**, Hans Straka and Boris P. Chagnaud

S.H. and **R.B**. contributed equally to the present study

***J Exp Biol*: accepted**

Contributions of RB

- Preliminary experiments and design of the study, together with BPC.
- All experiments and analyses required for the anatomical part of the study including the visualization of rhombomeric domains (Fig. 2).
- Back-filling method for use in calcium imaging.
- All experiments and analyses involved in the calcium imaging of tentacle motoneurons during fictive swimming (Fig. 3).
- Analysis of the duration of the tentacle nerve discharge compared to the duration of fictive swimming (Fig. 5A, B).
- Writing and revising, together with all other authors.

Date, place: 26.5.15, Planegg

Signature Roberto Banchi:

Signature Sara Hänzi:

Signature Prof. Dr. Hans Straka (Supervisor):

116

Spinal corollary discharge modulates motion detection during vertebrate locomotion

Boris P. Chagnaud, **Roberto Banchi**, John Simmers and Hans Straka

BPC and **RB** contributed equally to this work

This manuscript was submitted to *Nature Communication* and it is currently under revision in this journal.

Contributions of RB

- Design of the experiments together with BPC.
- Anatomical part of the study (Fig. 2)
- Establishment of the *in-vitro* preparation for calcium imaging during fictive swimming and techniques for backfilling of efferent neurons of the vestibular and lateral line system.
- Calcium imaging of efferent neurons during fictive swimming (Fig. 2).
- Duration encoding in the locomotor corollary discharge to the efferent nucleus (Fig. 3A).
- Swimming intensity and effects on the spinal corollary discharge (Fig. 3G).
- Ablation studies and sequential spinal cord activity recordings to reveal the origin of the locomotor corollary discharge together with BPC (Fig. 4).
- Developing of the *en-passant* electrophysiological technique for recordings of afferent-efferent activity in the intact vestibular-lateral line system.
- Corollary discharge induced lateral line peripheral adaptation during locomotion (Fig. 5).
- Writing and revising, together with all other authors.

Date, place: 11.06.2018, Plovdiv

Signature Roberto Banchi:

Signature Dr. Boris Chagnaud:

Signature Prof. Dr. Hans Straka (Supervisor):

117